

# Experimental chemical budgets of OH, HO<sub>2</sub> and RO<sub>2</sub> radicals in rural air in West-Germany during the JULIAC campaign 2019

Changmin Cho<sup>1,\*</sup>, Hendrik Fuchs<sup>1</sup>, Andreas Hofzumahaus<sup>1</sup>, Frank Holland<sup>1</sup>, William J. Bloss<sup>3</sup>, Birger Bohn<sup>1</sup>, Hans-Peter Dorn<sup>1</sup>, Marvin Glowania<sup>1</sup>, Thorsten Hohaus<sup>1</sup>, Lu Liu<sup>1</sup>, Paul S. Monks<sup>2</sup>, Doreen Niether<sup>1</sup>, Franz Rohrer<sup>1</sup>, Roberto Sommariva<sup>2,3</sup>, Zhaofeng Tan<sup>1</sup>, Ralf Tillmann<sup>1</sup>, Astrid Kiendler-Scharr<sup>1</sup>, Andreas Wahner<sup>1</sup>, and Anna Novelli<sup>1</sup>

<sup>1</sup>Forschungszentrum Jülich, Institute of Energy and Climate Research: Troposphere (IEK-8), Jülich, Germany

<sup>2</sup>Department of Chemistry, University of Leicester, Leicester, UK

<sup>3</sup>School of Geography, Earth and Environmental Sciences, University of Birmingham, Birmingham, UK

\*Now at: School of Earth Sciences and Environmental Engineering, Gwangju Institute of Science and Technology (GIST), Gwangju, South Korea

*Correspondence to:* Hendrik Fuchs (h.fuchs@fz-juelich.de) and Anna Novelli (a.novelli@fz-juelich.de)

## Abstract.

Photochemical processes in ambient air were studied using the atmospheric simulation chamber SAPHIR at Forschungszentrum Jülich, Germany. Ambient air was continuously drawn into the chamber through a 50 m high inlet line and passed through the chamber for one month in each season throughout 2019. The residence time of the air inside the chamber was about one hour. As the research center is surrounded by a mixed deciduous forest and is located close to the city Jülich, the sampled air was influenced by both anthropogenic and biogenic emissions. Measurements of hydroxyl (OH), hydroperoxyl (HO<sub>2</sub>) and organic peroxy (RO<sub>2</sub>) radicals were achieved by a laser-induced fluorescence instrument. The radical measurements together with measurements of OH reactivity ( $k_{\text{OH}}$ , the inverse of the OH lifetime) and a comprehensive set of trace gas concentrations and aerosol properties allowed for the investigation of the seasonal and diurnal variation of radical production and destruction pathways. In spring and summer periods, median OH concentrations reached  $6 \times 10^6 \text{ cm}^{-3}$  at noon, and median concentrations of both, HO<sub>2</sub> and RO<sub>2</sub> radicals, were  $3 \times 10^8 \text{ cm}^{-3}$ . The measured OH reactivity was between 4 and  $18 \text{ s}^{-1}$  in both seasons. The total reaction rate of peroxy radicals with NO was found to be consistent with production rates of odd oxygen ( $\text{O}_x = \text{NO}_2 + \text{O}_3$ ) determined from NO<sub>2</sub> and O<sub>3</sub> concentration measurements. The chemical budgets of radicals were analysed for the spring and summer seasons, when peroxy radical concentrations were above the detection limit. For most conditions, the concentrations of radicals were mainly sustained by the regeneration of OH via reactions of HO<sub>2</sub> and RO<sub>2</sub> radicals with nitric oxide (NO). The median diurnal profiles of the total radical production and destruction rates showed maxima between 3 to 6 ppbv h<sup>-1</sup> for OH, HO<sub>2</sub> and RO<sub>2</sub>. Total RO<sub>x</sub> (OH, HO<sub>2</sub> and RO<sub>2</sub>) initiation and termination rates were below 3 ppbv h<sup>-1</sup>. The highest OH radical turnover rate of 13 ppbv h<sup>-1</sup> was observed during a high-temperature (max 40°C) period in August. In this period, the highest HO<sub>2</sub>, RO<sub>2</sub> and RO<sub>x</sub> turnover rates were around 11, 10 and 4 ppbv h<sup>-1</sup>, respectively. When NO mixing ratios were between 1 ppbv to 3 ppbv, OH and HO<sub>2</sub> production and destruction rates were balanced, but unexplained RO<sub>2</sub> and RO<sub>x</sub> production reactions with median rates of 2 ppbv h<sup>-1</sup> and 0.4 ppbv h<sup>-1</sup>, respectively, were required to balance their destruction. For NO mixing ratios above 3 ppbv, the peroxy radical reaction rates with NO were highly

40 uncertain due to the low peroxy radical concentrations close to the limit of NO interferences in the HO<sub>2</sub>  
41 and RO<sub>2</sub> measurements. For NO mixing ratios below 1 ppbv, a missing source for OH and a missing sink  
42 for HO<sub>2</sub> were found with maximum rates of 3.0 ppbv h<sup>-1</sup> and 2.0 ppbv h<sup>-1</sup>, respectively. The missing OH  
43 source consisted likely of a combination of a missing inter-radical HO<sub>2</sub> to OH conversion reaction (up to  
44 2 ppbv h<sup>-1</sup>) and a missing primary radical source (0.5 – 1.4 ppbv h<sup>-1</sup>). The dataset collected in this  
45 campaign allowed to analyze the potential impact of OH regeneration from RO<sub>2</sub> isomerization reactions  
46 from isoprene, HO<sub>2</sub> uptake on aerosol, and RO<sub>2</sub> production from chlorine chemistry on radical production  
47 and destruction rates. These processes were negligible for the chemical conditions encountered in this  
48 study.

## 49 **1 Introduction**

50 The hydroxyl (OH) radical is the dominant daytime atmospheric oxidant. It reacts with most trace gases  
51 in the troposphere and thereby controls the rate of their removal and chemical transformation. In the  
52 lower troposphere, OH is primarily produced by solar photolysis of ozone (O<sub>3</sub>) and nitrous acid (HONO).  
53 The reaction of OH with trace gases leads to the formation of hydroperoxy (HO<sub>2</sub>) or organic peroxy (RO<sub>2</sub>,  
54 with R = organic group) radicals, which undergo further radical reactions. Generally, these reactions are  
55 cyclic chain reactions, in which OH, HO<sub>2</sub>, and RO<sub>2</sub> are converted into each other, while at the same time  
56 emitted pollutants are oxidized and converted into secondary pollutants such ozone and oxygenated  
57 volatile organic compounds (OVOCs). Because the conversion of radicals occurs on a time scale of  
58 seconds to minutes, they are often referred to as the RO<sub>x</sub> family (OH + HO<sub>2</sub> + RO<sub>2</sub>). The most important  
59 radical reactions in the lower are summarized in Table 1. Understanding the radical chemistry is the basis  
60 for reliable predictions of the atmospheric lifetime and chemical transformation of air pollutants and  
61 climate-relevant gases by atmospheric chemistry models (Stone et al., 2012).

62 The level of agreement between simulated and observed radical concentrations in various environments  
63 shows the degree of understanding of the underlying radical chemical mechanism. Even though good  
64 agreement is found in some cases (Tan et al., 2001; Konrad et al., 2003; Mihelcic et al., 2003; Lelieveld et  
65 al., 2008; Kubistin et al., 2010; Whalley et al., 2011), there are significant unexplained discrepancies  
66 between modelled and measured OH in forested regions (Wolfe et al., 2011; Griffith et al., 2013; Kim et  
67 al., 2013; Hens et al., 2013; Wolfe et al., 2014) and of HO<sub>2</sub> and RO<sub>2</sub> in polluted areas (Ren et al., 2003;  
68 Ren et al., 2006; Kanaya et al., 2007; Dusanter et al., 2009; Chen et al., 2010; Ren et al., 2013; Brune et  
69 al., 2016; Tan et al., 2018; Slater et al., 2020; Whalley et al., 2021), while different results are found  
70 depending on the abundance of nitric oxide (NO) in rural environments (Hofzumahaus et al., 2009; Lou et  
71 al., 2010; Elshorbany et al., 2012; Kanaya et al., 2012; Tan et al., 2017).

72 A chemical budget analysis using measured OH, HO<sub>2</sub> and RO<sub>2</sub> radical concentrations can help assessing  
73 the strength of different radical production and loss paths. This allows to identify possible missing  
74 chemical processes by comparing the total production and destruction rates for the different radicals as  
75 concentrations are expected to be in steady-state due to their short chemical lifetime. A large number of  
76 measurements needs to be available (e.g., OH reactivity, OH, peroxy radicals), therefore, there have been  
77 only few studies focusing on the analysis of the chemical budget for OH radicals so far (Handisides et al.,  
78 2003; Hofzumahaus et al., 2009; Brune et al., 2016; Whalley et al., 2018; Tan et al., 2019; Whalley et al.,  
79 2021).

80 Results from field campaigns in China showed a larger OH radical destruction rate compared to its  
81 production rate in the afternoon, which points to an unaccounted OH radical source. Discrepancies were  
82 highest, when NO mixing ratios were lower than 2 ppbv (Hofzumahaus et al., 2009; Tan et al., 2019;  
83 Whalley et al., 2021). On the other hand, studies in urban areas in California (Brune et al., 2016) and in  
84 London (Whalley et al., 2018) as well as in a rural area in Hohenpeissenberg (Handisides et al., 2003)  
85 showed no significant gap between the OH production and destruction rates. Recently, radical  
86 measurements including RO<sub>2</sub> enabled the investigation of HO<sub>2</sub>, RO<sub>2</sub>, and RO<sub>x</sub> production and destruction  
87 rates in field campaigns in China (Tan et al., 2019; Whalley et al., 2021). Tan et al. (2019) showed that a  
88 RO<sub>2</sub> loss process was required in a campaign in Wangdu in summer, while HO<sub>2</sub> production and  
89 destruction rates were balanced. This suggests a missing conversion of RO<sub>2</sub> to OH in addition to the  
90 reaction of peroxy radicals with NO. Furthermore, Whalley et al. (2021) found large imbalances between  
91 peroxy radical production and destruction rates in Beijing indicating a substantially slower propagation of  
92 RO<sub>2</sub> to HO<sub>2</sub> radicals than anticipated.

93 In this study, OH, HO<sub>2</sub>, and RO<sub>2</sub> radical concentrations as well as OH reactivity, the inverse of the OH  
94 radical lifetime, were measured in the atmospheric simulation chamber SAPHIR on campus of  
95 Forschungszentrum Jülich (FZJ), Germany, in the Jülich Atmospheric Chemistry Project Campaign  
96 (JULIAC). Ambient air was sampled from 50 m height into the SAPHIR chamber. From this data set, a  
97 chemical budget analysis of OH, HO<sub>2</sub>, RO<sub>2</sub> radicals, and their sum (RO<sub>x</sub>) was done using measured  
98 concentrations allowing to investigate, if all radical production and destruction processes were accounted  
99 for during spring and summer.

100 **Table 1.** Chemical reactions and rate constants used for the analysis of the chemical budgets of radicals.  
 101 Values of reaction rate constants are given for standard conditions (298 K, 1 atm). Actual numbers are  
 102 used for the calculations.

	Reaction	$k(298\text{ K, 1 atm}) / \text{cm}^3\text{ s}^{-1}$	$k_{\text{ERR}}^{\text{a}}$	Reference
<b>Radical initiation reactions</b>				
R1	$\text{HONO} + \text{h}\nu \rightarrow \text{OH} + \text{NO}$	$j_{\text{HONO}}^{\text{b}}$		
R2	$\text{O}_3 + \text{h}\nu \rightarrow \text{O}^1\text{D} + \text{O}_2$	$j_{\text{O}^1\text{D}}^{\text{b}}$		
R2a	$\text{O}^1\text{D} + \text{H}_2\text{O} \rightarrow 2\text{OH}$	$2.1 \times 10^{-10}$	$\pm 13\%$	IUPAC
R2b	$\text{O}^1\text{D} + \text{M} \rightarrow \text{O}^3\text{P} + \text{M}$	$3.3 \times 10^{-11}$	$\pm 10\%$	IUPAC and JPL
R3	$\text{HCHO} + \text{h}\nu \rightarrow 2\text{HO}_2 + \text{CO}$	$j_{\text{HCHO}}^{\text{b}}$		
R4	$\text{CH}_3\text{CHO} + \text{h}\nu \rightarrow \text{CH}_3\text{O}_2 + \text{HO}_2 + \text{CO}$	$j_{\text{CH}_3\text{CHO}}^{\text{b}}$		
R5	alkenes + $\text{O}_3 \rightarrow \text{OH}, \text{HO}_2, \text{RO}_2 + \text{products}$			
R5a	propene + $\text{O}_3 \rightarrow \text{products}^{\text{c}}$	$1.0 \times 10^{-17}$	$\pm 20\%$	IUPAC
R5b	cis-but-2-ene + $\text{O}_3 \rightarrow \text{product}^{\text{d}}$	$1.3 \times 10^{-16}$	$\pm 12\%$	IUPAC
R5c	1-pentene + $\text{O}_3 \rightarrow \text{products}^{\text{e}}$	$1.0 \times 10^{-17}$	$\pm 20\%$	MCMv3.3.1
R5d	2-hexene + $\text{O}_3 \rightarrow \text{products}^{\text{f}}$	$1.1 \times 10^{-17}$	$\pm 20\%$	MCMv3.3.1
R5e	isoprene + $\text{O}_3 \rightarrow \text{products}^{\text{g}}$	$1.3 \times 10^{-17}$	$\pm 10\%$	MCMv3.3.1
R5f	$\alpha$ -pinene + $\text{O}_3 \rightarrow \text{products}^{\text{h}}$	$9.6 \times 10^{-17}$	$\pm 20\%$	IUPAC
<b>Radical interconversion reactions</b>				
R6	$\text{HCHO} + \text{OH} + \text{O}_2 \rightarrow \text{CO} + \text{H}_2\text{O} + \text{HO}_2$	$8.5 \times 10^{-12}$	$\pm 10\%$	IUPAC
R7	$\text{CO} + \text{OH} + \text{O}_2 \rightarrow \text{CO}_2 + \text{HO}_2$	$2.3 \times 10^{-13}$	$\pm 6\%$	IUPAC
R8	$\text{VOCs} + \text{OH} + \text{O}_2 \rightarrow \text{RO}_2 + \text{H}_2\text{O}$	$j^{\text{j}}$		
R9	$\text{RO}_2 + \text{NO} \rightarrow \text{products} + \text{HO}_2 + \text{NO}_2$	$8.6 \times 10^{-12}$	$\pm 30\%$	Jenkin et al. (2019)
R10	$\text{HO}_2 + \text{NO} \rightarrow \text{OH} + \text{NO}_2$	$8.5 \times 10^{-12}$	$\pm 13\%$	IUPAC
R11	$\text{HO}_2 + \text{O}_3 \rightarrow \text{OH} + 2\text{O}_2$	$2.0 \times 10^{-15}$	$\pm 29\%$	IUPAC
<b>Radical termination reactions</b>				
R12	$\text{NO}_2 + \text{OH} \rightarrow \text{HNO}_3$	$1.0 \times 10^{-11}$	$\pm 30\%$	IUPAC
R13	$\text{NO} + \text{OH} \rightarrow \text{HONO}$	$9.7 \times 10^{-12}$	$\pm 13\%$	IUPAC
R14	$\text{RO}_2 + \text{NO} \rightarrow \text{RONO}_2$	$4.6 \times 10^{-13}$	$\pm 30\%$	Jenkin et al. (2019)
R15	$\text{RO}_2 + \text{RO}_2 \rightarrow \text{products}$	$3.5 \times 10^{-13}$	$\pm 50\%$	Jenkin et al. (2019)
R16	$\text{RO}_2 + \text{HO}_2 \rightarrow \text{ROOH} + \text{O}_2$	$2.3 \times 10^{-11}$	$\pm 50\%$	Jenkin et al. (2019)
R17	$\text{HO}_2 + \text{HO}_2 \rightarrow \text{H}_2\text{O}_2 + \text{O}_2$	$4.5 \times 10^{-12\text{i}}$	$\pm 20\%$	IUPAC
<b>Isoprene reactions</b>				
R18	isoprene + $\text{OH} \rightarrow \text{products}$	$1.0 \times 10^{-10}$	$\pm 8\%$	IUPAC
R19	isoprene- $\text{RO}_2$ (1,6-H shift) + $\text{OH} \rightarrow \text{products}$	$0.01\text{--}0.06\text{ s}^{-1}$		Peeters et al. (2014)
<b>Cl reactions</b>				
R20	$\text{ClNO}_2 + \text{h}\nu \rightarrow \text{Cl} + \text{NO}_2$	$j_{\text{ClNO}_2}^{\text{b}}$		
R21	$\text{Cl}_2 + \text{h}\nu \rightarrow 2\text{Cl}$	$j_{\text{Cl}_2}^{\text{b}}$		
R22	$\text{VOCs} + \text{Cl} \rightarrow \text{RO}_2 + \text{HCl}$	$j^{\text{j}}$		

103 <sup>a</sup> 1 $\sigma$  uncertainty

104 <sup>b</sup> Measured photolysis frequencies

105 <sup>c</sup> Yield for OH: 0.36, HO<sub>2</sub>: 0.10, RO<sub>2</sub>: 0.42 from Novelli et al. (2021)

106 <sup>d</sup> Yield for OH: 0.36, HO<sub>2</sub>: 0.15, RO<sub>2</sub>: 0.51 from Novelli et al. (2021)

107 <sup>e</sup> Yield for OH: 0.32, HO<sub>2</sub>: 0.09, RO<sub>2</sub>: 0.37 from Novelli et al. (2021)

108 <sup>f</sup> Yield for OH: 0.48, HO<sub>2</sub>: 0.11, RO<sub>2</sub>: 0.59 from Novelli et al. (2021)

109 <sup>g</sup> Yield for OH: 0.26, HO<sub>2</sub>: 0.26 from Malkin et al. (2010)

110 <sup>h</sup> Yield for OH: 0.8 from Cox et al. (2020)

111 <sup>i</sup> at 1% water vapour mixing ratio

112 <sup>j</sup> Highly variable depending on the specific VOC.

113

114 **2 Methodology**

115 **2.1 The JULIAC campaign**

116 The Jülich Atmospheric Chemistry Project (JULIAC) campaign was conducted at Forschungszentrum  
 117 Jülich (FZJ, 50.9° N, 6.4° E), Germany. The project consisted of four one-month long intensive  
 118 campaigns studying atmospheric chemistry in ambient air in each season throughout 2019. The location is  
 119 surrounded by a deciduous forest and is located in a rural environment near a town, Jülich (33,000  
 120 inhabitants), 25 km northeast, 40 km west, and 43 km southwest from three large cities, Aachen, Cologne  
 121 and Düsseldorf, respectively. Therefore, ambient air is influenced by both biogenic and anthropogenic  
 122 emission sources.

123 The investigation of the photochemistry was performed in the SAPHIR chamber, which was equipped  
 124 with a large set of instruments measuring radicals, trace gases and aerosol (Table 2). The SAPHIR  
 125 chamber has a cylindrical shape and is made of a double-wall Teflon (FEP) film. A slight overpressure  
 126 (35 Pa) is maintained in the chamber and the space between the two films is permanently flushed with  
 127 pure nitrogen (Linde, purity: > 99:99990 %) to prevent outside air penetrating the inner chamber. The

**Table 2.** Specification of instruments used in the JULIAC campaign for the analysis in this work.

Species	Measurement technique	Time resolution(1σ)	Limit of detection	1σ accuracy
OH	LIF	270 s	$0.7 \times 10^6 \text{ cm}^{-3}$	18%
OH	DOAS	134 s	$0.8 \times 10^6 \text{ cm}^{-3}$	6.5%
HO <sub>2</sub>	LIF	47 s	$1 \times 10^7 \text{ cm}^{-3}$	18%
RO <sub>2</sub>	LIF	47s	$2 \times 10^7 \text{ cm}^{-3}$	18%
OH reactivity ( $k_{\text{OH}}$ )	LP-LIF	180 s	$0.2 \text{ s}^{-1}$	10%
Photolysis frequencies	Spectroradiometer	60 s		18%
O <sub>3</sub>	UV photometry	60 s	0.5 ppbv	2%
NO <sub>x</sub>	Chemiluminescence <sup>a</sup>	60 s	NO: 20 pptv	NO: 5 %
(NO+NO <sub>2</sub> )			NO <sub>2</sub> : 30 pptv	NO <sub>2</sub> : 7%
CO, CO <sub>2</sub> , CH <sub>4</sub> , H <sub>2</sub> O	Cavity ring-down spectroscopy	60 s	CO and CH <sub>4</sub> : 1 ppbv CO <sub>2</sub> : 25 ppbv H <sub>2</sub> O: 0.1 %	5%
HONO	LOPAP	180 s	5 pptv	10%
HCHO	Cavity ring-down spectroscopy	300 s	0.1 ppbv	10%
ClNO <sub>2</sub>	I-CIMS	60 s	2.8 pptv	8.5%
VOCs	PTR-TOF-MS	30 s	15 pptv	14%
	VOCUS PTR-TOF-MS	30 s		
Aerosol surface area	SMPS	7 min	10nm – 1μm	N/A

<sup>a</sup> NO<sub>2</sub> was converted to NO before detection using a custom-built photolytic converter.

128 chamber is equipped with a shutter system allowing the air to be either shielded from or exposed to solar  
129 radiation.

130 In the JULIAC campaign, ambient air was sampled at a high flow rate of  $660 \text{ m}^3 \text{ h}^{-1}$  from 50 m high inlet  
131 line (104 mm inner diameter, SilcoNert® coated stainless steel) by means of an oil-free turbo blower  
132 (Aerzener Maschinenfabrik, AERZEN Turbo G3 Typ: TB 50-0.6 S). Large particles ( $>10 \mu\text{m}$  diameter)  
133 were removed by a SilcoNert® coated cyclone (LTG, ZSB-6). The temperatures in the inlet line and  
134 cyclone were controlled to be slightly higher than ambient temperature (+1 to  $2 \text{ }^\circ\text{C}$ ) to avoid water vapor  
135 condensation in the inlet system. A 3/2-way valve directed part of the air (flow rate of  $250 \text{ m}^3 \text{ h}^{-1}$ ) into the  
136 chamber. Two fans inside the chamber ensured fast mixing on a time scale of a few minutes. As a result,  
137 the chamber behaved as a continuously stirred photochemical flow reactor with a mean residence time of  
138 air of 1.1 h. During the transition time of 3.5 s from the tip of the inlet to the SAPHIR chamber,  
139 atmospheric  $\text{RO}_x$  radicals are lost on walls, but concentrations are rapidly re-established in the sampled  
140 ambient air inside the sunlit chamber.

141 The use of the chamber as a flow reactor has advantages compared to field measurements in the open air.  
142 Perturbations of the studied chemistry due to local emissions of VOCs or  $\text{NO}_x$  can be avoided. Transient  
143 fluctuations of reactants in the sampled air, for example due to spikes of NO from passing cars, are  
144 smoothed out in the chamber. Due to the homogeneous mixing, instruments connected to the chamber  
145 measure the same air composition and segregation effects on reaction rates are insignificant.

146 The air composition could be influenced by the inlet line and chamber surfaces. As the whole inlet line is  
147 heated and chemically inert due to the SilcoNert® coating, no relevant wall loss or desorption of trace  
148 gases is expected from the inlet. This assumption was confirmed by comparing OH reactivity measured at  
149 several positions of the inlet line. No significant differences were found between measurements, if the air  
150 was either sampled upstream of the cyclone or downstream of the blower. Wall losses of trace gases  
151 (VOCs,  $\text{NO}_x$ ,  $\text{O}_3$ ) inside the SAPHIR chamber were found to be negligible in previous experiments (e.g.,  
152 Kaminski et al., 2017, Rolletter et al., 2020).

153 Nitrous acid (HONO) and formaldehyde (HCHO) are known to be emitted from the chamber film when it  
154 is exposed to solar radiation (Rohrer et al. (2005)). These emissions significantly increase the  
155 concentrations of HONO and HCHO in the chamber. Due to the transmission through the Teflon film and  
156 shading from construction elements of the chamber, the absolute actinic flux density is reduced by 20 to  
157 40 % compared to outside the chamber. It is worth noting, however, that the relative spectral distribution  
158 of the solar radiation is not changed by the transmission through the chamber film (Bohn and Zilken,  
159 2005).

160 The floor underneath the chamber is heated by the solar radiation. Although it is not in direct contact to  
161 the foil, the air temperature in the chamber was on average  $0.7^\circ\text{C}$  higher during winter and autumn and  
162  $1.9^\circ\text{C}$  higher during spring and summer than the temperature outside of the chamber at daytime. Since  
163 photochemistry was studied in the chamber, all data of chemical and physical conditions shown in this  
164 work refer to conditions inside the chamber.

165 The measurements in the campaign were at least once a week interrupted for calibration and maintenance  
166 of instruments. Some days were also excluded from the analysis in this work because the chamber shutter

167 system was kept closed to protect the chamber film during bad weather from strong wind gusts and/or  
168 precipitation. Reference experiments with clean synthetic air were performed to investigate possible  
169 changes in the strength of chamber emissions and to check for instrumental backgrounds. In addition,  
170 chemical actinometry experiments, in which NO<sub>2</sub> was photolyzed in synthetic air, were performed before  
171 and after each intensive period. The comparison of actinometric and spectroradiometric  $j_{\text{NO}_2}$  values was  
172 used to track and correct for changes in light transmission due to aging of the chamber wall (Bohn et al.,  
173 2005).

174

## 175 **2.2 Instrumentation**

### 176 **2.2.1 OH, HO<sub>2</sub> and RO<sub>2</sub> radical and OH reactivity ( $k_{\text{OH}}$ ) measurements**

177  
178 OH, HO<sub>2</sub>, and RO<sub>2</sub> radicals were measured by the FZJ – LIF which included a newly developed chemical  
179 modulation reactor (CMR) for interference-corrected measurements of OH radicals (Cho et al., 2021).  
180 The signals of the instrument were calibrated against well-defined radical concentrations that were  
181 produced from water photolysis in synthetic air at a wavelength of 185nm using radiation of a mercury  
182 lamp. A detailed description of the LIF instrument and its calibration can be found in previous  
183 publications (Holland et al., 2003; Fuchs et al., 2008; Fuchs et al., 2011; Fuchs et al., 2012).

184 Shortly, the OH radical is sampled through a nozzle with a 0.4 mm diameter pinhole and is excited by a  
185 pulsed laser at a wavelength of 308 nm in a low-pressure (4 hPa) fluorescence cell. The emitted resonant  
186 fluorescence is detected with a time delay by a time-gated micro-channel plate detector (MCP). In the  
187 JULIAC campaign, a chemical modulation reactor (CMR) was implemented on top of the OH cell to  
188 quantify potential interferences. This is achieved by periodically removing ambient OH by an OH  
189 scavenger that is injected in the reactor (propane, Air Liquide, purity>99.95%, (5.0±0.1) % mixture in  
190 nitrogen) before the air enters the fluorescence cell. During the campaign, the observed interference could  
191 be fully explained by the well-characterized interference from the photolysis of ozone in humid air inside  
192 the detection cell. No evidence for an unexplained interference was found (Cho et al., 2021). The limit of  
193 detection for OH was  $0.7 \times 10^6 \text{ cm}^{-3}$  and the accuracy was 18 % ( $1\sigma$ ).

194 OH radical concentrations were also measured by differential optical absorption spectroscopy (DOAS)  
195 using a multiple folded light path for absorption inside along the chamber. The DOAS technique is a  
196 calibration-free technique (Hausmann et al., 1997; Schlosser et al., 2007; Schlosser et al., 2009). The limit  
197 of detection was  $0.8 \times 10^6 \text{ cm}^{-3}$  and the  $1\sigma$ -accuracy was 6.5 %. Due to a technical laser problem, the  
198 DOAS instrument was not available in spring.

199 HO<sub>2</sub> radicals were detected by the LIF instrument in a separate detection cell, where HO<sub>2</sub> is chemically  
200 converted to OH radicals in the reaction with NO (Air Liquide, 1% NO in N<sub>2</sub>, purity > 99.5 %) that is  
201 injected in the fluorescence cell (Fuchs et al., 2011). During the JULIAC campaign, two different  
202 concentrations ( $2.5 \times 10^{13} \text{ cm}^{-3}$  and  $1.0 \times 10^{14} \text{ cm}^{-3}$ ) of NO in the fluorescence cell were used to  
203 observe possible interference from specific RO<sub>2</sub> radicals as highlighted by Fuchs et al. (2011). No  
204 difference between HO<sub>2</sub> measurements at high and low NO concentrations was found suggesting that  
205 there was no significant interference from RO<sub>2</sub>.

206 In addition, the sum of OH, HO<sub>2</sub>, and RO<sub>2</sub> (RO<sub>x</sub>) was measured by the RO<sub>x</sub>-LIF system. Air is sampled  
207 into a chemical converter (pressure of ~ 25 hPa), where a mixture of NO (Air Liquide, 500 ppmv NO in  
208 N<sub>2</sub>, purity > 99.5%) and CO (Air Liquide, 10% CO in N<sub>2</sub>, purity > 99.997%) is injected. The NO converts  
209 RO<sub>2</sub> radicals to HO<sub>2</sub> radicals and CO converts OH radicals formed from the reaction of HO<sub>2</sub> radicals with  
210 NO back to HO<sub>2</sub>. Therefore, an equilibrium between OH and HO<sub>2</sub> is established. Concentrations are  
211 chosen, so that the equilibrium is on the side of HO<sub>2</sub>. In a low-pressure cell downstream of the converter  
212 HO<sub>2</sub> radicals are converted to OH radicals by injecting excess NO (Air Liquide, pure NO, purity>99.5%)  
213 (Fuchs et al., 2008) that shifts the equilibrium between OH and HO<sub>2</sub> to OH. The RO<sub>2</sub> concentration is  
214 obtained from the difference between the sum measurement of RO<sub>x</sub> and measurements of OH and HO<sub>2</sub>  
215 concentrations in the other two detection cells. The RO<sub>2</sub> detection sensitivity was calibrated for methyl  
216 peroxy radicals (CH<sub>3</sub>O<sub>2</sub>) which are produced from the reaction of OH with methane (CH<sub>4</sub>) in the  
217 calibration system. The resulting calibration is also applicable to the majority of other atmospheric alkyl  
218 peroxy radicals (Fuchs et al., 2008; Fuchs et al., 2011) and recent laboratory tests performed with a  
219 variety of VOCs including monoterpenes and chained alkanes for the CO and NO mixing ratios  
220 applied in the RO<sub>x</sub> converter during the JULIAC campaign showed a decrease of less than 15% of  
221 sensitivity as compared to methyl peroxy radicals which is within the accuracy of the instrument.

222 The signals in the HO<sub>2</sub> and RO<sub>2</sub> detection systems contain a background signal observed when NO is  
223 injected into the detection cells, even if no radicals are present in the air sampled. The background signal  
224 can be characterized when the inlet of the detection system is overflowed with synthetic air, which is part  
225 of the calibration procedures. During JULIAC the background varied from calibration to calibration and  
226 was often larger than the smallest signals measured in ambient air from the chamber (Table S1). The  
227 highest background signals obtained from calibrations is therefore regarded as an upper limit and the  
228 variability is considered as an additional uncertainty in the measured HO<sub>2</sub> and RO<sub>2</sub> concentrations. HO<sub>2</sub>  
229 and RO<sub>2</sub> background signals, which are subtracted in the evaluation of HO<sub>2</sub> and RO<sub>2</sub> measurements, were  
230 taken from reference experiments in the dark clean chamber, when no HO<sub>2</sub> or RO<sub>2</sub> radicals are expected.  
231 The subtracted signals for each period are available in Table S1 and in most cases were equivalent to  
232 concentrations lower than  $1 \times 10^7 \text{ cm}^{-3}$  for both HO<sub>2</sub> and RO<sub>2</sub> measurements.

233 The total OH reactivity ( $k_{\text{OH}}$ ), the inverse of the chemical lifetime of OH radicals, was measured in  
234 ambient air by a laser-flash photolysis LIF instrument (Lou et al., 2010; Fuchs et al., 2017). A high  
235 concentration of OH radicals is produced by flash photolysis (266 nm, 1 Hz repetition rate) of ozone in  
236 humid air (Reaction R2) in a flow tube that is on top of an OH fluorescence cell. The pseudo first-order  
237 decay of OH in the chemical reactions with atmospheric reactants is measured, giving directly the OH  
238 reactivity.

### 239 **2.2.2 Other trace gases, aerosol properties and photolysis frequencies measurements**

240 A comprehensive set of instruments operated during the JULIAC campaign (Table 2) analyzed the air  
241 composition inside the chamber. Photolysis frequencies inside the chamber were derived from solar  
242 actinic flux densities measured by a spectroradiometer mounted on the roof of the nearby institute  
243 building. Chamber values were calculated using a model approach considering shading effects and the  
244 influence of the chamber film (Bohn et al., 2005; Bohn and Zilken, 2005). Formaldehyde (HCHO) was  
245 detected by cavity ring-down spectroscopy (Picarro, G2307, Glowania et al. (2021)). NO and NO<sub>2</sub> were  
246 measured by chemiluminescence (Eco Physics, TR780, NO<sub>2</sub> conversion by a custom-built photolytic



247 converter). In addition, HONO was measured by long-path absorption photometry (LOPAP, Kleffmann et  
 248 al. (2006); Häsel et al. (2009)), CO, CO<sub>2</sub>, CH<sub>4</sub>, and H<sub>2</sub>O by cavity ring-down spectroscopy (Picarro,  
 249 G2401), and O<sub>3</sub> by UV absorption (Ansyco-41M and Thermo scientific-49I). Volatile organic compounds  
 250 (VOCs) were detected by a proton-transfer-reaction time-of-flight mass spectrometer (PTR-TOF-MS,  
 251 Ionicon) (Jordan et al., 2009) and a VOCUS PTR-TOF-MS instrument (Aerodyne). The VOCs included  
 252 in this study are listed in Table S2 and include isoprene and some carbonyl compounds. Total aerosol  
 253 surface area was determined from measurements by a scanning mobility particle sizer (SMPS). In the  
 254 summer and autumn periods, nitryl chloride (ClNO<sub>2</sub>) was detected by a chemical ionization mass  
 255 spectrometer using iodine as reagent ion (I-CIMS) (Sommariva et al., 2018; Tan et al., 2022).

256 In addition to measurements in the chamber, concentrations of O<sub>3</sub> and NO<sub>x</sub> were also measured in the  
 257 inlet system before the air flowed into the SAPHIR chamber. For these measurements, a combined system  
 258 (Eco Physics, CraNO<sub>x</sub>) consisting of an ozone photometer and a chemiluminescence instrument for NO<sub>x</sub>  
 259 was deployed. Measurements were used to determine the photochemical ozone production in the JULIAC  
 260 campaign. Further description of the measurement set-up and concept of the evaluation will be discussed  
 261 in details in a further publication.

262

## 263 2.3 Chemical budget calculations

264 A chemical budget analysis, similar as in Tan et al. (2019) and Whalley et al. (2021), was applied for OH,  
 265 HO<sub>2</sub>, RO<sub>2</sub> and the sum of all three radicals (RO<sub>x</sub>) to the data set from the JULIAC campaign. All  
 266 reactions typically considered to be relevant for the generation and destruction of these radicals are  
 267 considered (Table 1). Rate constants and their uncertainties were mainly taken from IUPAC  
 268 recommendations (Atkinson et al., 2004; Atkinson et al., 2006; Cox et al., 2020) or more recent studies. If  
 269 not otherwise specified, radical production and destruction rates are calculated from measured  
 270 concentrations of reactants.

### 271 2.3.1 Chemical budget of OH radicals

272 The production rate of OH radicals includes primary production reactions (Reaction R1, R2 and R5) and  
 273 radical interconversion reactions (Reaction R10 and R11):

$$274 P_{OH} = j_{HONO}[HONO] + \varphi_{OH}j_{O^1D}[O_3] + k_{10}[NO][HO_2] + k_{11}[O_3][HO_2] \\ 275 + \Sigma\{\varphi_{OH}^i k_5^i [alkene]^i [O_3]\} + P_{OH,Isop.} \quad (1)$$

276 Here,  $\varphi_{OH}$  is the effective OH yield of the ozone photolysis including the reaction of excited oxygen  
 277 atoms O(<sup>1</sup>D) with H<sub>2</sub>O producing two OH radicals.  $\varphi_{OH}^i$  is the OH yield of the ozonolysis reaction of  
 278 alkenes, and  $k_5^i$  represents the rate constants of the corresponding reactions.

279  $P_{OH,Isop}$  is the effective production of OH radicals from unimolecular reactions (1,6-hydrogen shift  
 280 reactions) of isoprene-RO<sub>2</sub> radicals (Z- $\delta$ -RO<sub>2</sub>-I and II, Peeters et al. (2014)) and the subsequent chemistry  
 281 of products.. As there was no measurement of speciated RO<sub>2</sub> radicals, isoprene-RO<sub>2</sub> radical  
 282 concentrations are estimated from steady-state conditions considering their production from the reaction

283 of isoprene with OH and their destruction in bimolecular reaction (reaction rate  $k_{bi}$ ) and unimolecular  
 284 reactions (bulk reaction rate  $k_{bulk\ 1,6-H}$  as defined in Peeters et al. (2014)):

$$285 \quad [RO_2(\text{isop.})]_{SS} = \frac{k_{18}[\text{Isoprene}][OH]}{k_{bi} + k_{bulk\ 1,6-H}} \quad (2)$$

$$286 \quad k_{bi} = (k_9 + k_{14})[NO] + k_{15}[RO_2] + k_{16}[HO_2] \quad (2a)$$

287 Bimolecular loss reactions include reactions with NO (Reaction R9 and R14),  $RO_2$  (Reaction R15) and  
 288  $HO_2$  (Reaction R16). The OH production from isoprene- $RO_2$  isomerization reactions is simplified in the  
 289 calculation of the total OH production in this work by assuming that each isomerization reaction produces  
 290 rapidly one OH radical from the subsequent reactions of products such as photolysis of hydroxy-peroxy  
 291 aldehyde (HPALD). In this case, the radical production rate is equal to the loss rate of the isoprene- $RO_2$   
 292 due to isomerization reactions ( $D_{Z-\delta-RO_2, \text{Isop.}}$ ):

$$293 \quad P_{OH, \text{Isop.}} = D_{Z-\delta-RO_2, \text{Isop.}} = k_{bulk\ 1,6-H} [RO_2(\text{isop.})]_{SS} \quad (4)$$

294 The total loss rate of OH radicals for the chemical budget analysis is determined by the product of the  
 295 total OH reactivity ( $k_{OH}$ ) and the OH radical concentration:

$$D_{OH} = k_{OH}[OH] \quad (5)$$

### 296 2.3.2 Chemical budget of $HO_2$ radicals

297 The production rate of  $HO_2$  radicals includes primary reactions (Reaction R3, R4 and R5) and  
 298 interconversion reactions (Reaction R6, R7 and R9, Table 1):

$$299 \quad P_{HO_2} = 2 j_{HCHO}[HCHO] + k_6[HCHO][OH] + k_7[CO][OH] + k_9[NO][RO_2] \\ + \sum\{\varphi_{HO_2}^i k_5^i [\text{alkene}]^i [O_3]\} \quad (6)$$

300 Here, the photolysis frequency of HCHO ( $j_{HCHO}$ ) include only paths generating radicals.  $\varphi_{HO_2}^i$  is the  
 301  $HO_2$  yield from the ozonolysis of alkenes. The reactions of OH with  $H_2$  and  $O_3$  are not considered due to  
 302 their negligible contributions to the  $HO_2$  production.

303 The loss rate of  $HO_2$  is determined by the reactions with NO (Reaction R10),  $O_3$  (Reaction R11),  $RO_2$   
 304 (Reaction R16) and  $HO_2$  (Reaction R17):

$$305 \quad D_{HO_2} = (k_{10}[NO] + k_{11}[O_3] + k_{16}[RO_2] + 2k_{17}[HO_2])[HO_2] \quad (7)$$

306 Here, the humidity dependence of  $k_{17}$  was taken into account. The reaction of  $HO_2$  radicals with  $NO_2$  is  
 307 not included as the thermal decomposition of peroxyxynitric acid ( $HO_2NO_2$ ) forming back  $HO_2$  radicals and  
 308  $NO_2$  is instantaneous for the temperatures experienced during the JULIAC campaign.

309 In a sensitivity calculation (Section 4.2.3), potential loss of  $HO_2$  due to heterogeneous uptake on aerosol  
 310 is investigated. The first order loss rate ( $k_{het.}$ ) can be described as:

$$311 \quad k_{het.} = \frac{Y_{eff} \cdot \nu_{HO_2} \cdot [AS]}{4} \quad (8)$$

312  $v_{\text{HO}_2}$  is the mean molecular velocity of  $\text{HO}_2$  ( $4.44 \times 10^5 \text{ cm s}^{-1}$  at 298 K),  $[\text{AS}]$  is the measured aerosol  
313 surface area concentration, and  $\gamma_{\text{eff}}$  is the effective uptake coefficient.

### 314 2.3.3 Chemical budget of $\text{RO}_2$ radicals

315 Primary sources of  $\text{RO}_2$  radicals include all oxidation reactions of VOCs with OH, Cl,  $\text{NO}_3$  radicals and  
316  $\text{O}_3$ . As the number of measured VOC species in this study was limited (Table S2) and because it is  
317 generally difficult to capture the entire spectrum of atmospheric VOCs (Goldstein and Galbally, 2007;  
318 Lou et al., 2010), the measured total OH reactivity ( $k_{\text{OH}}$ ) can be used to calculate the  $\text{RO}_2$  radicals  
319 production from the reactions of VOCs with OH. First, the contributions from CO, NO,  $\text{NO}_2$ , HCHO and  
320  $\text{O}_3$  is removed from the measured OH reactivity as these species do not form  $\text{RO}_2$  radicals in the reaction  
321 with OH. It is then assumed that the remaining fraction can be attributed to organic compounds (VOC  
322 reactivity ( $k_{\text{VOC}}$ )) including measured and unmeasured VOCs, which produce  $\text{RO}_2$  radicals in their  
323 reaction with OH.

324 For some aromatics, such as toluene, benzene, xylene, etc., the prompt formation of  $\text{HO}_2$  is expected by  
325 their reaction with OH (Nehr et al., 2011; Nehr et al., 2014; Jenkin et al., 2019). However, in this  
326 campaign, their concentrations were small and their average contributions to the OH reactivity from  
327 VOCs were only 2.8%. Therefore, their potential impacts on the  $\text{RO}_2$  production are negligible (less than  
328 1%).

329 In addition,  $\text{RO}_2$  production from ozonolysis needs to be included. In this work, only the reactions of  
330 measured organic compounds are considered. The contribution to the  $\text{RO}_2$  production from the oxidation  
331 of VOCs by the  $\text{NO}_3$  radical was negligible during daytime due to the low VOC load (low OH reactivity),  
332 so that  $\text{NO}_3$  destruction by photolysis and reaction with NO dominated.

333 Reactions of chloride (Cl) also produce  $\text{RO}_2$  radicals, but the concentration was not measured in the  
334 JULIAC campaign. However, one of the most important precursor species, nitryl chloride ( $\text{ClNO}_2$ ), was  
335 detected during the campaign (except in spring, Tan et al. (2022)).  $\text{ClNO}_2$  can accumulate during  
336 nighttime, but it is photolyzed after sunrise yielding  $\text{NO}_2$  and Cl atoms (Reaction R20). Assuming as an  
337 upper limit that each Cl atom reacts with a VOCs (Tanaka et al., 2003), the  $\text{RO}_2$  production rate from Cl  
338 radicals can be calculated as:

$$339 P_{\text{RO}_2, \text{Cl}} = j_{\text{ClNO}_2} [\text{ClNO}_2] \quad (9)$$

340 The total  $\text{RO}_2$  production rate is then calculated as:

$$341 P_{\text{RO}_2} = k_{\text{VOC}} [\text{OH}] + \sum (\varphi_{\text{RO}_2}^i k_{\text{R5}}^i [\text{alkene}]^i [\text{O}_3]) + P_{\text{RO}_2, \text{Cl}} \quad (10)$$

342 Here,  $\varphi_{\text{RO}_2}^i$  is the  $\text{RO}_2$  yield from the ozonolysis of alkenes species (Table 1).

343 With respect to the destruction rate of  $\text{RO}_2$ , its reactions with NO,  $\text{HO}_2$ , and other  $\text{RO}_2$  and unimolecular  
344 reactions of specific isoprene- $\text{RO}_2$  radicals ( $\text{D}_{\text{Z}-\delta-\text{RO}_2, \text{Isop}}$ ) (Eq. 4) are considered in this work:

$$345 \text{D}_{\text{RO}_2} = ((k_9 + k_{14}) [\text{NO}] + 2k_{15} [\text{RO}_2] + k_{16} [\text{HO}_2]) [\text{RO}_2] + \text{D}_{\text{Z}-\delta-\text{RO}_2, \text{Isop}} \quad (11)$$

### 346 2.3.4 Chemical budget of $\text{RO}_x$ radicals

347 In the chemical budget of the sum of OH, HO<sub>2</sub> and RO<sub>2</sub> (RO<sub>x</sub>), inter-radical conversion reactions cancel  
348 out and only initiation and termination reactions are included. Therefore, the RO<sub>x</sub> radical budget analysis  
349 allows to investigate if primary radical source reactions or termination processes are missing in the  
350 chemical mechanism used (Table 1).

351 The production rate of the RO<sub>x</sub> radicals is given by the sum of rates from radical initiation reactions  
352 (Reaction R1-R5, R20-R22, Table 1):

$$353 P_{RO_x} = j_{HONO}[HONO] + \varphi_{OH}j_{O^1D}[O_3] + 2j_{HCHO}[HCHO] \\ 354 + \sum((\varphi_{OH}^i + \varphi_{HO_2}^i + \varphi_{RO_2}^i)k_5^i[\text{alkene}]^i[O_3]) + P_{RO_2,Cl} \quad (12)$$

355 Radicals can be additionally produced from the photolysis of other oxygenated organic compounds  
356 (OVOCs, e.g., Reaction R4) not included in Eq. 12. Their potential impact is further discussed in Section  
357 4.2.2.

358 The loss rate of the RO<sub>x</sub> radical is calculated by the sum of rates from radical termination reactions  
359 (Reaction R12-R17):

$$360 D_{RO_x} = (k_{13}[NO] + k_{12}[NO_2])[OH] + k_{14}[NO][RO_2] + 2k_{15}[RO_2]^2 + 2k_{16}[HO_2][RO_2] + 2k_{17}[HO_2]^2 \\ 361 \quad (13)$$

### 362 **2.3.5 Uncertainties in the calculated production and destruction rates**

363 The uncertainty of each production or loss rate is calculated by Gaussian summation of the 1σ errors of  
364 the measured quantities (Table 2) and the uncertainties of the reaction rate constants (Table 1).

365 For reactions of RO<sub>2</sub> with NO (Reaction R9, R14), HO<sub>2</sub> (Reaction R16) and RO<sub>2</sub> (Reaction R15), generic  
366 rate constants are used for the sum of RO<sub>2</sub> radicals (Table 1, Jenkin et al. (2019)). Rate constants of the  
367 NO reaction with RO<sub>2</sub> derived from hydrocarbons (<C<sub>5</sub>) and with oxygenated peroxy radicals range from  
368 7.7 × 10<sup>-12</sup> cm<sup>3</sup> s<sup>-1</sup> to 1.1 × 10<sup>-11</sup> cm<sup>3</sup> s<sup>-1</sup> (Jenkin et al., 2019). The 1σ-uncertainty of the rate constants  
369 varies from 6 to 30 %. In the error calculations here, an upper limit value of 30 % is applied. However,  
370 for reactions of RO<sub>2</sub> with HO<sub>2</sub> and with RO<sub>2</sub>, the range of rate constants varies by more than an order of  
371 magnitude. In the calculations, an uncertainty of 50% is used for the reaction rate constants of RO<sub>2</sub> with  
372 HO<sub>2</sub> and with RO<sub>2</sub>.

373 As there are no measurements of speciated RO<sub>2</sub> radicals, a yield of 5% for the formation of organic  
374 nitrates is assumed for all RO<sub>2</sub> but the yield can vary between 1% for methyl peroxy radicals (CH<sub>3</sub>O<sub>2</sub>) and  
375 more than 20 % for RO<sub>2</sub> from monoterpene species. This simplification can introduce systematic errors in  
376 the calculations (Section 4.2.1).

377

### 378 **2.4 Odd oxygen production rate**

379 In the troposphere, ozone is formed exclusively by the oxidation of NO to NO<sub>2</sub> through reaction with RO<sub>2</sub>  
380 (Reaction R9) and HO<sub>2</sub> (Reaction R10), followed by NO<sub>2</sub> photolysis (Fishman and Carney, 1984; Sillman  
381 et al., 1990; Kleinman et al., 2002).

382 During the day, the photolysis of NO<sub>2</sub> and the back reaction of NO with O<sub>3</sub> form a rapid photochemical  
383 equilibrium between O<sub>3</sub> and NO<sub>2</sub>. The sum of O<sub>3</sub> and NO<sub>2</sub> is therefore defined as odd oxygen (O<sub>X</sub>) (Han  
384 et al., 2011; Goldberg et al., 2015). The relative composition of O<sub>X</sub> depends on the NO<sub>2</sub> photolysis  
385 frequency and the NO concentration. For the conditions of the spring and summer periods in the JULIAC  
386 campaign, O<sub>X</sub> consisted predominantly (> 85%) of O<sub>3</sub>.

387 In this work, the net production rate of O<sub>X</sub> (P<sub>O<sub>X</sub></sub>) was determined experimentally from the increase of O<sub>X</sub>  
388 in the sunlit SAPHIR chamber. Furthermore, measurements of radicals and NO<sub>X</sub> were used to calculate  
389 P<sub>O<sub>X</sub></sub> from the rate of O<sub>X</sub> formation reactions (Reaction R9, R10), and O<sub>X</sub> loss by the reaction of NO<sub>2</sub> with  
390 OH (Reaction R12) (Mihelcic et al., 2003; Cazorla et al., 2012; Niether et al., 2022)):

$$391 \quad P_{O_X,net} = k_9[NO][RO_2] + k_{10}[NO][HO_2] - k_{12}[NO_2][OH] \quad (14)$$

392 This calculation neglects minor O<sub>X</sub> destruction processes such as the reaction of O<sub>3</sub> with NO<sub>2</sub>, OH, HO<sub>2</sub>,  
393 Cl or alkenes since they did not play a notable role during the day in this campaign.

## 394 **3 Results**

### 395 **3.1 Data quality of radical measurements**

396 Performing measurements in the SAPHIR chamber allowed to test the accuracy of radical measurements  
397 in different ways that are typically not available in field experiments. First, OH radicals was measured by  
398 2 independent instruments, the OH-DOAS and LIF instruments (Cho et al., 2021). Second, the O<sub>X</sub>  
399 production rate calculated from measured concentrations of HO<sub>2</sub> and RO<sub>2</sub> could be compared to the  
400 observed increase of O<sub>X</sub> concentrations in the chamber, which can be solely attributed to chemical  
401 reactions. This is possible, because other factors typically impacting the O<sub>X</sub> concentration in field  
402 experiments such as transportation processes are not effective.

403 OH concentrations were measured by the LIF instrument applying the chemical modulation scheme and  
404 the DOAS in the winter, summer and autumn periods of the campaign. As OH concentrations were close  
405 to the limit of detection in autumn and winter, a meaningful comparison of measurements was only  
406 possible for the summer period. A detailed comparison of measurements can be found in Cho et al. (2021).  
407 In general, the OH measurements of the two instruments agreed within their measurement errors (Table 1)  
408 giving a slope of 1.1±0.02 in a linear regression analysis. The good agreement confirms that the newly  
409 developed chemical modulation system of the LIF instrument allowed for interference-free OH  
410 concentration measurements for conditions of the campaign. Only in the period from 22 to 26 August,  
411 which was characterized by exceptionally high temperatures (30 to 40°C), OH concentrations measured  
412 by the LIF instrument were systematically higher by 25% than those measured by the DOAS instrument  
413 for unknown reasons (Cho et al., 2021). OH concentrations measured by the DOAS instrument were used  
414 for the analysis of the radical budgets in this period.

415 Net O<sub>X</sub> production rates were determined from the measured increase of O<sub>X</sub> concentrations in the  
416 chamber and compared to calculations from the turnover rates of HO<sub>2</sub> and RO<sub>2</sub> reactions with NO. This  
417 calculation takes also the NO<sub>2</sub> loss due to its reaction with OH into account (Eq. 14). The odd oxygen  
418 production rate did not exceed 1 ppbv h<sup>-1</sup> in winter and autumn due to the general low photochemical

419 activity in these seasons. In spring and summer, the  $O_x$  production rate showed clear diurnal variations  
 420 with noontime maxima that reached up to  $16 \text{ ppbv h}^{-1}$ . In these seasons, both methods for determining the  
 421  $O_x$  production rate agreed within  $\pm 15\%$  ( $1\sigma$ ). Observed discrepancies were less than  $1 \text{ ppbv h}^{-1}$ , when  
 422  $NO$  mixing ratios were lower than  $1 \text{ ppbv}$ , but reached values of  $3 \text{ ppbv h}^{-1}$  for  $NO$  mixing ratios of  $3 - 4$   
 423  $\text{ppbv } NO$ . The largest discrepancy of  $8.5 \text{ ppbv h}^{-1}$  was found in the morning on 29 April, when the  $NO$   
 424 mixing ratio exceeded  $9 \text{ ppbv}$ . High  $NO$  values suppressed  $HO_2$  and  $RO_2$  concentrations to values below  
 425  $2.0 \times 10^7 \text{ cm}^{-3}$ , which is within the range of the background corrections for the  $HO_2$  and  $RO_2$   
 426 measurements (Table S1). Under these conditions, an erroneous background subtraction may have caused  
 427 the observed discrepancies.

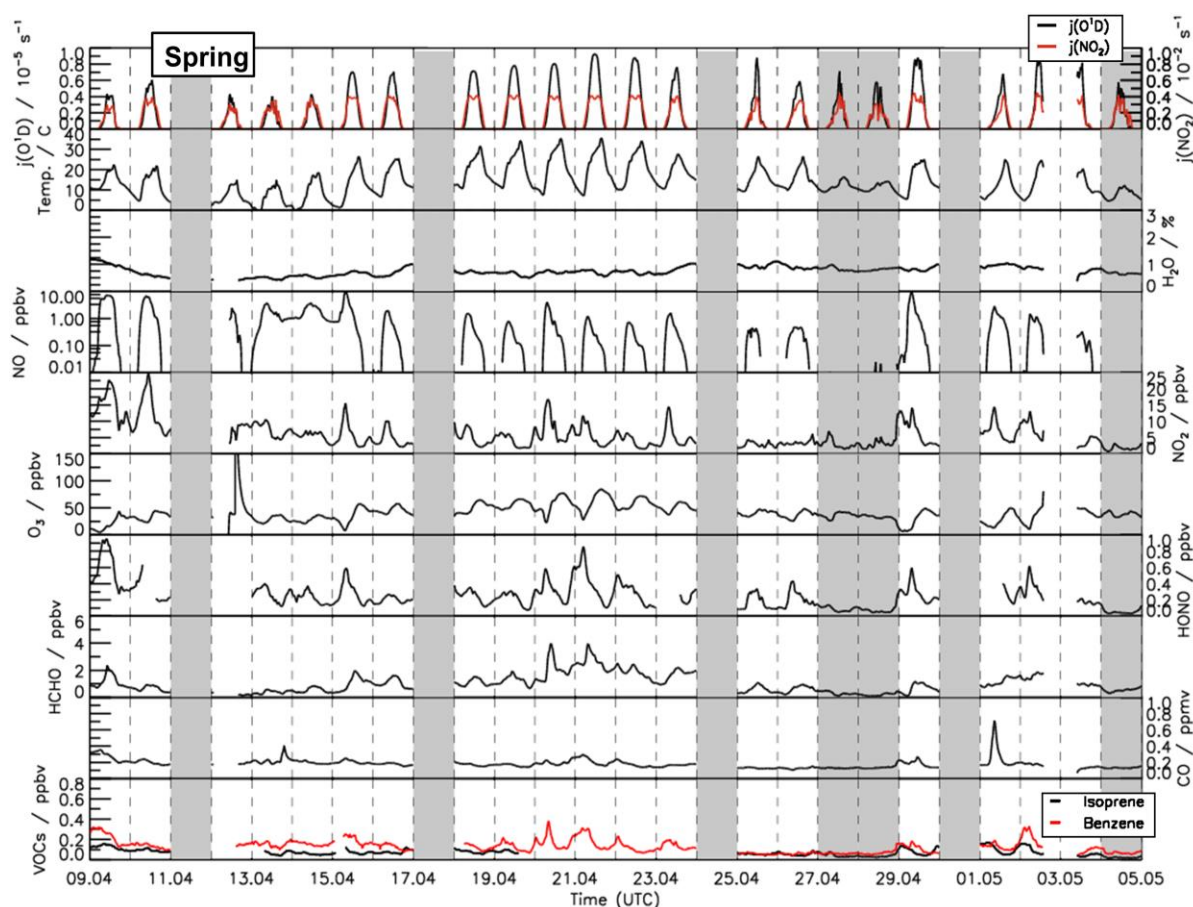


**Figure 1:** Time series of temperature and trace gas concentrations during the spring period of the JULIAC campaign (Cho et al., 2022). Vertical dashed lines denote midnight. Grey shaded areas indicate calibration days, when no measurements were done and days when the chamber roof was closed due to bad weather conditions.

428

### 429 3.2 Meteorological and chemical conditions during the JULIAC campaign

430 A broad range of meteorological and chemical conditions was encountered during the JULIAC campaign.  
 431 During the winter and autumn periods (Fig. S1 and S2), the sky was often overcast and it rained

432 frequently. Temperatures were generally below 10°C and the photolysis frequencies of ozone ( $j_{\text{O}_3}$ ) and  
433 nitrogen dioxide ( $j_{\text{NO}_2}$ ) mostly remained below  $1.5 \times 10^{-6} \text{ s}^{-1}$  and  $2 \times 10^{-3} \text{ s}^{-1}$ , respectively. During  
434 spring and summer, temperatures in the chamber were up to 35°C in mid-April and 40°C between 24 and  
435 31 August (Fig. 1 and 2). Photolysis frequencies in the chamber were  $1 \times 10^{-5} \text{ s}^{-1}$  ( $j_{\text{O}_3}$ ) and  $4 \times 10^{-3} \text{ s}^{-1}$   
436 ( $j_{\text{NO}_2}$ ).

437 The air was sampled at all times from 50 m above ground. The temperature at different heights measured  
438 between 5 m and 120 m at a meteorological tower near the SAPHIR chamber showed that the air was  
439 well mixed within this height range during the day. Therefore, it can be assumed for the chemical  
440 composition of the air sampled into the chamber to be representative for the air within the atmospheric  
441 boundary layer. At night, vertical temperature profiles showed atmospheric stratification below 100 m.  
442 The air at 50 m can be assumed to be isolated from the ground and therefore not being affected by surface  
443 emissions or deposition on surfaces at the ground.

444 Overall, relatively clean air was sampled during the whole JULIAC campaign indicated by CO and NO  
445 mixing ratios below 0.3 ppmv and 2 ppbv, respectively. Concentrations of anthropogenic organic  
446 compounds (e.g. benzene and toluene) were low with mixing ratios of less than 0.5 ppbv. Even though the  
447 measurement site is surrounded by a deciduous forest, the concentrations of biogenic organic compounds  
448 such as isoprene and monoterpenes were also low (median 0.8 ppbv and 0.15 ppbv, respectively)  
449 compared to previously reported values measured on the campus of FZJ in summer, when isoprene  
450 concentrations ranged between 0.5 to 4 ppbv (Komenda et al., 2003; Spirig et al., 2005; Kanaya et al.,  
451 2012). A possible reason for the low values could be damages of trees from severe droughts in the  
452 previous year (BMEL, 2021).

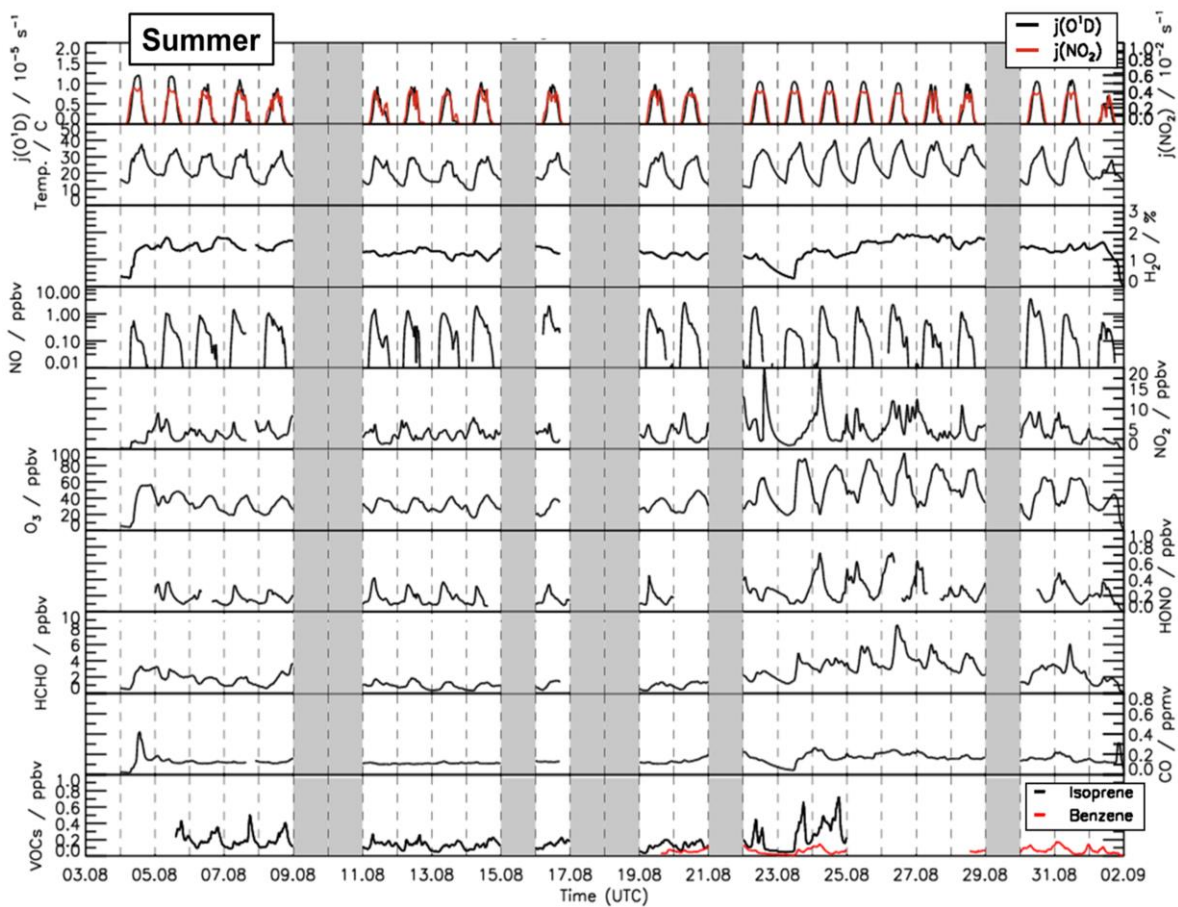


**Figure 2:** Time series of temperature and trace gas concentrations during the summer period of the JULIAC campaign (Cho et al., 2022). Vertical dashed lines denote midnight. Grey shaded areas indicate calibration days, when no measurements were done and days when the chamber roof was closed due to bad weather conditions.



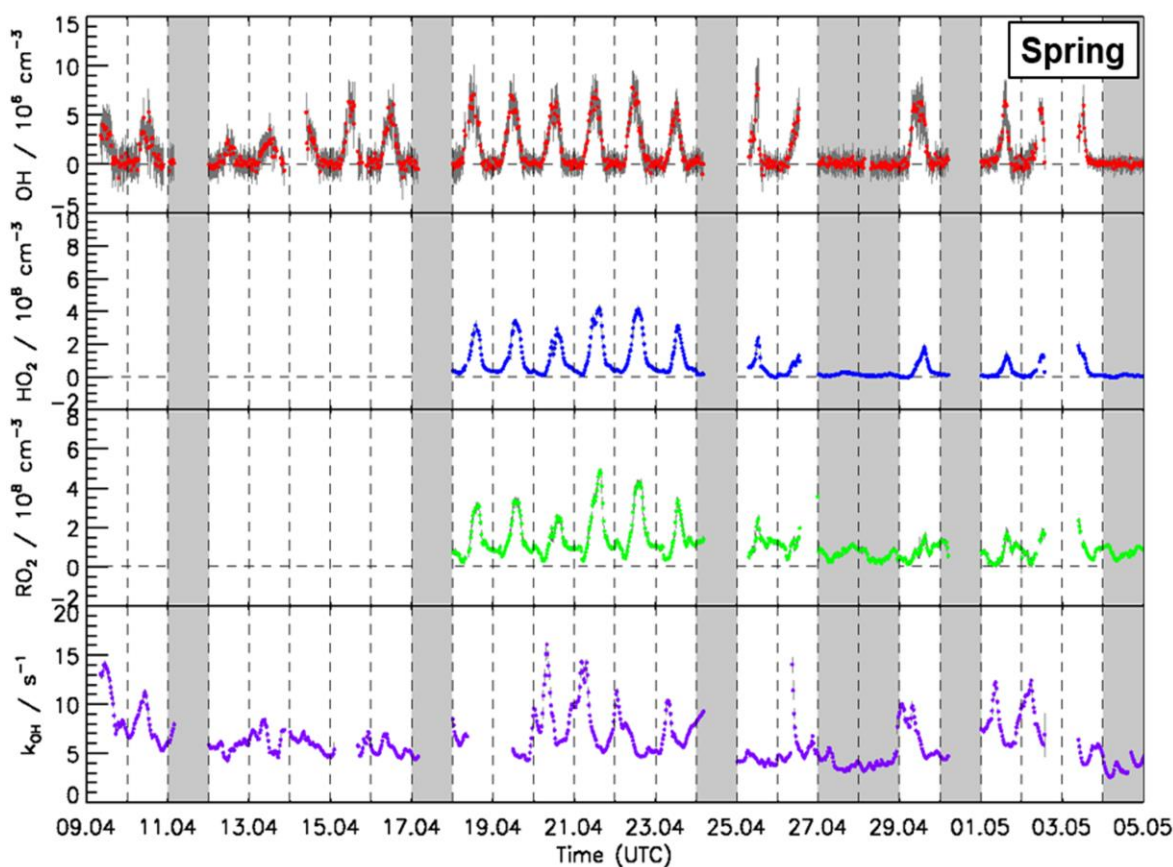


**Figure 3:** Time series of OH, HO<sub>2</sub>, and RO<sub>2</sub> radical concentration measured by the FZJ-LIF-CMR instrument and measurements of the OH reactivity ( $k_{\text{OH}}$ ) measured in the spring period of the JULIAC campaign (Cho et al., 2022). Vertical bars represent  $1\sigma$  statistical errors. Vertical dashed lines denote midnight. Grey shaded areas indicate calibration days when no measurements were done and days when the chamber roof was closed due to bad weather conditions.

### 454 3.3 OH, HO<sub>2</sub>, and RO<sub>2</sub> radical concentrations and OH reactivity during winter and autumn periods 455 of the JULIAC campaign

456 During winter (Fig. S3) and autumn (Fig. S4), daytime OH radical concentrations were below  $1 \times$   
 457  $10^6 \text{ cm}^{-3}$ , mainly due to a low primary radical production. Daytime peroxy radical (HO<sub>2</sub> and RO<sub>2</sub>)  
 458 concentrations during these periods were also very low with average values below  $2 \times 10^7 \text{ cm}^{-3}$  (Fig. S5)  
 459 close to the limit of detection of RO<sub>2</sub> radicals (Table 2) and within the uncertainty of the background  
 460 corrections for HO<sub>2</sub> and RO<sub>2</sub> (Table S1). During winter and autumn, HO<sub>2</sub> concentrations typically  
 461 increased in the morning and reached peak concentrations of  $2 \times 10^7 \text{ cm}^{-3}$  at noon. Concentrations  
 462 decreased in the evening and night with minimum values right before sunrise. In contrast, nighttime RO<sub>2</sub>  
 463 concentrations increased to values between 3 to  $4 \times 10^7 \text{ cm}^{-3}$  after sunset, when the chemical loss due to  
 464 their reaction with NO became negligible, while RO<sub>2</sub> radicals were still produced from reactions of VOC  
 465 with NO<sub>3</sub> and O<sub>3</sub>. NO concentrations were essentially zero at that time, because NO production by the  
 466 photolysis of NO<sub>2</sub> stopped and NO rapidly reacted with ozone. RO<sub>2</sub> radical concentrations decreased in

467 the morning to values that were similar to that of HO<sub>2</sub> radicals as can be expected for conditions with high  
468 NO mixing ratios, which lead to a fast loss of RO<sub>2</sub> and HO<sub>2</sub> in their reactions with NO.

469 The measured OH reactivity ( $k_{OH}$ ) ranged between 4 and 33 s<sup>-1</sup> during winter and autumn periods. The  
470 highest value was observed on 21 January, when a highly polluted plume containing 50 ppbv of NO was  
471 sampled.

472 The measured OH reactivity can be compared to OH reactivity calculated by summing up the product  
473 between measured OH reactant concentrations and their reaction rate constants with the OH radical. On  
474 average, 1.3 s<sup>-1</sup> (18 %) of the measured OH reactivity could not be explained by the measured OH  
475 reactants during the winter and autumn periods (Fig. S5). NO<sub>x</sub>, CH<sub>4</sub>, CO, and VOCs contributed  
476 approximately 43, 3, 20 and 13 %, respectively, to the measured OH reactivity.

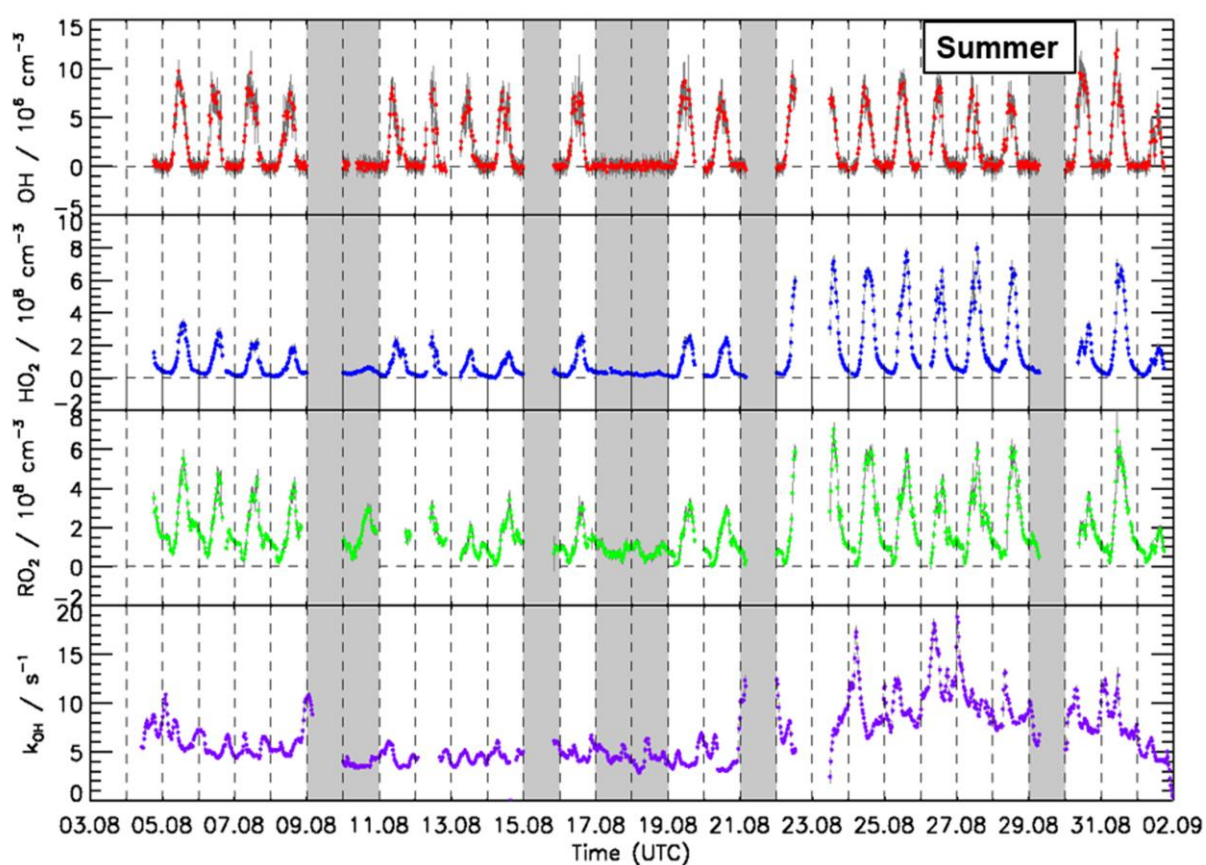


**Figure 4:** Time series of OH, HO<sub>2</sub>, and RO<sub>2</sub> concentration measured by the FZJ-LIF-CMR instrument and measurements of the OH reactivity ( $k_{OH}$ ) in the summer period of the JULIAC campaign (Cho et al., 2022). Vertical bars represent 1 $\sigma$  statistical errors. Vertical dashed lines denote midnight. Grey shaded areas indicate calibration days when no measurements were done and days when the chamber roof was closed due to bad weather conditions.

477

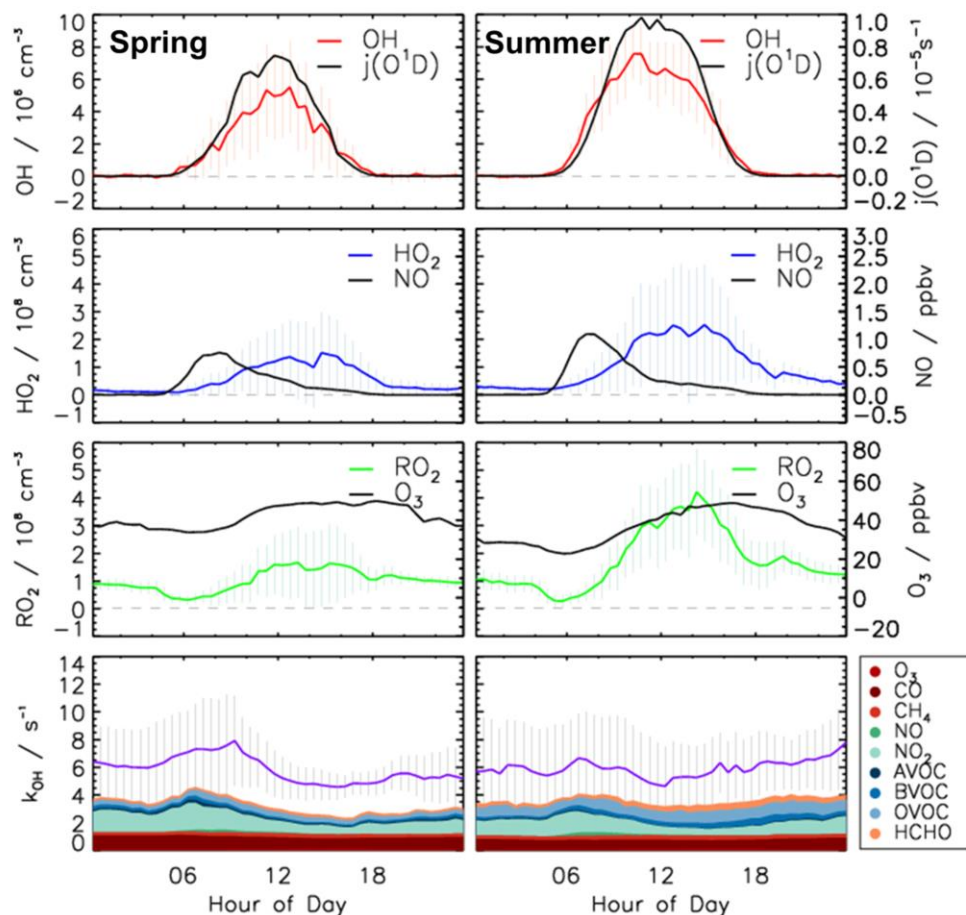


**Figure 5:** Median values of the diurnal profiles of OH, HO<sub>2</sub>, RO<sub>2</sub>, k<sub>OH</sub>, j<sub>OH</sub>, NO and O<sub>3</sub> measured in the spring and summer periods of the JULIAC campaign. Colored areas represent the contributions of measured reactants to the total OH reactivity. Vertical lines give 25<sup>th</sup> and 75<sup>th</sup> percentile values.

478

### 479 3.4 OH, HO<sub>2</sub>, and RO<sub>2</sub> radical concentrations and OH reactivity during the spring and summer 480 periods of the JULIAC campaign

481 During spring and summer (Fig. 3, 4 and 5), maximum daytime OH concentrations were between 6 and 8  
482  $\times 10^6 \text{ cm}^{-3}$ . The highest OH concentration ( $1.2 \times 10^7 \text{ cm}^{-3}$ ) occurred on 31 August. The diurnal OH  
483 concentration profile shows a high correlation with the ozone photolysis frequency ( $j_{O^1D}$ ) as observed in  
484 previous field campaigns (e.g., Ehhalt and Rohrer (2000); Handisides et al. (2003); Holland et al. (2003)).

485 Unfortunately, the measurements of HO<sub>2</sub> and RO<sub>2</sub> radicals were not available for the first two weeks of  
486 the spring campaign due to a malfunction of the instrument. Daily maximum HO<sub>2</sub> and RO<sub>2</sub> concentrations  
487 were in the range of 2 to 4  $\times 10^8 \text{ cm}^{-3}$  during the spring period and the first half of the summer period.  
488 Maximum HO<sub>2</sub> and RO<sub>2</sub> concentrations were  $8.0 \times 10^8 \text{ cm}^{-3}$  and  $7.0 \times 10^8 \text{ cm}^{-3}$ , respectively, during  
489 the second half of summer period. In spring and summer, peroxy radical concentrations showed a distinct  
490 diurnal pattern. Both HO<sub>2</sub> and RO<sub>2</sub> radical concentrations were suppressed in the early morning (between  
491 04:00 and 07:00) due to the reaction with elevated NO mixing ratios of up to 1.5 ppbv. Maximum peroxy

492 radical concentrations were usually reached in the afternoon (~14:00), when NO concentrations were  
493 lowest.

494 The measured OH reactivity values were in the range of 4 to 18 s<sup>-1</sup>. High values were observed between  
495 23 and 31 August due to high emissions of biogenic volatile organic compounds (BVOCs) from plants at  
496 high ambient temperatures. The OH reactivity that cannot be attributed to the measured OH reactants was  
497 on average, 2.5 s<sup>-1</sup> (40%), which is much higher than observed in the winter and autumn periods (Fig. S5).  
498 CO and CH<sub>4</sub> contributed 10% and 4%, respectively. Due to the high emissions of biogenic organic  
499 compounds in spring and summer, the attributed contribution of organic compounds to the total measured  
500 OH reactivity was 20 % and the contribution of NO<sub>x</sub> was only 19 %, much less compared to the winter  
501 and autumn periods. Isoprene had the largest contribution among all VOCs accounting for up to 5 % of  
502 the total measured OH reactivity. Unfortunately, the number of detected VOC species in the JULIAC  
503 campaign was small (Table S2).

504 In the JULIAC campaign, nighttime OH concentrations were clearly below the limit of detection of the

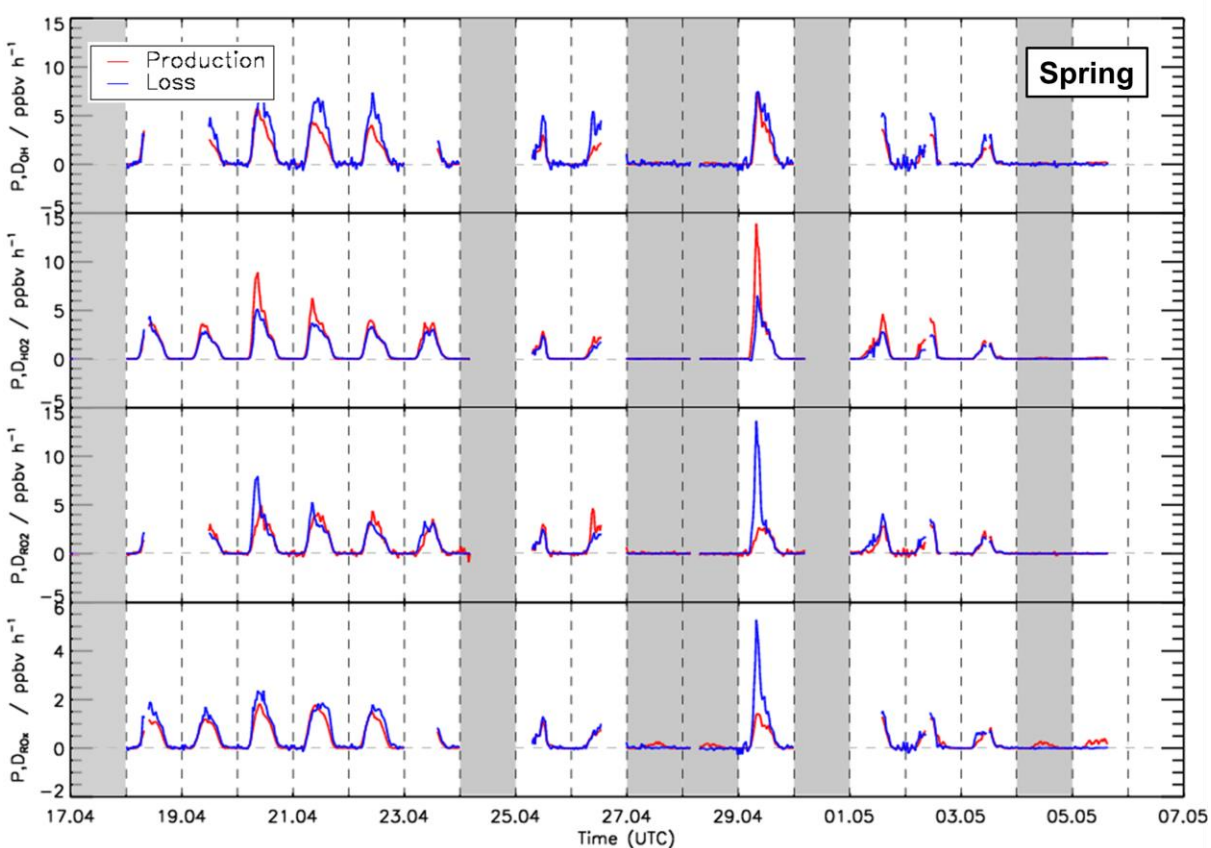


**Figure 6:** Time series of total production and destruction rates of OH, HO<sub>2</sub>, RO<sub>2</sub>, and RO<sub>x</sub> radicals in the spring period of the JULIAC campaign. Vertical dashed lines denote midnight. Grey areas indicate calibration days and days when the chamber roof was closed.

505 FZJ-CMR-LIF instrument ( $0.7 \times 10^6 \text{ cm}^{-3}$ ). When all nighttime data are averaged, mean OH  
506 concentrations with  $1\sigma$  standard errors of  $(3 \pm 1) \times 10^4 \text{ cm}^{-3}$  and  $(5 \pm 3) \times 10^4 \text{ cm}^{-3}$  are obtained for  
507 the spring and summer periods, respectively. These low values support the absence of instrumentally

508 produced OH and indicate a very low nocturnal OH production at 50 m height in the absence of NO and  
 509 solar UV.

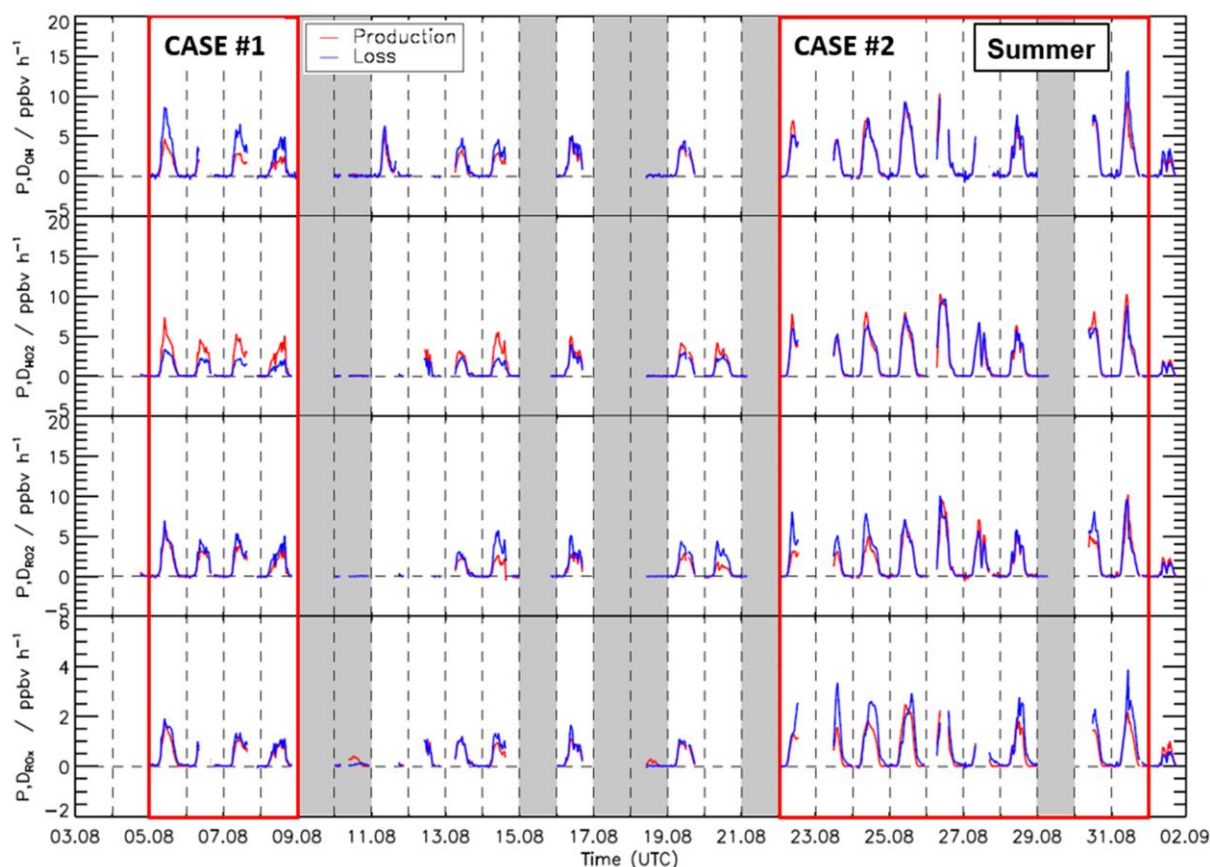


**Figure 7:** Time series of total production and destruction rates of OH, HO<sub>2</sub>, RO<sub>2</sub>, and RO<sub>x</sub> radicals in the summer period of the JULIAC campaign. Vertical dashed lines denote midnight. Grey areas indicate calibration days and days when the chamber roof was closed. The red boxes denote periods that are discussed in more detail (Case 1 and Case 2).

### 510 3.5 Chemical budgets of OH, HO<sub>2</sub>, RO<sub>2</sub> and RO<sub>x</sub> radicals in the spring and summer periods

511 Due to the very low photochemical activity observed in autumn and winter, which resulted in radical  
 512 concentrations close to the detection limit of the instrument, the chemical budget analysis is only  
 513 discussed for data from the spring and summer periods. It focuses on daytime conditions.

514 Time series of turnover rates of reactions involving OH, HO<sub>2</sub>, RO<sub>2</sub> and RO<sub>x</sub> radicals in the spring and  
 515 summer periods are presented in Fig. 6 and 7, respectively, and median diurnal profiles in Fig. 8. Typical  
 516 daytime turnover rates of OH, HO<sub>2</sub> and RO<sub>2</sub> radicals were between 3 ppbv h<sup>-1</sup> and 10 ppbv h<sup>-1</sup>. The rates  
 517 of RO<sub>x</sub> production and destruction ranged from 1 ppbv hr<sup>-1</sup> to 3 ppbv hr<sup>-1</sup>, which is 2 to 4 times lower  
 518 than those of OH, HO<sub>2</sub>, and RO<sub>2</sub>, because radical conversion reactions cancel out. The highest OH  
 519 turnover rate of 13 ppbv h<sup>-1</sup> was observed on 31 August, when the air temperature in the chamber reached  
 520 up to 40°C. Unusually high turnover rates for HO<sub>2</sub>, RO<sub>2</sub>, and RO<sub>x</sub> radicals occurred on 29 April with

521 values of 14 ppbv h<sup>-1</sup>, 15 ppbv h<sup>-1</sup>, and 4 ppbv h<sup>-1</sup>, respectively, when the NO mixing ratio exceeded 9  
522 ppbv. For the reasons stated in Section 3.1, the HO<sub>2</sub> and RO<sub>2</sub> data on this date are considered highly  
523 uncertain and were excluded from further analysis of the chemical budgets.

524 Diurnal variations of total radical production and destruction rates, as well as of the contributions of the  
525 most important reactions, are shown as median values for the entire spring and summer period in Fig. 8.  
526 For OH, the reaction of HO<sub>2</sub> with NO (Reaction R10) was the dominant production pathway contributing  
527 more than 70 % to the total production rate in both spring and summer periods. The photolysis of HONO  
528 (Reaction R1) was the most important primary OH source during daytime contributing approximately 20 %  
529 to the total OH production. The reaction of HO<sub>2</sub> with ozone (Reaction R11), the photolysis of ozone  
530 (Reaction R2), and the ozonolysis of alkenes (Reaction R5) contributed less than 3 % to the total OH  
531 production. The maximum median total OH production rate of 3.5 ppbv hr<sup>-1</sup> was observed in the morning  
532 shortly after the peak NO concentration in both spring and summer (Fig. 5). Values gradually decreased  
533 until sunset. Median total OH destruction rates were higher than production rates and reached up to 5  
534 ppbv hr<sup>-1</sup> and 6 ppbv hr<sup>-1</sup> at noon in spring and summer, respectively. The contributions of different  
535 reactions to the total OH destruction rate is described by the contribution of OH reactants to the OH  
536 reactivity (Section 3.4, Fig. 5).

537 Short-lived radicals are expected to be in a steady state, and therefore radical production and destruction  
538 rates must be balanced. An imbalance between the calculated rates indicates inaccurate data or a missing  
539 radical production or destruction process. The daily peak of the OH production rates was typically lower  
540 than the destruction rate by approximately 1.8 ppbv h<sup>-1</sup> in the spring and 2.5 ppbv h<sup>-1</sup> in the summer period  
541 (36 and 43 % of the total OH destruction rate). These discrepancies are higher than the uncertainty of the  
542 calculation (Fig. 8).

543 80% of the HO<sub>2</sub> production rate consisted of the reaction of RO<sub>2</sub> with NO (Reaction R9). The remaining  
544 part of the HO<sub>2</sub> production rate was due to the photolysis of formaldehyde (9 %) and the reaction of  
545 formaldehyde with OH (10 %). Other reactions producing HO<sub>2</sub> played a minor role (< 1 %). The HO<sub>2</sub>  
546 destruction was mostly due to the reaction of HO<sub>2</sub> with NO (Reaction R10) contributing on average 88 %  
547 to the total production rate. The loss due to reaction of HO<sub>2</sub> with RO<sub>2</sub> radicals (Reaction R16) contributed  
548 on average 9 % to the total loss.

549 Median values of the total HO<sub>2</sub> destruction and production rates were well balanced in the spring period,  
550 with the production rate being slightly higher than the destruction rate. The maximum difference of 1  
551 ppbv hr<sup>-1</sup>, however, was insignificant compared to the uncertainty of the calculation. A similar tendency  
552 but more pronounced feature was observed in summer. Here, the median value of production rate was  
553 higher than that of the destruction rate by 1.8 ppbv hr<sup>-1</sup> (38 % of the total HO<sub>2</sub> production rate) but  
554 differences were variable (Fig. 7). This aspect is discussed in more detail for two periods (Sections 3.7  
555 and 3.8), which exhibited different degrees of imbalances in the radical budgets.

556 The  $\text{RO}_2$  production rate was dominated by the reaction of VOCs with OH (Reaction R8). The  
 557 contributions of ozonolysis of measured alkenes to the  $\text{RO}_2$  production were very small (less than 1 %).  
 558 The reaction of  $\text{RO}_2$  with NO (Reaction R9) dominated the  $\text{RO}_2$  destruction and contributed more than 90 %  
 559 to the total loss rate. In the late afternoon, the  $\text{RO}_2$  termination reaction with  $\text{HO}_2$  gained in importance

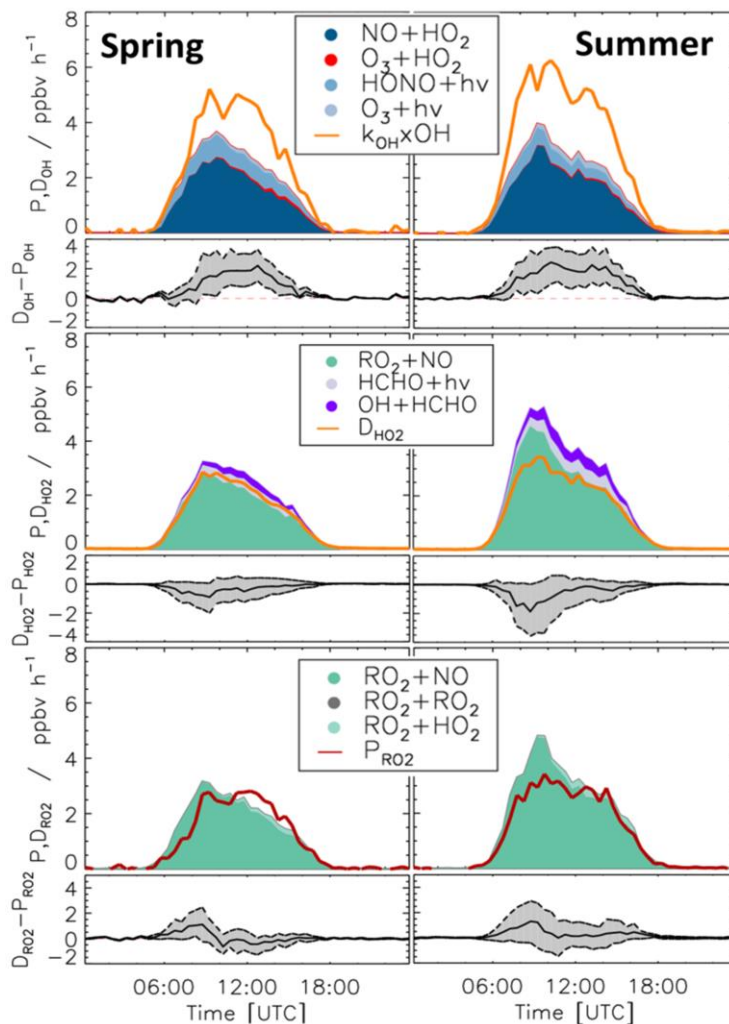


**Figure 8:** Median values of production and destruction rates of OH,  $\text{HO}_2$ , and  $\text{RO}_2$  radicals in the spring and summer periods of the JULIAC campaign, with data from 29 April excluded. In addition, the differences between the destruction and production rates are shown. Grey areas indicate the  $1\sigma$  uncertainty derived from experimental errors of the measured quantities (Table 2) and of the reaction rate constants (Table 1). The reactions that have insignificant contributions to the production or destruction rates are not shown.

560 with contributions of up to 10 %. Although slight imbalances of up to 1 ppbv were observed in the early  
 561 morning, the  $\text{RO}_2$  production and destruction rates were generally balanced within the uncertainty of  
 562 calculations in both spring and summer.

563 Figure 9 shows the calculated RO<sub>x</sub> production and destruction rates. The photolysis of HONO (Reaction  
 564 R1), HCHO (Reaction R3) and O<sub>3</sub> (Reaction R2) were the dominant processes initiating radical chemistry  
 565 and contributed to the total RO<sub>x</sub> production rate on average 45 %, 38 % and 15 %, respectively, in both  
 566 periods. In the morning, the reaction of OH with NO<sub>2</sub> (Reaction R12) was the most important radical  
 567 termination process contributing up to 65 % to the total RO<sub>x</sub> destruction rate. In addition, due to relatively  
 568 high NO mixing ratios in the early morning, the reactions of OH with NO (Reaction R13) and RO<sub>2</sub> with  
 569 NO, which yields organic nitrate (Reaction R14), were also significant radical termination processes  
 570 contributing 13 % and 17 % to the total RO<sub>x</sub> destruction rate, respectively. In the afternoon, radical self-  
 571 reactions (Reaction R15 – R17), and, in particular, the reaction of RO<sub>2</sub> with HO<sub>2</sub> (Reaction R16),  
 572 dominated the RO<sub>x</sub> destruction due to the low NO and NO<sub>2</sub> mixing ratios. In both periods, spring and  
 573 summer, the total RO<sub>x</sub> destruction rate was slightly higher than the production rate, in particular, in the  
 574 afternoon. The imbalance was up to 0.5 ppbv h<sup>-1</sup>, which is higher than the uncertainty of the calculations.

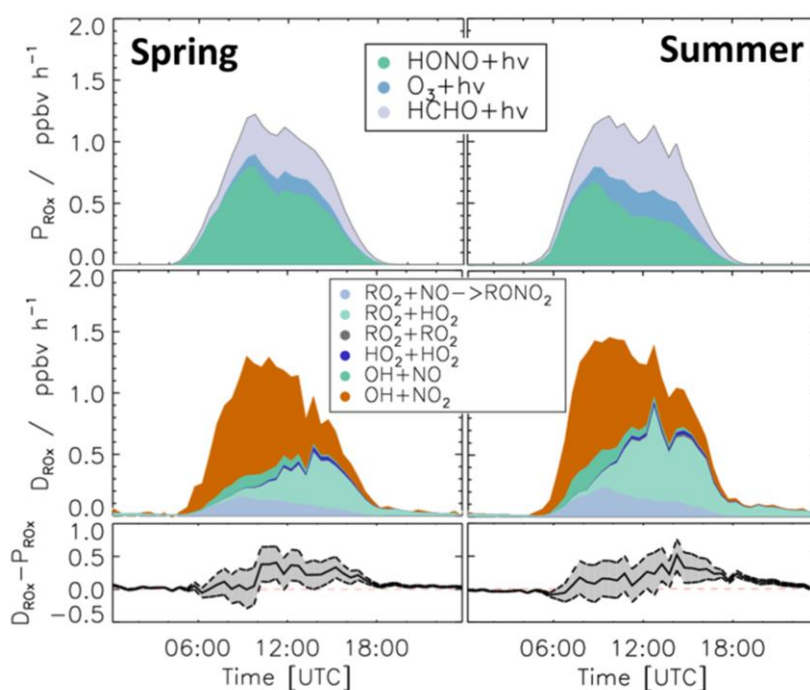


**Figure 9:** Median values of production and destruction rates of RO<sub>x</sub> radicals during the spring and summer periods of the JULIAC campaign. In addition, the differences between the destruction and production rates are shown. Grey areas indicate the 1 $\sigma$  uncertainty derived from experimental errors of the measured quantities (Table 2) and of the reaction rate constants (Table 1). The reactions that have insignificant contributions to the production or destruction rates are not shown.

575 Meteorological and chemical conditions were variable especially in the summer period causing variations  
 576 in the balance between radical production and destruction rates (Fig. 7 and Table S3). In the following,  
 577 the chemical budgets with the largest and smallest observed imbalances are discussed: August 5-8 (Case 1)  
 578 and August 22-31 (Case 2).

### 579 3.5.1 Case 1: 5 - 8 August 2019



580 For the period between 5 and 8 August, relatively low NO mixing ratios (maximum: 1 ppbv, median: 0.26  
581 ppbv) and typical summer temperature for this region (median: 27°C) were observed (Fig. 10 and Table  
582 S3).

583 As for the whole summer period (Fig. 8), the reactions of peroxy radicals with NO (Reaction R9, R10)  
584 dominated the inter-radical conversion reactions of OH, HO<sub>2</sub> and RO<sub>2</sub> in this period (Fig. 10). A  
585 significant imbalance between the OH production and destruction rates of up to 3.0 ppbv h<sup>-1</sup> (51 % of the  
586 total OH destruction rate) is found, which cannot be explained by the uncertainty of the calculations. The  
587 total HO<sub>2</sub> production rate was 2.0 ppbv h<sup>-1</sup> higher than the destruction rate (48 % of the total HO<sub>2</sub>  
588 production rate), whilst the RO<sub>2</sub> production and destruction rates were well balanced. Relatively small but  
589 nevertheless significant differences between RO<sub>x</sub> production and destruction rates (0.5 ppbv h<sup>-1</sup>) were  
590 observed during daytime (Fig. 11).

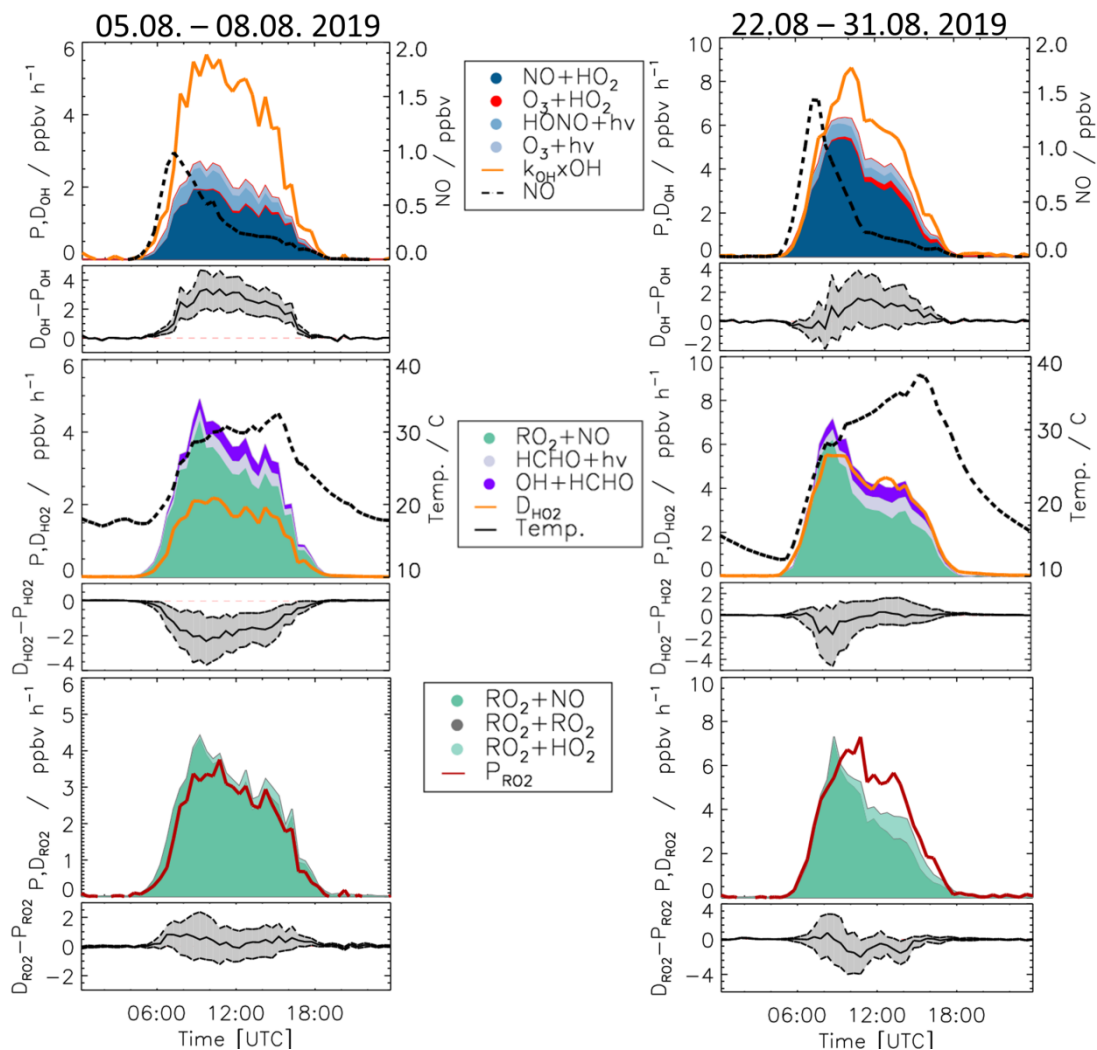


**Figure 10:** Production and destruction rates of OH, HO<sub>2</sub>, and RO<sub>2</sub> radicals for Case 1 (05.08. - 08.08. 2019) and Case 2 (22.08 - 31.08. 2019). In addition, the differences between the destruction and production rates are shown. Grey areas give the 1 $\sigma$  uncertainty derived from experimental errors of the measured quantities (Table 2) and of the reaction rate constants (Table 1). The reactions that have insignificant contributions to the production or destruction rates are not shown.

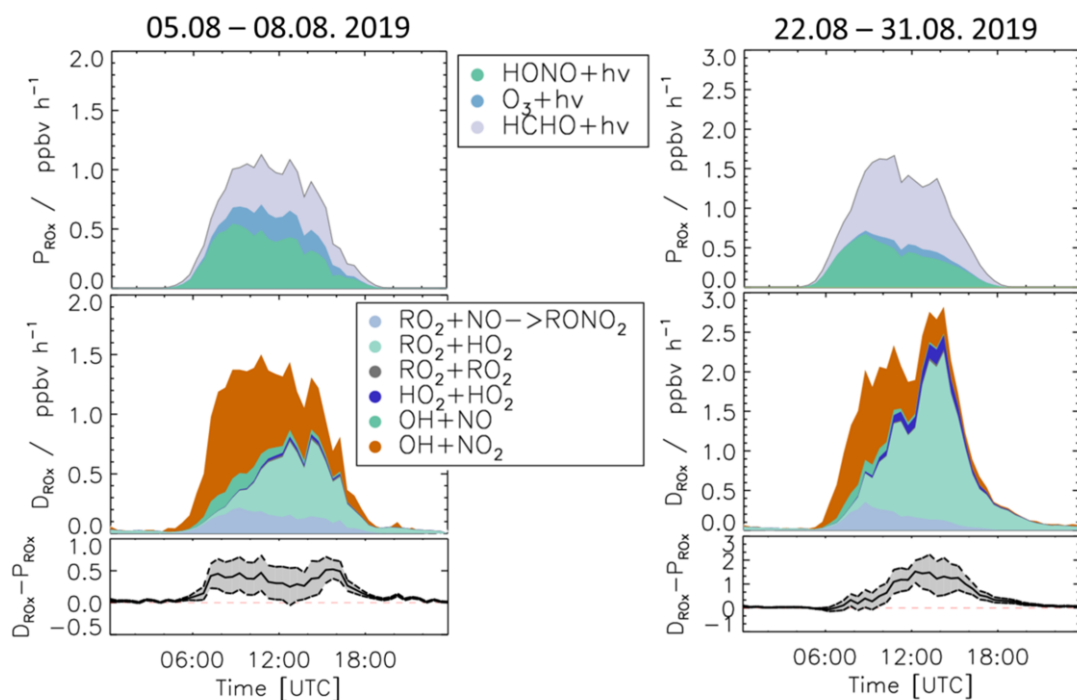


**Figure 11:** Production and destruction rates of  $\text{RO}_x$  for the periods of the case studies (Case 1 and Case 2). In addition, the differences between the destruction and production rates are shown. Grey areas indicate the  $1\sigma$  uncertainty derived from experimental errors of the measured quantities (Table 2) and of the reaction rate constants (Table 1). The reactions that have insignificant contributions to the production or destruction rates are not shown.

### 592 3.5.2 Case 2: 22 - 31 August 2019

593 During the period from 22 to 31 August, the temperature was generally high and reached a maximum  
 594 value of  $42^\circ\text{C}$  inside the chamber. The concentrations of radical precursors, HONO, HCHO and  $\text{O}_3$ , were  
 595 higher than those observed in Case 1 (Table S3). Ozone mixing ratios reached values up to 100 ppbv,  
 596 while daytime NO mixing ratios were similar as in Case 1 ( $<1.5$  ppbv, median value of 0.22 ppbv). The  
 597 conditions outside the chamber were characterized by stagnant air (wind speed  $< 4$  m/s at 50 m height)  
 598 with no precipitation. At these conditions, vigorous biogenic emissions can be expected (Vilà-Guerau de  
 599 Arellano et al., 2009; Sarkar et al., 2020). Enhanced biogenic VOC emissions and their photochemical  
 600 degradation can therefore explain the higher VOC and HCHO concentrations in Case 2 compared to the  
 601 cooler period beginning of the month (Table S3). The larger VOC reactivity and comparable OH  
 602 concentrations resulted in  $\text{HO}_2$  and  $\text{RO}_2$  concentrations that were approximately 2 to 3 times higher than  
 603 in Case 1 (Table S3).

604 Imbalances between the radical production and destruction rates were a factor of 2 smaller in the warmer  
 605 and more photochemically active period of Case 2 compared to Case 1. OH destruction rates were up to  
 606  $1.5$  ppbv  $\text{h}^{-1}$  (25 % of the total OH destruction rate) higher than the total production rate (Fig. 10). The  
 607  $\text{HO}_2$  production and destruction rates agree within  $\pm 1$  ppbv  $\text{h}^{-1}$ . The contributions from photolysis of

608 HCHO and the reaction of HCHO with OH to the HO<sub>2</sub> production rate were larger compared to other  
609 periods with values of up to 15% and 13%, respectively, due to high HCHO mixing ratios of up to 8 ppbv  
610 (Fig. 2). The RO<sub>2</sub> production and destruction rates showed imbalances by up to 1.5 ppbv h<sup>-1</sup> in the late  
611 afternoon.

612 While HONO photolysis was the dominating RO<sub>x</sub> source during most of the time in spring and summer  
613 (Fig. 9), HO<sub>2</sub> production from the photolysis of HCHO was the most important primary radical source in  
614 Case 2 due to the high concentration of HCHO (Fig. 11). Although the chemical budgets for each radical  
615 species were essentially closed within the experimental uncertainty, the total loss rate of RO<sub>x</sub> was  
616 consistently higher than the production rate during daytime. The deviation was higher than the  
617 experimental uncertainty and reached a maximum value of 1.4 ppbv h<sup>-1</sup> at noontime.

### 618 **3.5.3 NO dependence of radical production and destruction rates**

619 One of the most influential parameters for the radical chemistry is the concentration of NO, since the  
620 reaction with NO dominates the conversion rate of RO<sub>2</sub> to HO<sub>2</sub> (Reaction R10) and HO<sub>2</sub> to OH (Reaction  
621 R9) (Fig. 10). Figure 12 shows the NO dependence of median values of the calculated production and  
622 destruction rates for the different radicals for the spring and summer period.

623 For OH, the production rates are consistently lower than the destruction rates by about 1.5 ppbv h<sup>-1</sup> for  
624 NO mixing ratios lower than 1 ppbv NO. At higher NO, the OH budget is balanced within the  
625 experimental uncertainty. For HO<sub>2</sub>, an inverse pattern is observed. Below 1 ppbv NO, the production rate  
626 is higher than the destruction rate by about 1 ppbv h<sup>-1</sup>. Only for lowest NO mixing ratios, the production  
627 and destruction rates are balanced. For NO mixing ratios above 1 ppbv, the chemical budget of HO<sub>2</sub> is  
628 essentially closed. For NO mixing ratios of 3.5 ppbv, the difference between production and destruction  
629 rate is noticeably high with 4 ppbv h<sup>-1</sup> but has also a large uncertainty. For RO<sub>2</sub> radicals, the chemical  
630 budget is closed for NO mixing ratios below 1 ppbv but an increasing discrepancy between the loss and  
631 production rates is observed with increasing NO mixing ratios. While the production rate is relatively  
632 constant with a value of 2.5 ppbv h<sup>-1</sup>, the loss rate increases to values of up to 7.5 ppbv h<sup>-1</sup> at 3.5 ppbv NO.  
633 The budget of RO<sub>x</sub>, in which radical inter-conversion reactions cancel out, is mostly balanced over the  
634 whole range of NO. Only for lowest and highest NO mixing ratios the destruction rate is 0.6 ppbv h<sup>-1</sup>  
635 higher than the production rate.

636

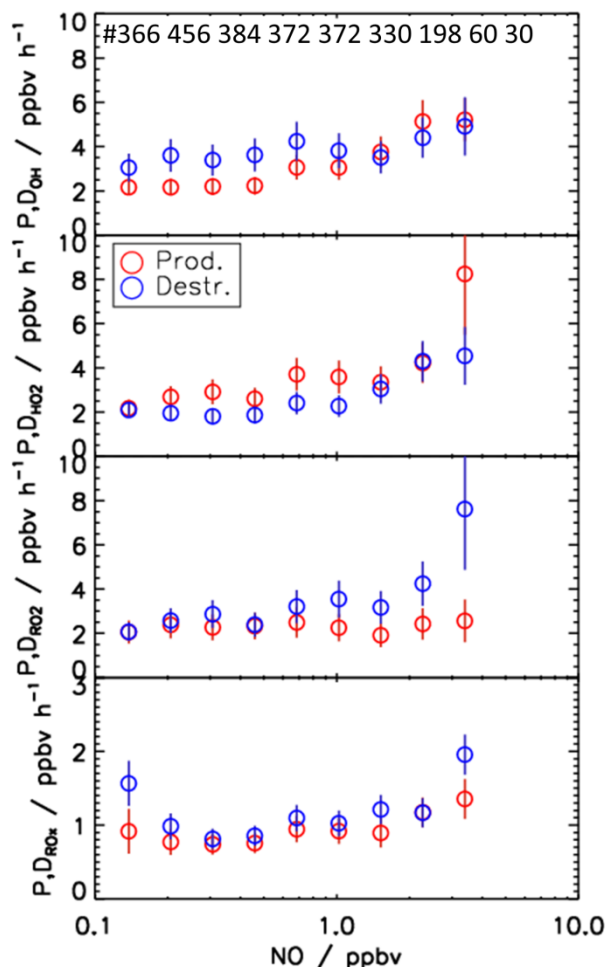


**Figure 12:** NO dependence of median production and destruction rates of OH, HO<sub>2</sub>, RO<sub>2</sub>, and RO<sub>x</sub> radicals. Median values include all data from the spring and summer periods of the JULIAC campaign (NO intervals: ln(NO) = 0.4 ppbv). Vertical bars represent the 1σ uncertainty from experimental errors of the measured quantities (Table 2) and of the reaction rate constants (Table 1). The number of data points in each NO bin is represented on the top panel.

637

## 638 4 Discussion

### 639 4.1 Discrepancies in the chemical budgets of radicals

640 The highest imbalances in the chemical budgets of radicals are found for OH radicals. In spring and  
 641 summer, their production rate was consistently lower than the loss rate (Fig. 8). This deficit was largest  
 642 beginning of August (Case 1, Fig. 10) when the discrepancy reached  $(3.0 \pm 1)$  ppbv h<sup>-1</sup>.

643 Imbalances in the radical budgets can be observed for different reasons. They can be caused by missing  
 644 processes or incorrect rate constants in the calculations of the production or destruction rates (Section 4.2).  
 645 It is also possible that measured concentrations that are used for the calculation contain unknown errors.

646 The technically difficult radical measurements have a large potential for artefacts (Hofzumahaus and  
647 Heard, 2016). Precautions were taken to minimize measurement interferences for OH and HO<sub>2</sub> in this  
648 campaign:

- 649 • The measurements of OH by the LIF instrument were interference-corrected using chemical  
650 modulation and agreed with simultaneous OH measurements by the DOAS instrument within the  
651 experimental uncertainties. The measured OH reactivity quantifies the total chemical loss rate of  
652 OH caused by atmospheric reactants and has a total accuracy of 10%. Thus, the destruction rate  
653 of OH, which is the product of the concentration and reactivity of OH, is known within 20 % and  
654 is unlikely biased by unknown OH interferences or unknown atmospheric reactants.
- 655 • The O<sub>x</sub> production rate calculated from the reaction of peroxy radicals with NO agrees with the  
656 measured increase of O<sub>x</sub> concentrations within ±1 ppbv h<sup>-1</sup> for most conditions (Section 3.1). As  
657 more than 70 % of the OH production is due to the reaction of HO<sub>2</sub> with NO (Reaction R10), a  
658 bias of more than 1 ppbv h<sup>-1</sup> due to an unaccounted HO<sub>2</sub> measurement error seems unlikely.
- 659 • The analysis of the chemical budget of OH in previous chamber experiments performed at  
660 various chemical conditions showed no evidence for a missing OH source originating from  
661 chamber wall effects (Kaminski et al., 2017; Fuchs et al., 2018; Novelli et al., 2018; Rolletter et  
662 al., 2019; Rolletter et al., 2020).

663 Thus, there is no evidence for instrumental errors that are not included in the estimated errors of the  
664 calculated turnover rates. The observed imbalances in the OH budget of up to 3 ppbv h<sup>-1</sup> are therefore  
665 most likely due to a missing OH source.

666 The missing OH production is correlated with the imbalance in the HO<sub>2</sub> budget, for which the production  
667 rate is larger than the loss rate at low NO mixing ratios (Fig. 12). This is most clearly seen in the period of  
668 Case 1, when the discrepancy reaches (2.0±1) ppbv h<sup>-1</sup> (Fig. 10). The production rate of HO<sub>2</sub> is nearly  
669 equal to the RO<sub>2</sub> loss rate (P<sub>HO<sub>2</sub></sub> ≈ D<sub>RO<sub>2</sub></sub>) because both are controlled by the reaction of RO<sub>2</sub> with NO  
670 (Reaction R9). Furthermore, the RO<sub>2</sub> loss rate is well balanced by the RO<sub>2</sub> production rate within the  
671 experimental uncertainty of ±1 ppbv h<sup>-1</sup> (Fig. 8 and 10). Thus, there is no hint that the calculated turnover  
672 rate of the RO<sub>2</sub> + NO reaction had a bias higher than 1 ppbv h<sup>-1</sup>. In addition, turnover rates of the  
673 reactions of HO<sub>2</sub> and RO<sub>2</sub> with NO producing ozone are consistent with the observed O<sub>x</sub> increase in the  
674 chamber (Section 3.1). This suggests that these rates are correct in the chemical budget analysis. For the  
675 above reasons, the discrepancy between HO<sub>2</sub> production and destruction rates is most likely due to a  
676 missing HO<sub>2</sub> loss process and not by measurement errors of HO<sub>2</sub>, RO<sub>2</sub> or NO.

677 RO<sub>x</sub> destruction rates are generally higher than the production rates but differences are on average lower  
678 than 0.5 ppbv h<sup>-1</sup> (Fig. 9). In the periods of Case 1 and Case 2, the corresponding discrepancies reach 0.5  
679 ppbv h<sup>-1</sup> and 1.4 ppbv h<sup>-1</sup>, respectively (Fig. 10). If these discrepancies were due to a missing primary OH  
680 source, they could also explain a small part (17 %) of the imbalance in the chemical OH budget in Case 1,  
681 and the complete imbalance in the OH budget in Case 2.

682 It is difficult to identify the exact cause for the differences in OH and HO<sub>2</sub> budgets observed for Case 1  
683 and 2 only with the available data. Case 2 was characterized by high temperature with increased BVOC  
684 emissions and high levels of HCHO (Table S3). No clear correlation was found between the ratio of the  
685 production and destruction rates of the radicals and the concentration of chemical species such as NO,  
686 NO<sub>2</sub>, O<sub>3</sub>, HCHO, etc. A weak correlation was observed with temperature with an improved balance in the

687 budgets the higher the temperature was. This could indicate that the unaccounted processes become less  
688 competitive for high radical turnover rates with chemical conditions being dominated by organic  
689 compounds from biogenic emissions.

690 In conclusion, the radical budget analysis suggests the presence of a missing OH source and a missing  
691 HO<sub>2</sub> loss process with a similar turnover rate at NO mixing ratios below 1 ppbv for typical temperatures  
692 in summer. The opposing imbalances in the OH and HO<sub>2</sub> budgets could be due to an unknown  
693 mechanism that converts HO<sub>2</sub> to OH, or they could indicate a missing primary OH source and a similar  
694 fast, but independent termination reaction removing HO<sub>2</sub>. The remaining imbalance in the RO<sub>x</sub> budget  
695 would be consistent with an unaccounted primary OH source. This fits best the observations in Case 2  
696 characterized by high temperatures and VOC emissions.

697 For NO mixing ratios that are higher than 1 ppbv, production and destruction rates of OH and HO<sub>2</sub>  
698 radicals are generally balanced (Fig. 12). An exception is observed for HO<sub>2</sub> for highest NO mixing ratios  
699 of 3.5 ppbv, for which the production rate is 3.5 ppbv h<sup>-1</sup> higher than the loss rate.

700 For RO<sub>2</sub>, the radical budget is not closed, but the loss rate increases with NO in contrast to the production  
701 rate. The difference reaches a value of 5 ppbv h<sup>-1</sup> at 3.5 ppbv NO. In the same range of NO mixing ratios,  
702 the odd oxygen production rate ( $P_{O_x}$ ) calculated by peroxy radicals (Eq. 14) overestimates the observed  
703 increase in the O<sub>x</sub> mixing ratio by about 3 ppbv h<sup>-1</sup>. This difference points to a systematic error in the  
704 peroxy radical measurements explaining a considerable part of the imbalance in the RO<sub>2</sub> budget. A  
705 reduction of the RO<sub>2</sub> concentration by  $3 \times 10^7$  cm<sup>-3</sup> would reduce the HO<sub>2</sub> production rate by 3 ppbv h<sup>-1</sup>  
706 and resolve the discrepancy in the odd oxygen production calculations for the highest NO mixing ratio.  
707 The presumed bias in the RO<sub>2</sub> measurement may be caused by an incorrect background subtraction that  
708 becomes most relevant at high NO concentrations (Section 3.1). However, even after correction of this  
709 bias a discrepancy in the RO<sub>2</sub> budget would remain requiring an additional RO<sub>2</sub> source of approximately  
710 2 ppbv h<sup>-1</sup> to be balanced.

711 Further information on the nature of the missing RO<sub>2</sub> source can be obtained from the chemical budget of  
712 RO<sub>x</sub>, for which the production rate is 0.5 ppbv h<sup>-1</sup> smaller than the loss rate at 3.5 ppbv NO (Fig. 12).  
713 This discrepancy cannot be explained by the instrumental uncertainties in HO<sub>2</sub> and RO<sub>2</sub> measurements,  
714 because the RO<sub>x</sub> budget at high NO in the morning was dominated by OH reactions with NO<sub>2</sub> and (Fig.  
715 9). Thus, the imbalance in the RO<sub>x</sub> budget at high NO indicates a missing primary radical source, which  
716 on a single day (29 April) even reached 3 ppbv hr<sup>-1</sup> (Fig. 6). As the OH budget is balanced for most of  
717 the time and the corresponding HO<sub>2</sub> budget does not require an additional HO<sub>2</sub> source, a missing primary  
718 RO<sub>2</sub> source is a likely explanation for the discrepancy in the RO<sub>x</sub> budget. This would also explain part of  
719 the imbalance in the RO<sub>2</sub> budget at high NO concentrations.

720

#### 721 4.2 Potentially missing chemical processes

722 The above discussion shows that imbalances between calculated production and destruction rates are  
723 highly variable over time and change with chemical conditions. As main general features in spring and  
724 summer, the radical budget analysis indicates unaccounted OH production processes with a typical  
725 strength of 1.5 – 3 ppbv h<sup>-1</sup> at low NO concentrations, which coincides with a missing HO<sub>2</sub> sink of 1 – 2

726 ppbv h<sup>-1</sup>. At high NO mixing ratios (> 1 ppbv), the radical budgets for OH and HO<sub>2</sub> radicals are relatively  
727 well balanced, but RO<sub>2</sub> production processes of about 2 ppbv h<sup>-1</sup> appear to be missing in the RO<sub>2</sub> radical  
728 budget. In the following, potential reasons for the observed discrepancies in the radical budgets are  
729 discussed.

#### 730 **4.2.1 Differences in the chemical behavior of specific RO<sub>2</sub> radicals**

731 As no speciated RO<sub>2</sub> radicals were detected but the sum of all RO<sub>2</sub> species, effective rate coefficients for  
732 the reaction of all RO<sub>2</sub> species with NO (Reaction R9, R14), RO<sub>2</sub> (Reaction R15), and HO<sub>2</sub> (Reaction R16)  
733 are used from structure-activity relationship (SAR) by Jenkin et al. (2019) for the calculations of turnover  
734 rates. Potential systematic errors due to this simplification for reactions of RO<sub>2</sub> with RO<sub>2</sub> and HO<sub>2</sub> are  
735 expected to be negligible due to their small contributions to the total turnover rates.

736 In contrast, the reaction of RO<sub>2</sub> with NO plays an important role in the chemical budgets of HO<sub>2</sub> and RO<sub>2</sub>.  
737 The reaction has one channel that converts RO<sub>2</sub> to HO<sub>2</sub> (Reaction R9) and one radical termination channel  
738 that produces organic nitrates (RONO<sub>2</sub>) (Reaction R14). The unknown speciation of RO<sub>2</sub> causes  
739 uncertainty with respect to the total rate constant of the RO<sub>2</sub> + NO reaction ( $k_9 + k_{14}$ ). An effective value  
740 of  $9 \times 10^{-12} \text{ cm}^{-3} \text{ s}^{-1}$  was taken from (Jenkin et al., 2019). A high limit for the total rate coefficient of  
741 RO<sub>2</sub> + NO (for example  $1.1 \times 10^{-11} \text{ cm}^{-3} \text{ s}^{-1}$ , 298K for c-C<sub>5</sub>H<sub>9</sub>O<sub>2</sub>) would slightly increase the imbalances  
742 between production and destruction rates for HO<sub>2</sub> and RO<sub>2</sub> radicals by 13 % for both spring and summer.  
743 A lower limit would be the rate constant of the reaction of methyl peroxy radicals (CH<sub>3</sub>O<sub>2</sub>) with NO  
744 having a value of  $7.7 \times 10^{-12} \text{ cm}^{-3} \text{ s}^{-1}$  (298 K)., Applying this number in the calculations for HO<sub>2</sub>  
745 production and RO<sub>2</sub> destruction rates (Fig. S6) for the period when observed discrepancies in the HO<sub>2</sub>  
746 budget were highest (Case 1) further improves the already well balanced budget of RO<sub>2</sub> radicals. This  
747 also reduces the imbalance between HO<sub>2</sub> destruction and destruction rates, but the effect is rather small  
748 (approximately 10%) and not sufficient to explain the total difference. For the other periods such as the  
749 spring period and the period of Case 2, a reduced reaction rate would worsen the observed imbalances.

750 An additional uncertainty in the HO<sub>2</sub> production rate comes from the assumed yield of organic nitrates in  
751 the reaction of RO<sub>2</sub> with NO. Typical organic nitrate yields range from 5 % to 20 % (Jenkin et al., 2019).  
752 The low limit value is applied in the calculations above. Using a value of 20 % decreases the discrepancy  
753 between HO<sub>2</sub> production and destruction rates from 2.0 to 1.5 ppbv h<sup>-1</sup> for the period of Case 1.

754 It is worth noting that the organic nitrate yield is generally higher for larger hydrocarbons, but the rate  
755 constant for the RO<sub>2</sub> + NO reaction is also often higher, so that there are compensating effects in the  
756 production efficiency of HO<sub>2</sub>. In addition, it is expected that only a fraction of RO<sub>2</sub> radicals is produced  
757 from large hydrocarbons due to the major composition of RO<sub>2</sub> would be methyl peroxy radicals.

758 For the above reasons, the unknown speciation of RO<sub>2</sub> is unlikely the reason for the observed imbalances  
759 in the HO<sub>2</sub> budget that are most prominent in the period of Case 1.

#### 760 **4.2.2 Unaccounted primary radical sources**

761 Primary RO<sub>x</sub> radical production that may not be appropriately accounted for in the calculations could be  
762 OH, HO<sub>2</sub>, and RO<sub>2</sub> production from the ozonolysis of alkenes. Only few alkene compounds were  
763 measured in the JULIAC campaign. The contribution from the ozonolysis of these alkenes to the radical  
764 production was very small with values in the range of 0.005 to 0.03 ppbv h<sup>-1</sup> (Section 3.5). The ozonolysis



765 of small alkenes such as propene and cis-2-butene that were not measured but are often abundant for  
766 example in forested areas (Goldstein et al., 1996; Rhew et al., 2017), may have significantly contributed  
767 to the radical production.

768 The potential impact of unmeasured alkenes on the primary radical production is tested by assuming that  
769 the OH reactivity that cannot be explained by measured OH reactants (on average,  $2.5 \text{ s}^{-1}$ ) originates from  
770 1.5 ppbv propene and 1.0 ppbv cis-2-butene. The radical production by ozonolysis of the additional  
771 propene and cis-2-butene increases the production from ozonolysis of measured species by more than an  
772 order of magnitude in both spring and summer periods of the JULIAC campaign (Fig. S7) The  
773 discrepancies between the total  $\text{RO}_x$  production and destruction rates is significantly decreased for the  
774 period of the 2 Case studies by approximately  $0.2 \text{ ppbv h}^{-1}$ . However, the additional OH production is by  
775 far insufficient to explain the missing OH source that was generally found during the JULIAC campaign.  
776 In addition, the corresponding OH and  $\text{O}_3$  reactivity from the additional alkene compounds is about a  
777 factor of 6 larger than of alkenes (e.g., ethene, propene, trans-2-butene, cis-2-pentene) that were measured  
778 in ambient air next to the SAPHIR chamber in the HOxComp campaign in July 2005 (Elshorbany et al.,  
779 2012; Kanaya et al., 2012).

780 The photolysis of oxygenated organic compounds is another source for radicals that could be  
781 underestimated in the calculations. Only the photolysis of HCHO is included in the production rate of  
782  $\text{HO}_2$  and  $\text{RO}_x$  at all times of the campaign. In addition, acetaldehyde ( $\text{CH}_3\text{CHO}$ ), methyl vinyl ketone  
783 (MVK), methacrolein (MACR), and methylglyoxal were measured during part of the campaign and were  
784 not included in the analysis in Section 3. Calculations show that radical production rate from their  
785 photolysis was less than  $0.1 \text{ ppbv h}^{-1}$ . Thus, photolysis of unmeasured OVOCs was very likely  
786 unimportant in the present study. This is consistent with similar small contributions from photolysis of  
787 OVOCs other than HCHO found in in the HOxComp campaign (Kanaya et al., 2012). In addition, during  
788 the HOxCOMP campaign the modelled OH reactivity could be matched with the measured reactivity by  
789 including either additional primary emissions (Kanaya et al., 2012) or model-produced oxygenated  
790 secondary products (Elshorbany et al., 2012). Neither of the additional species contributed enough to  
791 close the radical budgets. If it is assumed that the missing OH reactivity ( $2.5 \text{ s}^{-1}$ ) is all due to glyoxal (9  
792 ppb) an additional OH production of  $0.3 \text{ ppbv h}^{-1}$  could be expected. This would still not be enough to  
793 close the radical budget suggesting that unmeasured OVOCs do not play a large role.

794 The photolysis of  $\text{ClNO}_2$  constitutes a primary radical source (Reaction R20, R22) that can be found in  
795 coastal environments (e.g., Osthoff et al. (2008)) and mid-continental regions (e.g., Thornton et al.  
796 (2010)). The availability of  $\text{ClNO}_2$  data during the summer period allowed assessing the potential impact  
797 of its photolysis on the  $\text{RO}_2$  radical production (Eq. 9). Due to the low mixing ratio of  $\text{ClNO}_2$  of less than  
798  $0.4 \text{ ppbv}$  (Tan et al., 2022), the  $\text{RO}_2$  production from Cl oxidation processes was insignificant ( $<0.1 \text{ ppbv}$   
799  $\text{h}^{-1}$ ) and cannot explain the observed discrepancies in the primary production and destruction rates of  
800 radicals in the summer period and in the case studies. The instrument detecting  $\text{ClNO}_2$  was not available  
801 in the spring period of the campaign. Therefore, the extent to which  $\text{ClNO}_2$  photolysis contributed in  
802 spring, for example to the large missing  $\text{RO}_x$  source (up to  $3 \text{ ppbv hr}^{-1}$ ) on 29 April, remains unknown.

#### 803 4.2.3 Unaccounted radical termination reactions

804 Heterogeneous uptake of  $\text{HO}_2$  on aerosol is a potential termination reaction that is not included in the  $\text{HO}_2$   
805 and  $\text{RO}_x$  destruction rates above. However, the impact of including the heterogeneous  $\text{HO}_2$  loss on

806 aerosol surface (Eq. 8) on the total loss rate is insignificant (less than 1 %), even if a high effective uptake  
807 coefficient of 0.2 is assumed (Fig. S7).

808 As HO<sub>2</sub> uptake is a radical termination process, its relative contribution to the total RO<sub>x</sub> loss rate can be  
809 higher compared to the relative contribution to the total HO<sub>2</sub> loss rate. However, the only notable  
810 influence would be for the period of Case 2 (8 % of total RO<sub>x</sub> loss rate), when the aerosol surface area  
811 concentration was high with values of up to  $3.0 \times 10^2 \mu\text{m}^2 \text{cm}^{-3}$ .

812 The estimate for the heterogeneous HO<sub>2</sub> loss rate has a high uncertainty because the uptake coefficient  
813 highly depends on the aerosol properties that were not fully characterized in this campaign. Previous  
814 laboratory investigations showed a large variability for the uptake coefficient with values ranging from  
815 0.08 to 0.6 depending on the aerosol chemical composition and the physical state (George et al., 2007;  
816 Taketani et al., 2008, 2009; George et al., 2013; Lakey et al., 2015; Song et al., 2020; Tan et al., 2020).  
817 Even the largest reported HO<sub>2</sub> uptake coefficients cannot explain the observed differences in the chemical  
818 budget of HO<sub>2</sub> radicals. Therefore, heterogeneous HO<sub>2</sub> reactions can be ruled out as an explanation for the  
819 unexplained HO<sub>2</sub> loss rate.

#### 820 **4.2.4 Unaccounted radical inter-conversion reactions**

821 In the last decade, it has been discovered that unimolecular reactions of RO<sub>2</sub> can significantly increase  
822 atmospheric OH concentrations in low-NO environments where they can compete with the reaction of  
823 RO<sub>2</sub> with NO. The most important, atmospherically relevant example is the production of OH from the  
824 isomerization of isoprene-RO<sub>2</sub> radicals (Peeters et al., 2009; da Silva et al., 2010; Peeters and Müller,  
825 2010; Crouse et al., 2011; Fuchs et al., 2013; Peeters et al., 2014; Teng et al., 2017; Novelli et al., 2020).  
826 The SAPHIR chamber is surrounded by a deciduous forest that emits isoprene especially in summer.  
827 Compared to previous campaigns on the campus where up to several ppbv of isoprene were measured  
828 (Komenda et al., 2003; Spirig et al., 2005; Kanaya et al., 2012), concentrations were relatively low during  
829 the JULIAC campaign (< 0.4 ppbv, on average).

830 The effect of the conversion of RO<sub>2</sub> to OH by the isomerization of isoprene-RO<sub>2</sub> (Eq. 4) is tested in the  
831 analysis of the OH and RO<sub>2</sub> budgets. In the afternoon of days in the spring period and the period of Case  
832 2, the total OH production increases only 1 % due to the low isoprene mixing ratios (< 0.2 ppbv) and the  
833 competition of unimolecular reactions with bimolecular reactions of RO<sub>2</sub> with NO. Even in the summer  
834 period, when isoprene mixing ratios were up to 0.8 ppbv, the contribution of isomerization reactions from  
835 isoprene-RO<sub>2</sub> radicals to the total turnover rate of RO<sub>2</sub> is still small with values of less than 4 %. This  
836 implies that unimolecular decomposition reactions of isoprene-RO<sub>2</sub> radicals made a minor contribution to  
837 the RO<sub>2</sub> destruction and OH production rates.

838 Another known isomerization process that produces OH applies to RO<sub>2</sub> that are formed by OH oxidation  
839 of methacrolein (MACR) (Crouse et al., 2012; Fuchs et al., 2014), which is an oxidation product of  
840 isoprene. MACR mixing ratios were up to 0.5 ppbv in the JULIAC campaign. Because the rate constant  
841 for the OH reaction of MACR is smaller than for isoprene, OH regeneration from MACR-RO<sub>2</sub> radicals is  
842 even less important than from isoprene-RO<sub>2</sub>.

843 For acyl and carbonyl peroxy radicals it was shown that the reaction of RO<sub>2</sub> with HO<sub>2</sub>, which mainly  
844 forms hydroperoxides (ROOH) (Reaction R16), can produce OH with yields up to 80% (Hasson et al.,

845 2004; Dillon and Crowley, 2008; Groß et al., 2014; Praske et al., 2015; Winiberg et al., 2016; Fuchs et al.,  
846 2018; Jenkin et al., 2019). It is also noteworthy that the rate constant for the reaction of HO<sub>2</sub> with this  
847 class of RO<sub>2</sub> species is almost a factor of 2 higher than for other RO<sub>2</sub> species (Jenkin et al., 2019).  
848 However, even if it is assumed that all the measured RO<sub>2</sub> are acyl and carbonyl peroxy radicals, the  
849 formation of OH from their reaction with NO could only explain up to 0.5 ppbv h<sup>-1</sup> of the imbalances in  
850 both OH and HO<sub>2</sub> budgets.

851 Studies in the remote marine boundary layer show that HO<sub>2</sub> to OH conversion mediated by halogen  
852 oxides (XO, X = Cl, Br, I) (e.g., Bloss et al. (2005); Sommariva et al. (2006); Kanaya et al. (2007); Stone  
853 et al. (2018); Fan and Li (2022)) can significantly contribute to the interconversion of radicals and destroy  
854 ozone:



859 This conversion mechanism would only be effective at low NO, when the consumption of XO by NO  
860 (Reaction R25) is comparatively slow and when X is not depleted by other reactions as in the case of Cl  
861 by reactions with VOCs (Reaction R22).

862 For BrO, the rate constants for Reaction R23 and R25 are about the same ( $2.1 \times 10^{-11} \text{ cm}^3 \text{ s}^{-1}$  at 298 K,  
863 (J. B. Burkholder, 2019). Thus, the reaction of BrO with HO<sub>2</sub> would only be dominant, if the NO  
864 concentration were smaller than the concentration of HO<sub>2</sub>, i.e., less than 10 pptv in this campaign. For IO,  
865 the situation is similar and NO mixing ratios would need to be less than 40 pptv. Such low NO mixing  
866 ratios were not observed during daytime and rule out significant halogen oxide mediated HO<sub>2</sub> to OH  
867 conversion. The required XO concentrations to achieve an HO<sub>2</sub> loss rate of 1 ppbv h<sup>-1</sup> at an HO<sub>2</sub>  
868 concentration of  $2 \times 10^8 \text{ cm}^3$  would be 66 pptv BrO or 16 pptv IO, which exceeds the abundances  
869 reported for marine environments, where halogen sources are known to exist, by more than an order of  
870 magnitude. For these reasons, halogen oxide chemistry cannot explain the missing HO<sub>2</sub> sink and missing  
871 OH source in this study.

### 872 **4.3 Comparison with results from other field campaigns**

873 Although the chemical and physical conditions were partly influenced by the chamber properties (Section  
874 2.1), the radical concentrations observed during spring and summer were within the range of values that  
875 have been observed in other field studies in summertime in urban and suburban areas (Tan et al., 2001;  
876 Ren et al., 2003; Kanaya et al., 2007; Mao et al., 2010; Lu et al., 2013; Brune et al., 2016; Tan et al., 2017;  
877 Whalley et al., 2018; Tan et al., 2019). The impact of the decreased solar radiation by the chamber  
878 transmission on the radical production was compensated by the radical production from the photolysis of  
879 HONO and HCHO emitted from the chamber film.

880 This effect is also shown in the relationship between the OH concentration and the photolysis frequencies  
881 of ozone,  $j_{\text{O}_3}$  (Section 3.4). The slope ( $8.0 \times 10^{11} \text{ cm}^{-3} \text{ s}^{-1}$ ) of the correlation for the data from the

882 JULIAC campaign is much higher than obtained for data in other field campaigns in similar environments  
883 (Ehhalt and Rohrer, 2000; Handisides et al., 2003; Holland et al., 2003; Tan et al., 2017) due to the high  
884 OH production by the photolysis of chamber-produced HONO (Reaction R1). This is further confirmed  
885 by the similarity in OH and HO<sub>2</sub> radical concentrations between this campaign and what was observed in  
886 the HO<sub>x</sub>Comp campaign when measurements were performed in front of the SAPHIR chamber for 3 days  
887 in July 2005 (Elshorbany et al., 2012).

888 In contrast, daytime OH concentrations observed during winter and autumn in the JULIAC campaign  
889 were lower than OH concentrations observed in previous wintertime field campaigns (Heard et al., 2004;  
890 Ren et al., 2006; Kanaya et al., 2007; Tan et al., 2018; Ma et al., 2019). This is due to the lower photolysis  
891 frequencies in the chamber compared to outdoors, which is not compensated by chamber-produced HONO  
892 in wintertime, because the emission strength is low at low temperature and low solar radiation.

893 Very low nighttime OH concentration in all seasons of the JULIAC campaign (Section 3.4) is consistent  
894 with observations in previous field campaigns in rural areas in Germany (Ehhalt and Rohrer, 2000;  
895 Handisides et al., 2003; Holland et al., 2003), in which nighttime OH concentrations were less than  
896  $1 \times 10^5 \text{ cm}^{-3}$ . However, in several other field studies performed in urban areas, nighttime OH  
897 concentrations were in the range of  $0.2$  to  $3 \times 10^6 \text{ cm}^{-3}$ , for example in China (Lu et al., 2014; Rohrer et  
898 al., 2014; Tan et al., 2017; Tan et al., 2018; Ma et al., 2019; Tan et al., 2019; Wang et al., 2019; Whalley  
899 et al., 2021), in the US (Martinez et al., 2003; Brune et al., 2016; Griffith et al., 2016), and in the UK (Ren  
900 et al., 2003; Vaughan et al., 2012). In these studies, the high nighttime OH concentrations could not be  
901 explained by model predictions and raised questions about the presence of potential interferences in  
902 nighttime OH signals measured by LIF instruments (Mao et al., 2012; Lu et al., 2014; Novelli et al.,  
903 2014).

904 Similar studies investigating the chemical budgets of OH, HO<sub>2</sub>, RO<sub>2</sub>, and RO<sub>x</sub> radicals like in this study  
905 have been performed for data from field campaigns in a suburban area in the Pearl River Delta (PRD),  
906 China, in autumn 2014 (Tan et al., 2019), and in central Beijing, China, (Whalley et al., 2021) in summer  
907 2017.

908 Tan et al. (2019) observed median values of turnover rates of OH, HO<sub>2</sub> and RO<sub>2</sub> radicals ranging from 10  
909 to 15 ppbv h<sup>-1</sup>, while rates for RO<sub>x</sub> initiation and termination rates were on the order of 3 to 4 ppbv h<sup>-1</sup>  
910 during daytime for chemical conditions affected by anthropogenic emissions. From the comparison  
911 between the radical production and destruction rates, a missing OH source and a missing RO<sub>2</sub> sink with a  
912 similar rate up to 7 ppbv h<sup>-1</sup> (45 % of the total OH turnover) were found at low NO mixing ratios below 1  
913 ppbv, while HO<sub>2</sub> production and destruction rates were balanced. The authors suggested that an additional  
914 chemical mechanism is required that efficiently converts RO<sub>2</sub> to OH without the involvement of NO. One  
915 possibility proposed by Tan et al. (2019) is that HO<sub>x</sub> radicals are formed from the auto-oxidation of  
916 specific RO<sub>2</sub> species which include multifunctional groups such as -OH, -OOH, or -CHO groups.

917 The analysis of the chemical budget of OH radicals in the JULIAC campaign shows that an unaccounted  
918 OH source with a rate ranging between 2 and 3 ppbv h<sup>-1</sup> (about 50 % of the total OH destruction rate) is  
919 required at low NO mixing ratios to balance OH production and destruction rates. This rate is smaller than  
920 the rate determined in Tan et al. (2019). However, considering that the OH radical turnover rates in the  
921 JULIAC campaign were about half compared to values in the campaign in the PRD area, the relative  
922 importance of the unaccounted OH source was comparable in both campaigns. However, the mechanism

923 suggested by Tan et al. (2019) is likely not the only explanation for discrepancies in the radical budgets  
924 observed in this study. In the JULIAC campaign, to balance the budget of RO<sub>2</sub> radicals rather requires an  
925 additional radical source than additional loss processes particularly at high NO mixing ratios above 1  
926 ppbv, and the missing OH sources are likely originating from an HO<sub>2</sub> to OH conversion process and/or a  
927 missing primary OH source.

928 Whalley et al. (2021) also investigated the chemical budgets for radicals over a wide range of NO mixing  
929 ratios (0.1 to 104 ppbv) from measurement performed in central Beijing, China. Compared to the results  
930 in Tan et al. (2019) and to results in this study, the rates of RO<sub>x</sub> initiation and termination reactions were  
931 2 to 4 times higher. Also, the rates of radical propagation reactions for OH, HO<sub>2</sub> and RO<sub>2</sub> radicals were 5  
932 to 10 times higher due to fast inter-radical conversion reactions at conditions with high concentrations of  
933 NO. Similar to the results in this study, an OH source with a high rate of up to 15 ppbv h<sup>-1</sup> (50 % of the  
934 total OH destruction) was required to balance OH production and destruction rates for low NO mixing  
935 ratios. This unaccounted OH source is more than 3 times higher than that determined in the JULIAC  
936 campaign and in the campaign in China reported by Tan et al. (2019). The HO<sub>2</sub> production rate observed  
937 in Beijing largely exceeded the destruction rate by 3 to 5 times for low NO mixing ratios. In contrast,  
938 production and destruction of RO<sub>2</sub> and RO<sub>x</sub> radicals were well balanced. On the other hand, results for  
939 conditions of low NO concentrations, production and destruction of OH radicals were balanced at high  
940 NO mixing ratios, while very high imbalances of up to 50 ppbv h<sup>-1</sup> were observed for HO<sub>2</sub> and RO<sub>2</sub>  
941 radicals. Whalley et al. (2021) showed that reducing the rate constant of the reaction between RO<sub>2</sub> and  
942 NO by a factor of 10 could close the gaps between production and destruction rates. The authors  
943 suggested that the presence of a significant fraction of RO<sub>2</sub> radicals from the oxidation of large and  
944 multifunctional VOCs such as monoterpenes and long-chain alkanes could explain observations. These  
945 radicals can undergo multiple RO<sub>2</sub> to RO<sub>2</sub> conversion reactions by unimolecular isomerization of alkoxy  
946 radicals (RO), which are formed from the reaction of RO<sub>2</sub> with NO, so that no HO<sub>2</sub> is produced. Such a  
947 RO<sub>2</sub> radical reaction chain would be equivalent to an increased chemical lifetime of RO<sub>2</sub> radicals, if RO<sub>2</sub>  
948 species cannot be distinguished by instruments like in the sum measurements performed by RO<sub>x</sub>-LIF  
949 instruments. Whalley et al. (2021) showed that RO<sub>2</sub> production by this mechanism would largely  
950 reconcile discrepancies between modelled and measured RO<sub>2</sub> concentrations (the model-measurement  
951 ratio decreases from 6.2 to 1.8), if the OH reactivity that could not be accounted for by measured OH  
952 reactants is attributed to  $\alpha$ -pinene.

953 Applying a reduced rate constant for RO<sub>2</sub> to HO<sub>2</sub> propagation reactions as suggested in Whalley et al.  
954 (2021) in the calculations in this study could help explaining the observed discrepancies between HO<sub>2</sub> and  
955 RO<sub>2</sub> production and destruction rates. The largest effect is expected when high NO mixing ratios up to 10  
956 ppbv like on 29 April is experienced. In this case, a high reduction of the rate constant by a factor of 2 for  
957 all measured RO<sub>2</sub> would be required to close the observed gaps between production and destruction rates.  
958 Reduced reaction rate constants of the RO<sub>2</sub>+NO reaction could be expected for RO<sub>2</sub> from large VOCs.  
959 However, the fraction of these RO<sub>2</sub> species is expected to be small for conditions of this campaign, even  
960 if OH reactivity that is not explained by measured OH reactants is attributed to large VOCs. Therefore, it  
961 seems unlikely that the mechanism suggested by Whalley et al. (2021) affects the observed discrepancies  
962 in the radical budgets in this study.

963 It is interesting to point out that similar discrepancies in the OH and HO<sub>2</sub> budgets have been observed  
964 during the HOxComp campaign in July 2005 (Elshorbany et al., 2012). Although measurements were

965 only done for 3 days and despite that these were 14 years earlier than measurements in this work, the  
966 chemical composition was similar with comparable values of NO<sub>x</sub>, O<sub>3</sub>, isoprene concentrations and of  
967 OH reactivity. As observed in this study, a missing OH radical source in the range of 2 to 4 ppbv h<sup>-1</sup> was  
968 needed to close the OH budget for low-NO chemical regimes. The lack of measured RO<sub>2</sub> radicals did not  
969 allow to perform a measurement-only budget for HO<sub>2</sub> radicals. Nevertheless, model calculations  
970 overestimated measured HO<sub>2</sub> radicals after the correction for RO<sub>2</sub> radical interferences (Fuchs et al., 2011)  
971 by up to 30% at low NO (Elshorbany et al., 2012; Kanaya et al., 2012). Like in this study, good  
972 agreement was found between modelled and measured OH and HO<sub>2</sub> radical concentrations only if an  
973 unknown loss process for HO<sub>2</sub> radicals that would recycle OH was introduced.

#### 974 **4.4 Potential role of the missing radical processes on the evaluation of the ozone production rate**

975 The good agreement of the odd oxygen production rates calculated by the two different methods (Section  
976 3.1) not only gives high confidence in the measured peroxy radical concentrations but also confirms the  
977 current chemical understanding of tropospheric ozone formation from the reaction of peroxy radicals with  
978 NO. Therefore, results demonstrate that accurate predictions of radical concentrations in atmospheric  
979 models are crucial to accurately predict the surface ozone level.

980 However, the significant level of the missing radical processes found in this study implies the difficulties  
981 in the prediction of the radical concentrations by the models without constraining radicals by their  
982 measurements. In low NO mixing ratios, there are two opposing effects of the missing radical processes  
983 on the O<sub>3</sub> formation. At first, a missing OH source and therefore an underestimation of OH concentrations  
984 by the models would lower the loss of NO<sub>2</sub> by the reduced reaction rate with OH, and essentially produce  
985 more O<sub>3</sub> by its photolysis. Furthermore, the production of RO<sub>2</sub> would be under-predicted due to the lower  
986 OH concentrations in the models. At the same time, an unexplained HO<sub>2</sub> sink would result in the over-  
987 prediction in HO<sub>2</sub> concentrations and thus O<sub>3</sub> production. In high NO environments, missing RO<sub>2</sub> and  
988 RO<sub>x</sub> production processes would result in an underestimation of the O<sub>3</sub> production.

989

#### 990 **5 Summary and conclusions**

991 Ambient measurements of atmospheric radicals, trace gases, and aerosol properties were performed  
992 during the Jülich Atmospheric Chemistry Project campaign (JULIAC) using the atmospheric simulation  
993 chamber SAPHIR at Forschungszentrum Jülich, Germany. Ambient air was continuously drawn at a high  
994 rate into the chamber (1 hour residence time) through a 50 m high inlet line for one month in each season  
995 throughout 2019.

996 For parts of the campaign, measurements of OH concentrations were achieved by two different methods,  
997 laser-induced fluorescence with a chemical modulation system for zeroing (FZJ-LIF-CMR) and  
998 differential optical absorption spectroscopy (FZJ-DOAS). Measurements of both instruments agreed  
999 within 11 % (Cho et al., 2021).

1000 The production rate of odd oxygen (O<sub>x</sub>) was determined by using either measured HO<sub>2</sub> and RO<sub>2</sub>  
1001 concentrations or O<sub>3</sub> and NO<sub>2</sub> concentrations measured in the chamber and in the incoming flow. Results  
1002 showed excellent agreement between the two different methods confirming that HO<sub>2</sub> and RO<sub>2</sub> are

1003 responsible for the formation of tropospheric O<sub>3</sub> and giving additional confidence in the reliability of  
1004 peroxy radical concentration measurements performed in the JULIAC campaign.

1005 An analysis of the chemical budgets of OH, HO<sub>2</sub>, RO<sub>2</sub> and RO<sub>x</sub> radicals was performed for data obtained  
1006 in the spring and summer periods of the campaign. On average, daytime radical turnover rates ranged  
1007 between 3 to 6 ppbv h<sup>-1</sup> and 4 to 10 ppbv h<sup>-1</sup> in spring and summer, respectively, for OH, HO<sub>2</sub> and RO<sub>2</sub>  
1008 radicals, while total rates of RO<sub>x</sub> initiation and termination reactions were below 2.0 ppbv h<sup>-1</sup>. For most  
1009 conditions, radical production and destruction rates highly depended on the turnover rate of the reaction  
1010 of peroxy radicals with NO. For the total turnover rate of the sum of all radicals (RO<sub>x</sub>), the photolysis of  
1011 HONO and HCHO contributed most to the primary radical production and the reactions of OH with NO<sub>2</sub>  
1012 and RO<sub>2</sub> with HO<sub>2</sub> dominated the radical termination processes.

1013 Differences between radical production and destruction rates were often small and below the accuracy of  
1014 the calculations in the JULIAC campaign in winter and autumn. However, for both spring and summer,  
1015 an additional OH source is required to explain the observed discrepancy between production and  
1016 destruction rates. The OH production rate of this source would need be on average 2 ppbv h<sup>-1</sup> and 3 ppbv  
1017 h<sup>-1</sup> in the spring and summer period, respectively. This discrepancy is in the same range as observed for  
1018 measurements at the same location during the HO<sub>x</sub>Comp campaign in July 2005 (Elshorbany et al., 2012).

1019 Discrepancies between production and destruction rates of OH radicals were highest for conditions with  
1020 low NO mixing ratios in this study. This is similar to findings in other field campaigns in China (Tan et  
1021 al., 2017; Tan et al., 2019; Whalley et al., 2021). The high reliability of radical data in this study gives  
1022 further confidence that the discrepancies arise from unaccounted chemical processes rather than from  
1023 instrumental artefacts.

1024 The highest unaccounted OH source with a rate of 3.0 ppbv h<sup>-1</sup> (51 % of the observed total OH  
1025 destruction rate) is observed in the period from 5 August to 8 August (Case 1), when NO mixing ratios  
1026 were less than 1 ppbv and median maximum temperature in the chamber were 31°C. At the same time, an  
1027 additional HO<sub>2</sub> destruction process with a rate of up to 2.0 ppbv h<sup>-1</sup> is required to balance the HO<sub>2</sub>  
1028 production rate, while production and destruction rates for RO<sub>2</sub> radicals are well balanced. The opposing  
1029 imbalances in the OH and HO<sub>2</sub> budgets could be due to an unknown mechanism that converts HO<sub>2</sub> to OH,  
1030 or this could indicate a missing primary OH source and a similar fast, but independent termination  
1031 reaction removing HO<sub>2</sub>. If an unknown HO<sub>2</sub> to OH conversion mechanism played a major role, it would  
1032 not explain the complete rate of the missing OH source. Since the missing OH source is slightly larger  
1033 than the rate of the missing HO<sub>2</sub> sink, part of the missing OH source could have been originated from a  
1034 missing primary OH production process, because also a small difference between the total RO<sub>x</sub>  
1035 production and destruction rates are observed. The missing RO<sub>x</sub> source was up to 0.5 ppbv h<sup>-1</sup> for Case 1,  
1036 but was even higher with a rate of 1.4 ppbv h<sup>-1</sup> in the summer, when temperature was highest (Case 2).  
1037 Since the calculated reaction rate of the HO<sub>2</sub> and RO<sub>2</sub> radicals with NO were able to reproduce the  
1038 observed O<sub>x</sub> production within 1ppbv h<sup>-1</sup>, the unknown missing processes do not seem to have a direct  
1039 impact on net ozone production.

1040 For NO mixing ratios in range of 1 to 3 ppbv, production and destruction rates for OH and HO<sub>2</sub> radicals  
1041 were balanced, while additional sources of RO<sub>2</sub> and RO<sub>x</sub> having on average rates of 1.6 ppbv h<sup>-1</sup> and 0.4  
1042 ppbv h<sup>-1</sup>, respectively, were required to balance their production and destruction rates. Therefore, part of

1043 the missing RO<sub>2</sub> source can be explained by a primary radical source, but the remaining RO<sub>2</sub> source is  
1044 still unresolved.

1045 For high NO mixing ratios above 3 ppbv, 4 to 5 ppbv h<sup>-1</sup>, large discrepancies between production and  
1046 destruction rates of HO<sub>2</sub> and RO<sub>2</sub> radicals were found, but the calculations for these conditions have a  
1047 higher uncertainty due to low HO<sub>2</sub> and RO<sub>2</sub> concentrations close to background signals. Whereas the  
1048 imbalance in the budget for HO<sub>2</sub> radicals is due to an unaccounted loss processes, an additional RO<sub>2</sub>  
1049 production processes is required to close the chemical budget for RO<sub>2</sub> radicals. For the same conditions, a  
1050 primary RO<sub>x</sub> source with a rate of 0.5 ppbv h<sup>-1</sup> was needed to balance the RO<sub>x</sub> destruction rate. Therefore,  
1051 the missing primary RO<sub>x</sub> source is likely an unaccounted primary RO<sub>2</sub> source.

1052 Production of radicals from the oxidation of organic compounds by chlorine could have been one  
1053 additional source. Unfortunately, the potential impact of chlorine chemistry could not be examined in the  
1054 spring periods, when these conditions were experienced, because ClNO<sub>2</sub> measurements were not available.  
1055 During times when ClNO<sub>2</sub> concentrations were measured, chlorine chemistry initiated by the photolysis  
1056 of ClNO<sub>2</sub> did not significantly contribute to the radical production.

1057 For chemical conditions when the contribution of the reaction of HO<sub>2</sub> with NO to the OH production was  
1058 reduced, i.e. at lower NO levels, other radical formation pathways such as isomerization reactions of RO<sub>2</sub>  
1059 radicals, OH formation from ozonolysis of alkenes or photolysis of multifunctional organic compounds  
1060 could gain in importance and need to be properly accounted for. These processes remain relatively poorly  
1061 constrained due to the lack of direct measurements of e.g., multifunctional organic compounds.

1062 Although the exact mechanism for the missing production or destruction processes for OH, HO<sub>2</sub> and RO<sub>2</sub>  
1063 radicals could not be determined from measurements in this campaign, knowing the magnitudes of the  
1064 missing radical processes gives indicative information about the disagreements of model simulations and  
1065 observations for radicals and secondary air pollutants.

1066 More investigations of the chemical budgets of radicals for example in environments with high NO  
1067 mixing ratios including the determination of the impact of chlorine chemistry and with a detailed  
1068 characterization of the chemical composition of air masses with respect to the presence of complex  
1069 organic compounds would be beneficial for the understanding of radical chemistry as well as of the  
1070 formation of secondary air pollution such as ozone.

1071

## 1072 **Code and data availability**

1073 Data of the JULIAC campaign analyzed in this work is available from the Jülich Data repository  
1074 (<https://doi.org/10.26165/JUELICH-DATA/3J80BW>, Cho et al., 2022).

1075

## 1076 **Author contributions**

1077 AH designed JULIAC campaign and organized it together with HF and FH. CC performed the  
1078 measurements of radicals, analyzed the data, and wrote the paper together with AN and HF. All co-  
1079 authors contributed with data and helped the writing by intensive discussions of the manuscript.



1080

1081 **Competing interests**

1082 The authors declare that they have no conflict of interest.

1083

1084 **Financial Support**

1085 This project has received funding from the European Research Council (ERC) under the European  
1086 Union's Horizon 2020 research and innovation program (SARLEP grant agreement no. 681529) and from  
1087 the European Commission (EC) (Eurochamp 2020 project, grant agreement no. 730997).

1088

1089 **References**

1090 Atkinson, R., Baulch, D. L., Cox, R. A., Crowley, J. N., Hampson, R. F., Hynes, R. G., Jenkin, M. E.,  
1091 Rossi, M. J., and Troe, J.: Evaluated kinetic and photochemical data for atmospheric chemistry: Volume I  
1092 - gas phase reactions of O<sub>x</sub>, HO<sub>x</sub>, NO<sub>x</sub> and SO<sub>x</sub> species, *Atmos. Chem. Phys.*, 4, 1461-1738,  
1093 doi:10.5194/acp-4-1461-2004, 2004.

1094

1095 Atkinson, R., Baulch, D. L., Cox, R. A., Crowley, J. N., Hampson, R. F., Hynes, R. G., Jenkin, M. E.,  
1096 Rossi, M. J., Troe, J., and Subcommittee, I.: Evaluated kinetic and photochemical data for atmospheric  
1097 chemistry: Volume II - gas phase reactions of organic species, *Atmos. Chem. Phys.*, 6, 3625-4055,  
1098 doi:10.5194/acp-6-3625-2006, 2006.

1099

1100 Bloss, W. J., Lee, J. D., Johnson, G. P., Sommariva, R., Heard, D. E., Saiz-Lopez, A., Plane, J. M. C.,  
1101 McFiggans, G., Coe, H., Flynn, M., Williams, P., Rickard, A. R., and Fleming, Z. L.: Impact of halogen  
1102 monoxide chemistry upon boundary layer OH and HO<sub>2</sub> concentrations at a coastal site, *Geophysical*  
1103 *Research Letters*, 32, doi:10.1029/2004GL022084, 2005.

1104

1105 BMEL: (Federal Ministry of Food and Agriculture) : Ergebnisse der Waldzustandserhebung 2020, in,  
1106 Bonn, Germany, 2021.

1107

1108 Bohn, B., Rohrer, F., Brauers, T., and Wahner, A.: Actinometric measurements of NO<sub>2</sub> photolysis  
1109 frequencies in the atmosphere simulation chamber SAPHIR, *Atmos. Chem. Phys.*, 5, 493-503,  
1110 doi:10.5194/acp-5-493-2005, 2005.

1111

1112 Bohn, B., and Zilken, H.: Model-aided radiometric determination of photolysis frequencies in a sunlit  
1113 atmosphere simulation chamber, *Atmos. Chem. Phys.*, 5, 191-206, doi:10.5194/acp-5-191-2005, 2005.

1114

1115 Brune, W. H., Baier, B. C., Thomas, J., Ren, X., Cohen, R. C., Pusede, S. E., Browne, E. C., Goldstein, A.  
1116 H., Gentner, D. R., Keutsch, F. N., Thornton, J. A., Harrold, S., Lopez-Hilfiker, F. D., and Wennberg, P.

1117 O.: Ozone production chemistry in the presence of urban plumes, *Faraday Discuss.*, 189, 169-189,  
1118 doi:10.1039/C5FD00204D, 2016.

1119  
1120 Cazorla, M., Brune, W. H., Ren, X., and Lefer, B.: Direct measurement of ozone production rates in  
1121 Houston in 2009 and comparison with two estimation methods, *Atmos. Chem. Phys.*, 12, 1203-1212,  
1122 doi:10.5194/acp-12-1203-2012, 2012.

1123  
1124 Chen, S., Ren, X., Mao, J., Chen, Z., Brune, W. H., Lefer, B., Rappenglück, B., Flynn, J., Olson, J., and  
1125 Crawford, J. H.: A comparison of chemical mechanisms based on TRAMP-2006 field data, *Atmos.*  
1126 *Environ.*, 44, 4116-4125, doi:10.1016/j.atmosenv.2009.05.027, 2010.

1127  
1128 Cho, C., Hofzumahaus, A., Fuchs, H., Dorn, H. P., Glowania, M., Holland, F., Rohrer, F., Vardhan, V.,  
1129 Kiendler-Scharr, A., Wahner, A., and Novelli, A.: Characterization of a chemical modulation reactor  
1130 (CMR) for the measurement of atmospheric concentrations of hydroxyl radicals with a laser-induced  
1131 fluorescence instrument, *Atmos. Meas. Tech.*, 14, 1851-1877, doi:10.5194/amt-14-1851-2021, 2021.

1132  
1133 Cox, R. A., Ammann, M., Crowley, J. N., Herrmann, H., Jenkin, M. E., McNeill, V. F., Mellouki, A.,  
1134 Troe, J., and Wallington, T. J.: Evaluated kinetic and photochemical data for atmospheric chemistry:  
1135 Volume VII – Criegee intermediates, *Atmos. Chem. Phys.*, 20, 13497-13519, doi:10.5194/acp-20-13497-  
1136 2020, 2020.

1137  
1138 Crouse, J. D., Paulot, F., Kjaergaard, H. G., and Wennberg, P. O.: Peroxy radical isomerization in the  
1139 oxidation of isoprene, *Phys. Chem. Chem. Phys.*, 13, 13607-13613, doi:10.1039/C1CP21330J, 2011.

1140  
1141 Crouse, J. D., Knap, H. C., Ørnsø, K. B., Jørgensen, S., Paulot, F., Kjaergaard, H. G., and Wennberg, P.  
1142 O.: Atmospheric Fate of Methacrolein. 1. Peroxy Radical Isomerization Following Addition of OH and  
1143 O<sub>2</sub>, *J. Phys. Chem. A*, 116, 5756-5762, doi:10.1021/jp211560u, 2012.

1144  
1145 da Silva, G., Graham, C., and Wang, Z.-F.: Unimolecular β-hydroxyperoxy radical decomposition with  
1146 OH recycling in the photochemical oxidation of isoprene, *Environ. Sci. Technol.*, 44, 250-256,  
1147 doi:10.1021/es900924d, 2010.

1148  
1149 Dillon, T. J., and Crowley, J. N.: Direct detection of OH formation in the reactions of HO<sub>2</sub> with  
1150 CH<sub>3</sub>C(O)O<sub>2</sub> and other substituted peroxy radicals, *Atmos. Chem. Phys.*, 8, 4877-4889, doi:10.5194/acp-8-  
1151 4877-2008, 2008.

1152  
1153 Dusanter, S., Vimal, D., Stevens, P. S., Volkamer, R., Molina, L. T., Baker, A., Meinardi, S., Blake, D.,  
1154 Sheehy, P., Merten, A., Zhang, R., Zheng, J., Fortner, E. C., Junkermann, W., Dubey, M., Rahn, T.,  
1155 Eichinger, B., Lewandowski, P., Prueger, J., and Holder, H.: Measurements of OH and HO<sub>2</sub>  
1156 concentrations during the MCMA-2006 field campaign – Part 2: Model comparison and radical budget,  
1157 *Atmos. Chem. Phys.*, 9, 6655-6675, doi:10.5194/acp-9-6655-2009, 2009.

1158

1159 Ehhalt, D. H., and Rohrer, F.: Dependence of the OH concentration on solar UV, *J. Geophys. Res.:*  
1160 *Atmos.*, 105, 3565-3571, doi:10.1029/1999jd901070, 2000.

1161

1162 Elshorbany, Y. F., Kleffmann, J., Hofzumahaus, A., Kurtenbach, R., Wiesen, P., Brauers, T., Bohn, B.,  
1163 Dorn, H.-P., Fuchs, H., Holland, F., Rohrer, F., Tillmann, R., Wegener, R., Wahner, A., Kanaya, Y.,  
1164 Yoshino, A., Nishida, S., Kajii, Y., Martinez, M., Kubistin, D., Harder, H., Lelieveld, J., Elste, T., Plass-  
1165 Dülmer, C., Stange, G., Berresheim, H., and Schurath, U.: HOx budgets during HOxComp: A case study  
1166 of HOx chemistry under NOx-limited conditions, *J. Geophys. Res.: Atmos.*, 117,  
1167 doi:10.1029/2011JD017008, 2012.

1168

1169 Fan, S., and Li, Y.: The impacts of marine-emitted halogens on OH radicals in East Asia during summer,  
1170 *Atmos. Chem. Phys.*, 22, 7331-7351, doi:10.5194/acp-22-7331-2022, 2022.

1171

1172 Fishman, J., and Carney, T. A.: A one-dimensional photochemical model of the troposphere with  
1173 planetary boundary-layer parameterization, *J. Atmos. Chem.*, 1, 351-376, doi:10.1007/BF00053800, 1984.  
1174

1175

1176 Fuchs, H., Holland, F., and Hofzumahaus, A.: Measurement of tropospheric RO<sub>2</sub> and HO<sub>2</sub> radicals by a  
1177 laser-induced fluorescence instrument, *Rev. Sci. Instrum.*, 79, 084104, doi:10.1063/1.2968712, 2008.

1178

1179 Fuchs, H., Bohn, B., Hofzumahaus, A., Holland, F., Lu, K. D., Nehr, S., Rohrer, F., and Wahner, A.:  
1180 Detection of HO<sub>2</sub> by laser-induced fluorescence: calibration and interferences from RO<sub>2</sub> radicals, *Atmos.*  
1181 *Meas. Tech.*, 4, 1209-1225, doi:10.5194/amt-4-1209-2011, 2011.

1182

1183 Fuchs, H., Dorn, H. P., Bachner, M., Bohn, B., Brauers, T., Gomm, S., Hofzumahaus, A., Holland, F.,  
1184 Nehr, S., Rohrer, F., Tillmann, R., and Wahner, A.: Comparison of OH concentration measurements by  
1185 DOAS and LIF during SAPHIR chamber experiments at high OH reactivity and low NO concentration,  
1186 *Atmos. Meas. Tech.*, 5, 1611-1626, doi:10.5194/amt-5-1611-2012, 2012.

1187

1188 Fuchs, H., Hofzumahaus, A., Rohrer, F., Bohn, B., Brauers, T., Dorn, H. P., Häsel, R., Holland, F.,  
1189 Kaminski, M., Li, X., Lu, K., Nehr, S., Tillmann, R., Wegener, R., and Wahner, A.: Experimental  
1190 evidence for efficient hydroxyl radical regeneration in isoprene oxidation, *Nat. Geosci.*, 6, 1023-1026,  
1191 doi:10.1038/ngeo1964, 2013.

1192

1193 Fuchs, H., Acir, I. H., Bohn, B., Brauers, T., Dorn, H. P., Häsel, R., Hofzumahaus, A., Holland, F.,  
1194 Kaminski, M., Li, X., Lu, K., Lutz, A., Nehr, S., Rohrer, F., Tillmann, R., Wegener, R., and Wahner, A.:  
1195 OH regeneration from methacrolein oxidation investigated in the atmosphere simulation chamber  
1196 SAPHIR, *Atmos. Chem. Phys.*, 14, 7895-7908, doi:10.5194/acp-14-7895-2014, 2014.

1197

1198 Fuchs, H., Novelli, A., Rolletter, M., Hofzumahaus, A., Pfannerstill, E. Y., Kessel, S., Edtbauer, A.,  
1199 Williams, J., Michoud, V., Dusanter, S., Locoge, N., Zannoni, N., Gros, V., Truong, F., Sarda-Esteve, R.,  
1200 Cryer, D. R., Brumby, C. A., Whalley, L. K., Stone, D., Seakins, P. W., Heard, D. E., Schoemaeker, C.,  
1201 Blocquet, M., Coudert, S., Batut, S., Fittschen, C., Thames, A. B., Brune, W. H., Ernest, C., Harder, H.,  
1202 Muller, J. B. A., Elste, T., Kubistin, D., Andres, S., Bohn, B., Hohaus, T., Holland, F., Li, X., Rohrer, F.,

- 1203 Kiendler-Scharr, A., Tillmann, R., Wegener, R., Yu, Z., Zou, Q., and Wahner, A.: Comparison of OH  
1204 reactivity measurements in the atmospheric simulation chamber SAPHIR, *Atmos. Meas. Tech.*, 10, 4023-  
1205 4053, doi:10.5194/amt-10-4023-2017, 2017.
- 1206  
1207 Fuchs, H., Albrecht, S., Acir, I., Bohn, B., Breitenlechner, M., Dorn, H. P., Gkatzelis, G. I., Hofzumahaus,  
1208 A., Holland, F., Kaminski, M., Keutsch, F. N., Novelli, A., Reimer, D., Rohrer, F., Tillmann, R.,  
1209 Vereecken, L., Wegener, R., Zaytsev, A., Kiendler-Scharr, A., and Wahner, A.: Investigation of the  
1210 oxidation of methyl vinyl ketone (MVK) by OH radicals in the atmospheric simulation chamber SAPHIR,  
1211 *Atmos. Chem. Phys.*, 18, 8001-8016, doi:10.5194/acp-18-8001-2018, 2018.
- 1212  
1213 George, I. J., Vlasenko, A., Slowik, J. G., Broekhuizen, K., and Abbatt, J. P. D.: Heterogeneous oxidation  
1214 of saturated organic aerosols by hydroxyl radicals: uptake kinetics, condensed-phase products, and  
1215 particle size change, *Atmos. Chem. Phys.*, 7, 4187-4201, doi:10.5194/acp-7-4187-2007, 2007.
- 1216  
1217 George, I. J., Matthews, P. S. J., Whalley, L. K., Brooks, B., Goddard, A., Baeza-Romero, M. T., and  
1218 Heard, D. E.: Measurements of uptake coefficients for heterogeneous loss of HO<sub>2</sub> onto submicron  
1219 inorganic salt aerosols, *Phys. Chem. Chem. Phys.*, 15, 12829-12845, doi:10.1039/C3CP51831K, 2013.
- 1220  
1221 Glowania, M., Rohrer, F., Dorn, H. P., Hofzumahaus, A., Holland, F., Kiendler-Scharr, A., Wahner, A.,  
1222 and Fuchs, H.: Comparison of formaldehyde measurements by Hantzsch, CRDS and DOAS in the  
1223 SAPHIR chamber, *Atmos. Meas. Tech. Discuss.*, 2021, 1-23, doi:10.5194/amt-2021-10, 2021.
- 1224  
1225 Goldberg, D. L., Vinciguerra, T. P., Hosley, K. M., Loughner, C. P., Canty, T. P., Salawitch, R. J., and  
1226 Dickerson, R. R.: Evidence for an increase in the ozone photochemical lifetime in the eastern United  
1227 States using a regional air quality model, *J. Geophys. Res.: Atmos.*, 120, 12778-12793,  
1228 doi:10.1002/2015JD023930, 2015.
- 1229  
1230 Goldstein, A. H., Fan, S. M., Goulden, M. L., Munger, J. W., and Wofsy, S. C.: Emissions of ethene,  
1231 propene, and 1-butene by a midlatitude forest, *Journal of Geophysical Research: Atmospheres*, 101, 9149-  
1232 9157, doi:10.1029/96JD00334, 1996.
- 1233  
1234 Goldstein, A. H., and Galbally, I. E.: Known and Unexplored Organic Constituents in the Earth's  
1235 Atmosphere, *Environ. Sci. Technol.*, 41, 1514-1521, doi:10.1021/es072476p, 2007.
- 1236  
1237 Griffith, S. M., Hansen, R. F., Dusanter, S., Stevens, P. S., Alaghmand, M., Bertman, S. B., Carroll, M. A.,  
1238 Erickson, M., Galloway, M., Grossberg, N., Hottle, J., Hou, J., Jobson, B. T., Kamrath, A., Keutsch, F.  
1239 N., Lefer, B. L., Mielke, L. H., O'Brien, A., Shepson, P. B., Thurlow, M., Wallace, W., Zhang, N., and  
1240 Zhou, X. L.: OH and HO<sub>2</sub> radical chemistry during PROPHET 2008 and CABINEX 2009 - Part 1:  
1241 Measurements and model comparison, *Atmos. Chem. Phys.*, 13, 5403-5423, doi:10.5194/acp-13-5403-  
1242 2013, 2013.
- 1243  
1244 Griffith, S. M., Hansen, R. F., Dusanter, S., Michoud, V., Gilman, J. B., Kuster, W. C., Veres, P. R.,  
1245 Graus, M., de Gouw, J. A., Roberts, J., Young, C., Washenfelder, R., Brown, S. S., Thalman, R.,  
1246 Waxman, E., Volkamer, R., Tsai, C., Stutz, J., Flynn, J. H., Grossberg, N., Lefer, B., Alvarez, S. L.,

1247 Rappenglueck, B., Mielke, L. H., Osthoff, H. D., and Stevens, P. S.: Measurements of hydroxyl and  
1248 hydroperoxy radicals during CalNex-LA: Model comparisons and radical budgets, *J. Geophys. Res.:*  
1249 *Atmos.*, 121, 4211-4232, doi:10.1002/2015jd024358, 2016.

1250  
1251 Groß, C. B. M., Dillon, T. J., Schuster, G., Lelieveld, J., and Crowley, J. N.: Direct Kinetic Study of OH  
1252 and O<sub>3</sub> Formation in the Reaction of CH<sub>3</sub>C(O)O<sub>2</sub> with HO<sub>2</sub>, *J. Phys. Chem. A*, 118, 974-985,  
1253 doi:10.1021/jp412380z, 2014.

1254  
1255 Häsel, R., Brauers, T., Holland, F., and Wahner, A.: Development and application of a new mobile  
1256 LOPAP instrument for the measurement of HONO altitude profiles in the planetary boundary layer,  
1257 *Atmos. Meas. Tech. Discuss.*, 2009, 2027-2054, doi:10.5194/amtd-2-2027-2009, 2009.

1258  
1259 Han, S., Bian, H., Feng, Y., Liu, A., Li, X., Zeng, F., and Zhang, X.: Analysis of the Relationship  
1260 between O<sub>3</sub>, NO and NO<sub>2</sub> in Tianjin, China, *Aerosol Air Qual. Res.*, 11, 128-139,  
1261 doi:10.4209/aaqr.2010.07.0055, 2011.

1262  
1263 Handisides, G. M., Plass-Dülmer, C., Gilge, S., Bingemer, H., and Berresheim, H.: Hohenpeissenberg  
1264 Photochemical Experiment (HOPE 2000): Measurements and photostationary state calculations of OH  
1265 and peroxy radicals, *Atmos. Chem. Phys.*, 3, 1565-1588, doi:10.5194/acp-3-1565-2003, 2003.

1266  
1267 Hasson, A. S., Tyndall, G. S., and Orlando, J. J.: A Product Yield Study of the Reaction of HO<sub>2</sub> Radicals  
1268 with Ethyl Peroxy (C<sub>2</sub>H<sub>5</sub>O<sub>2</sub>), Acetyl Peroxy (CH<sub>3</sub>C(O)O<sub>2</sub>), and Acetonyl Peroxy (CH<sub>3</sub>C(O)CH<sub>2</sub>O<sub>2</sub>)  
1269 Radicals, *J. Phys. Chem. A*, 108, 5979-5989, doi:10.1021/jp048873t, 2004.

1270  
1271 Hens, K., Novelli, A., Martinez, M., Auld, J., Axinte, R., Bohn, B., Fischer, H., Keronen, P., Kubistin, D.,  
1272 Nölscher, A. C., Oswald, R., Paasonen, P., Petäjä, T., Regelin, E., Sander, R., Sinha, V., Sipilä, M.,  
1273 Taraborrelli, D., Tatum Ernest, C., Williams, J., Lelieveld, J., and Harder, H.: Observation and modelling  
1274 of HOx radicals in a boreal forest, *Atmos. Chem. Phys.*, 14, 8723-8747, doi:10.5194/acp-14-8723-2014,  
1275 2014.

1276  
1277 Hofzumahaus, A., Rohrer, F., Lu, K., Bohn, B., Brauers, T., Chang, C.-C., Fuchs, H., Holland, F., Kita,  
1278 K., Kondo, Y., Li, X., Lou, S., Shao, M., Zeng, L., Wahner, A., and Zhang, Y.: Amplified trace gas  
1279 removal in the troposphere, *Science*, 324, 1702-1704, doi:10.1126/science.1164566, 2009.

1280  
1281 Hofzumahaus, A., and Heard, D. H.: Assessment of local HOx and ROx measurement techniques:  
1282 achievements, challenges, and future directions - Outcomes of the 2015 international HOx workshop,  
1283 Forschungszentrum Jülich, Jülich, 20-21, 2016.

1284  
1285 Holland, F., Hofzumahaus, A., Schäfer, J., Kraus, A., and Pätz, H.-W.: Measurements of OH and HO<sub>2</sub>  
1286 radical concentrations and photolysis frequencies during BERLIOZ, *J. Geophys. Res.: Atmos.*, 108, 8246,  
1287 doi:10.1029/2001jd001393, 2003.

1288

1289 J. B. Burkholder, S. P. S., J. Abbatt, J. R. Barker, C. Cappa, J. D. Crouse, T. S. Dibble, R. E. Huie, C. E.  
1290 Kolb, M. J. Kurylo, V. L. Orkin, C. J. Percival, D. M. Wilmouth, and P. H. Wine: Chemical Kinetics and  
1291 Photochemical Data for Use in Atmospheric Studies, Evaluation No. 19, Jet Propulsion Laboratory,  
1292 Pasadena, 2019.

1293

1294 Jenkin, M. E., Valorso, R., Aumont, B., and Rickard, A. R.: Estimation of rate coefficients and branching  
1295 ratios for reactions of organic peroxy radicals for use in automated mechanism construction, *Atmos.*  
1296 *Chem. Phys.*, 19, 7691-7717, doi:10.5194/acp-19-7691-2019, 2019.

1297

1298 Jordan, A., Haidacher, S., Hanel, G., Hartungen, E., Märk, L., Seehauser, H., Schottkowsky, R., Sulzer, P.,  
1299 and Märk, T. D.: A high resolution and high sensitivity proton-transfer-reaction time-of-flight mass  
1300 spectrometer (PTR-TOF-MS), *Int. J. Mass Spectrom.*, 286, 122-128, doi:10.1016/j.ijms.2009.07.005,  
1301 2009.

1302

1303 Kaminski, M., Fuchs, H., Acir, I. H., Bohn, B., Brauers, T., Dorn, H. P., Häsel, R., Hofzumahaus, A., Li,  
1304 X., Lutz, A., Nehr, S., Rohrer, F., Tillmann, R., Vereecken, L., Wegener, R., and Wahner, A.:  
1305 Investigation of the  $\beta$ -pinene photooxidation by OH in the atmosphere simulation chamber SAPHIR,  
1306 *Atmos. Chem. Phys.*, 17, 6631-6650, doi:10.5194/acp-17-6631-2017, 2017.

1307

1308 Kanaya, Y., Cao, R., Akimoto, H., Fukuda, M., Komazaki, Y., Yokouchi, Y., Koike, M., Tanimoto, H.,  
1309 Takegawa, N., and Kondo, Y.: Urban photochemistry in central Tokyo: 1. Observed and modeled OH and  
1310 HO<sub>2</sub> radical concentrations during the winter and summer of 2004, *J. Geophys. Res.: Atmos.*, 112,  
1311 doi:10.1029/2007jd008670, 2007.

1312

1313 Kanaya, Y., Hofzumahaus, A., Dorn, H. P., Brauers, T., Fuchs, H., Holland, F., Rohrer, F., Bohn, B.,  
1314 Tillmann, R., Wegener, R., Wahner, A., Kajii, Y., Miyamoto, K., Nishida, S., Watanabe, K., Yoshino, A.,  
1315 Kubistin, D., Martinez, M., Rudolf, M., Harder, H., Berresheim, H., Elste, T., Plass-Dülmer, C., Stange,  
1316 G., Kleffmann, J., Elshorbany, Y., and Schurath, U.: Comparisons of observed and modeled OH and HO<sub>2</sub>  
1317 concentrations during the ambient measurement period of the HO<sub>x</sub>Comp field campaign, *Atmos. Chem.*  
1318 *Phys.*, 12, 2567-2585, doi:10.5194/acp-12-2567-2012, 2012.

1319

1320 Kim, S., Wolfe, G. M., Mauldin, L., Cantrell, C., Guenther, A., Karl, T., Turnipseed, A., Greenberg, J.,  
1321 Hall, S. R., Ullmann, K., Apel, E., Hornbrook, R., Kajii, Y., Nakashima, Y., Keutsch, F. N., DiGangi, J.  
1322 P., Henry, S. B., Kaser, L., Schnitzhofer, R., Graus, M., Hansel, A., Zheng, W., and Flocke, F. F.:  
1323 Evaluation of HO<sub>x</sub> sources and cycling using measurement-constrained model calculations in a 2-methyl-  
1324 3-butene-2-ol (MBO) and monoterpene (MT) dominated ecosystem, *Atmos. Chem. Phys.*, 13, 2031-2044,  
1325 doi:10.5194/acp-13-2031-2013, 2013.

1326

1327 Kleffmann, J., Lörzer, J. C., Wiesen, P., Kern, C., Trick, S., Volkamer, R., Rodenas, M., and Wirtz, K.:  
1328 Intercomparison of the DOAS and LOPAP techniques for the detection of nitrous acid (HONO), *Atmos.*  
1329 *Environ.*, 40, 3640-3652, doi:10.1016/j.atmosenv.2006.03.027, 2006.

1330

1331 Kleinman, L. I., Daum, P. H., Lee, Y.-N., Nunnermacker, L. J., Springston, S. R., Weinstein-Lloyd, J.,  
1332 and Rudolph, J.: Ozone production efficiency in an urban area, *J. Geophys. Res.: Atmos.*, 107, ACH 23-  
1333 21-ACH 23-12, doi:10.1029/2002JD002529, 2002.

1334  
1335 Komenda, M., Schaub, A., and Koppmann, R.: Description and characterization of an on-line system for  
1336 long-term measurements of isoprene, methyl vinyl ketone, and methacrolein in ambient air, *J.*  
1337 *Chromatogr. A*, 995, 185-201, doi:10.1016/S0021-9673(03)00518-1, 2003.

1338  
1339 Konrad, S., Schmitz, T., Buers, H.-J., Houben, N., Mannschreck, K., Mihelcic, D., Müsgen, P., Pätz, H.-  
1340 W., Holland, F., Hofzumahaus, A., Schäfer, H.-J., Schröder, S., Volz-Thomas, A., Bächmann, K.,  
1341 Schlomski, S., Moortgat, G., and Großmann, D.: Hydrocarbon measurements at Pabstthum during the  
1342 BERLIOZ campaign and modeling of free radicals, *J. Geophys. Res.: Atmos.*, 108,  
1343 doi:10.1029/2001JD000866, 2003.

1344  
1345 Kubistin, D., Harder, H., Martinez, M., Rudolf, M., Sander, R., Bozem, H., Eerdeken, G., Fischer, H.,  
1346 Gurk, C., Klüpfel, T., Königstedt, R., Parchatka, U., Schiller, C. L., Stickler, A., Taraborrelli, D.,  
1347 Williams, J., and Lelieveld, J.: Hydroxyl radicals in the tropical troposphere over the Suriname rainforest:  
1348 comparison of measurements with the box model MECCA, *Atmos. Chem. Phys.*, 10, 9705-9728,  
1349 doi:10.5194/acp-10-9705-2010, 2010.

1350  
1351 Lakey, P. S. J., George, I. J., Whalley, L. K., Baeza-Romero, M. T., and Heard, D. E.: Measurements of  
1352 the HO<sub>2</sub> Uptake Coefficients onto Single Component Organic Aerosols, *Environ. Sci. Technol.*, 49, 4878-  
1353 4885, doi:10.1021/acs.est.5b00948, 2015.

1354  
1355 Lelieveld, J., Butler, T. M., Crowley, J. N., Dillon, T. J., Fischer, H., Ganzeveld, L., Harder, H., Lawrence,  
1356 M. G., Martinez, M., Taraborrelli, D., and Williams, J.: Atmospheric oxidation capacity sustained by a  
1357 tropical forest, *Nature*, 452, 737, doi:10.1038/nature06870, 2008.

1358  
1359 Lou, S., Holland, F., Rohrer, F., Lu, K., Bohn, B., Brauers, T., Chang, C. C., Fuchs, H., Häseler, R., Kita,  
1360 K., Kondo, Y., Li, X., Shao, M., Zeng, L., Wahner, A., Zhang, Y., Wang, W., and Hofzumahaus, A.:  
1361 Atmospheric OH reactivities in the Pearl River Delta – China in summer 2006: measurement and model  
1362 results, *Atmos. Chem. Phys.*, 10, 11243-11260, doi:10.5194/acp-10-11243-2010, 2010.

1363  
1364 Lu, K. D., Hofzumahaus, A., Holland, F., Bohn, B., Brauers, T., Fuchs, H., Hu, M., Häseler, R., Kita, K.,  
1365 Kondo, Y., Li, X., Lou, S. R., Oebel, A., Shao, M., Zeng, L. M., Wahner, A., Zhu, T., Zhang, Y. H., and  
1366 Rohrer, F.: Missing OH source in a suburban environment near Beijing: observed and modelled OH and  
1367 HO<sub>2</sub> concentrations in summer 2006, *Atmos. Chem. Phys.*, 13, 1057-1080, doi:10.5194/acp-13-1057-  
1368 2013, 2013.

1369  
1370 Lu, K. D., Rohrer, F., Holland, F., Fuchs, H., Brauers, T., Oebel, A., Dlugi, R., Hu, M., Li, X., Lou, S. R.,  
1371 Shao, M., Zhu, T., Wahner, A., Zhang, Y. H., and Hofzumahaus, A.: Nighttime observation and  
1372 chemistry of HO<sub>x</sub> in the Pearl River Delta and Beijing in summer 2006, *Atmos. Chem. Phys.*, 14, 4979-  
1373 4999, doi:10.5194/acp-14-4979-2014, 2014.

1374

1375 Ma, X., Tan, Z., Lu, K., Yang, X., Liu, Y., Li, S., Li, X., Chen, S., Novelli, A., Cho, C., Zeng, L., Wahner,  
1376 A., and Zhang, Y.: Winter photochemistry in Beijing: Observation and model simulation of OH and HO<sub>2</sub>  
1377 radicals at an urban site, *Sci. Tot. Environ.*, 685, 85-95, doi:10.1016/j.scitotenv.2019.05.329, 2019.

1378  
1379 Malkin, T. L., Goddard, A., Heard, D. E., and Seakins, P. W.: Measurements of OH and HO<sub>2</sub> yields from  
1380 the gas phase ozonolysis of isoprene, *Atmos. Chem. Phys.*, 10, 1441-1459, doi:10.5194/acp-10-1441-  
1381 2010, 2010.

1382  
1383 Mao, J., Ren, X., Chen, S., Brune, W. H., Chen, Z., Martinez, M., Harder, H., Lefer, B., Rappenglück, B.,  
1384 Flynn, J., and Leuchner, M.: Atmospheric oxidation capacity in the summer of Houston 2006:  
1385 Comparison with summer measurements in other metropolitan studies, *Atmos. Environ.*, 44, 4107-4115,  
1386 doi:doi.org/10.1016/j.atmosenv.2009.01.013, 2010.

1387  
1388 Mao, J., Ren, X., Zhang, L., Van Duin, D. M., Cohen, R. C., Park, J. H., Goldstein, A. H., Paulot, F.,  
1389 Beaver, M. R., Crounse, J. D., Wennberg, P. O., DiGangi, J. P., Henry, S. B., Keutsch, F. N., Park, C.,  
1390 Schade, G. W., Wolfe, G. M., Thornton, J. A., and Brune, W. H.: Insights into hydroxyl measurements  
1391 and atmospheric oxidation in a California forest, *Atmos. Chem. Phys.*, 12, 8009-8020, doi:10.5194/acp-  
1392 12-8009-2012, 2012.

1393  
1394 Martinez, M., Harder, H., Kovacs, T. A., Simpas, J. B., Bassis, J., Leshner, R., Brune, W. H., Frost, G. J.,  
1395 Williams, E. J., Stroud, C. A., Jobson, B. T., Roberts, J. M., Hall, S. R., Shetter, R. E., Wert, B., Fried, A.,  
1396 Alicke, B., Stutz, J., Young, V. L., White, A. B., and Zamora, R. J.: OH and HO<sub>2</sub> concentrations, sources,  
1397 and loss rates during the Southern Oxidants Study in Nashville, Tennessee, summer 1999, *J. Geophys.*  
1398 *Res.: Atmos.*, 108, doi:10.1029/2003JD003551, 2003.

1399  
1400 Mihelcic, D., Holland, F., Hofzumahaus, A., Hoppe, L., Konrad, S., Müsgen, P., Pätz, H.-W., Schäfer, H.-  
1401 J., Schmitz, T., Volz-Thomas, A., Bächmann, K., Schlomski, S., Platt, U., Geyer, A., Alicke, B., and  
1402 Moortgat, G. K.: Peroxy radicals during BERLIOZ at Pabstthum: Measurements, radical budgets and  
1403 ozone production, *J. Geophys. Res.: Atmos.*, 108, doi:10.1029/2001JD001014, 2003.

1404  
1405 Nehr, S., Bohn, B., Fuchs, H., Hofzumahaus, A., and Wahner, A.: HO<sub>2</sub> formation from the OH + benzene  
1406 reaction in the presence of O<sub>2</sub>, *Physical Chemistry Chemical Physics*, 13, 10699-10708,  
1407 doi:10.1039/C1CP20334G, 2011.

1408  
1409 Nehr, S., Bohn, B., Dorn, H. P., Fuchs, H., Häsel, R., Hofzumahaus, A., Li, X., Rohrer, F., Tillmann, R.,  
1410 and Wahner, A.: Atmospheric photochemistry of aromatic hydrocarbons: OH budgets during SAPHIR  
1411 chamber experiments, *Atmos. Chem. Phys.*, 14, 6941-6952, doi:10.5194/acp-14-6941-2014, 2014.

1412  
1413 Niether, D., Cho, C., Rohrer, F. H., A. Novelli, A., Holland, F., Fuchs, H., Wesolek, C., Bohn, B., and  
1414 Wahner, A. K.-S., A. Tillmann, R.: Seasonal ozone production rate measurements by use of SAPHIR as a  
1415 large continuous flow reactor during the JULIAC campaign, *Atmos. Chem. Phys.*, In preparation, 2022.

1416  
1417 Novelli, A., Hens, K., Tatum Ernest, C., Kubistin, D., Regelin, E., Elste, T., Plass-Dülmer, C., Martinez,  
1418 M., Lelieveld, J., and Harder, H.: Characterisation of an inlet pre-injector laser-induced fluorescence



1419 instrument for the measurement of atmospheric hydroxyl radicals, *Atmos. Meas. Tech.*, 7, 3413-3430,  
1420 doi:10.5194/amt-7-3413-2014, 2014.

1421

1422 Novelli, A., Kaminski, M., Rolletter, M., Acir, I. H., Bohn, B., Dorn, H. P., Li, X., Lutz, A., Nehr, S.,  
1423 Rohrer, F., Tillmann, R., Wegener, R., Holland, F., Hofzumahaus, A., Kiendler-Scharr, A., Wahner, A.,  
1424 and Fuchs, H.: Evaluation of OH and HO<sub>2</sub> concentrations and their budgets during photooxidation of 2-  
1425 methyl-3-butene-2-ol (MBO) in the atmospheric simulation chamber SAPHIR, *Atmos. Chem. Phys.*, 18,  
1426 11409-11422, doi:10.5194/acp-18-11409-2018, 2018.

1427

1428 Novelli, A., Vereecken, L., Bohn, B., Dorn, H. P., Gkatzelis, G. I., Hofzumahaus, A., Holland, F., Reimer,  
1429 D., Rohrer, F., Rosanka, S., Taraborrelli, D., Tillmann, R., Wegener, R., Yu, Z., Kiendler-Scharr, A.,  
1430 Wahner, A., and Fuchs, H.: Importance of isomerization reactions for OH radical regeneration from the  
1431 photo-oxidation of isoprene investigated in the atmospheric simulation chamber SAPHIR, *Atmos. Chem.*  
1432 *Phys.*, 20, 3333-3355, doi:10.5194/acp-20-3333-2020, 2020.

1433

1434 Novelli, A., Cho, C., Fuchs, H., Hofzumahaus, A., Rohrer, F., Tillmann, R., Kiendler-Scharr, A., Wahner,  
1435 A., and Vereecken, L.: Experimental and theoretical study on the impact of a nitrate group on the  
1436 chemistry of alkoxy radicals, *Phys. Chem. Chem. Phys.*, 23, 5474-5495, doi:10.1039/d0cp05555g, 2021.

1437

1438 Osthoff, H. D., Roberts, J. M., Ravishankara, A. R., Williams, E. J., Lerner, B. M., Sommariva, R., Bates,  
1439 T. S., Coffman, D., Quinn, P. K., Dibb, J. E., Stark, H., Burkholder, J. B., Talukdar, R. K., Meagher, J.,  
1440 Fehsenfeld, F. C., and Brown, S. S.: High levels of nitryl chloride in the polluted subtropical marine  
1441 boundary layer, *Nature Geoscience*, 1, 324-328, doi:10.1038/ngeo177, 2008.

1442

1443 Peeters, J., Nguyen, T., and Vereecken, L.: HO<sub>x</sub> radical regeneration in the oxidation of isoprene, *Phys.*  
1444 *Chem. Chem. Phys.*, 11, 5935-5939, doi:10.1039/b908511d, 2009.

1445

1446 Peeters, J., and Müller, J.-F.: HO<sub>x</sub> radical regeneration in isoprene oxidation via peroxy radical  
1447 isomerisations. II: experimental evidence and global impact, *Phys. Chem. Chem. Phys.*, 12, 14227-14235,  
1448 doi:10.1039/C0CP00811G, 2010.

1449

1450 Peeters, J., Müller, J. F., Stavrou, T., and Vinh Son, N.: Hydroxyl radical recycling in isoprene  
1451 oxidation driven by hydrogen bonding and hydrogen tunneling: The upgraded LIM1 mechanism, *J. Phys.*  
1452 *Chem. A*, 118, doi:10.1021/jp5033146, 2014.

1453

1454 Praske, E., Crounse, J. D., Bates, K. H., Kurtén, T., Kjaergaard, H. G., and Wennberg, P. O.: Atmospheric  
1455 Fate of Methyl Vinyl Ketone: Peroxy Radical Reactions with NO and HO<sub>2</sub>, *J. Phys. Chem. A*, 119, 4562-  
1456 4572, doi:10.1021/jp5107058, 2015.

1457

1458 Ren, X., Harder, H., Martinez, M., Leshner, R. L., Olliger, A., Simpas, J. B., Brune, W. H., Schwab, J. J.,  
1459 Demerjian, K. L., He, Y., Zhou, X., and Gao, H.: OH and HO<sub>2</sub> Chemistry in the urban atmosphere of  
1460 New York City, *Atmos. Environ.*, 37, 3639-3651, doi:doi.org/10.1016/S1352-2310(03)00459-X, 2003.

1461

1462 Ren, X., Brune, W. H., Mao, J., Mitchell, M. J., Leshner, R. L., Simpas, J. B., Metcalf, A. R., Schwab, J. J.,  
1463 Cai, C., Li, Y., Demerjian, K. L., Felton, H. D., Boynton, G., Adams, A., Perry, J., He, Y., Zhou, X., and  
1464 Hou, J.: Behavior of OH and HO<sub>2</sub> in the winter atmosphere in New York City, *Atmos. Environ.*, 40, 252-  
1465 263, doi:10.1016/j.atmosenv.2005.11.073, 2006.

1466  
1467 Ren, X., van Duin, D., Cazorla, M., Chen, S., Mao, J., Zhang, L., Brune, W. H., Flynn, J. H., Grossberg,  
1468 N., Lefer, B. L., Rappenglück, B., Wong, K. W., Tsai, C., Stutz, J., Dibb, J. E., Thomas Jobson, B., Luke,  
1469 W. T., and Kelley, P.: Atmospheric oxidation chemistry and ozone production: Results from SHARP  
1470 2009 in Houston, Texas, *J. Geophys. Res.: Atmos.*, 118, 5770-5780, doi:10.1002/jgrd.50342, 2013.

1471  
1472 Rhew, R. C., Deventer, M. J., Turnipseed, A. A., Warneke, C., Ortega, J., Shen, S., Martinez, L., Koss, A.,  
1473 Lerner, B. M., Gilman, J. B., Smith, J. N., Guenther, A. B., and de Gouw, J. A.: Ethene, propene, butene  
1474 and isoprene emissions from a ponderosa pine forest measured by relaxed eddy accumulation, *Atmos.*  
1475 *Chem. Phys.*, 17, 13417-13438, doi:10.5194/acp-17-13417-2017, 2017.

1476  
1477 Rohrer, F., Bohn, B., Brauers, T., Brüning, D., Johnen, F. J., Wahner, A., and Kleffmann, J.:  
1478 Characterisation of the photolytic HONO-source in the atmosphere simulation chamber SAPHIR, *Atmos.*  
1479 *Chem. Phys.*, 5, 2189-2201, doi:10.5194/acp-5-2189-2005, 2005.

1480  
1481 Rohrer, F., Lu, K., Hofzumahaus, A., Bohn, B., Brauers, T., Chang, C.-C., Fuchs, H., Häseler, R.,  
1482 Holland, F., Hu, M., Kita, K., Kondo, Y., Li, X., Lou, S., Oebel, A., Shao, M., Zeng, L., Zhu, T., Zhang,  
1483 Y., and Wahner, A.: Maximum efficiency in the hydroxyl-radical-based self-cleansing of the troposphere,  
1484 *Nat. Geosci.*, 7, 559, doi:10.1038/ngeo2199, 2014.

1485  
1486 Rolletter, M., Kaminski, M., Acir, I. H., Bohn, B., Dorn, H. P., Li, X., Lutz, A., Nehr, S., Rohrer, F.,  
1487 Tillmann, R., Wegener, R., Hofzumahaus, A., Kiendler-Scharr, A., Wahner, A., and Fuchs, H.:  
1488 Investigation of the  $\alpha$ -pinene photooxidation by OH in the atmospheric simulation chamber SAPHIR,  
1489 *Atmos. Chem. Phys.*, 19, 11635-11649, doi:10.5194/acp-19-11635-2019, 2019.

1490  
1491 Rolletter, M., Blocquet, M., Kaminski, M., Bohn, B., Dorn, H. P., Hofzumahaus, A., Holland, F., Li, X.,  
1492 Rohrer, F., Tillmann, R., Wegener, R., Kiendler-Scharr, A., Wahner, A., and Fuchs, H.: Photooxidation of  
1493 pinonaldehyde at ambient conditions investigated in the atmospheric simulation chamber SAPHIR,  
1494 *Atmos. Chem. Phys.*, 20, 13701-13719, doi:10.5194/acp-20-13701-2020, 2020.

1495  
1496 Sarkar, C., Guenther, A. B., Park, J. H., Seco, R., Alves, E., Batalha, S., Santana, R., Kim, S., Smith, J.,  
1497 Tóta, J., and Vega, O.: PTR-TOF-MS eddy covariance measurements of isoprene and monoterpene fluxes  
1498 from an eastern Amazonian rainforest, *Atmos. Chem. Phys.*, 20, 7179-7191, doi:10.5194/acp-20-7179-  
1499 2020, 2020.

1500  
1501 Sillman, S., Logan, J. A., and Wofsy, S. C.: The sensitivity of ozone to nitrogen oxides and hydrocarbons  
1502 in regional ozone episodes, *J. Geophys. Res.: Atmos.*, 95, 1837-1851, doi:10.1029/JD095iD02p01837,  
1503 1990.

1504

1505 Slater, E. J., Whalley, L. K., Woodward-Massey, R., Ye, C., Lee, J. D., Squires, F., Hopkins, J. R.,  
1506 Dunmore, R. E., Shaw, M., Hamilton, J. F., Lewis, A. C., Crilley, L. R., Kramer, L., Bloss, W., Vu, T.,  
1507 Sun, Y., Xu, W., Yue, S., Ren, L., Acton, W. J. F., Hewitt, C. N., Wang, X., Fu, P., and Heard, D. E.:  
1508 Elevated levels of OH observed in haze events during wintertime in central Beijing, *Atmos. Chem. Phys.*,  
1509 20, 14847-14871, doi:10.5194/acp-20-14847-2020, 2020.

1510  
1511 Sommariva, R., Bloss, W. J., Brough, N., Carslaw, N., Flynn, M., Haggerstone, A. L., Heard, D. E.,  
1512 Hopkins, J. R., Lee, J. D., Lewis, A. C., McFiggans, G., Monks, P. S., Penkett, S. A., Pilling, M. J., Plane,  
1513 J. M. C., Read, K. A., Saiz-Lopez, A., Rickard, A. R., and Williams, P. I.: OH and HO<sub>2</sub> chemistry during  
1514 NAMBLEX: roles of oxygenates, halogen oxides and heterogeneous uptake, *Atmos. Chem. Phys.*, 6,  
1515 1135-1153, doi:10.5194/acp-6-1135-2006, 2006.

1516  
1517 Sommariva, R., Hollis, L. D. J., Sherwen, T., Baker, A. R., Ball, S. M., Bandy, B. J., Bell, T. G.,  
1518 Chowdhury, M. N., Cordell, R. L., Evans, M. J., Lee, J. D., Reed, C., Reeves, C. E., Roberts, J. M., Yang,  
1519 M., and Monks, P. S.: Seasonal and geographical variability of nitryl chloride and its precursors in  
1520 Northern Europe, *Atmos. Sci. Lett.*, 19, e844, doi:10.1002/asl.844, 2018.

1521  
1522 Song, H., Chen, X., Lu, K., Zou, Q., Tan, Z., Fuchs, H., Wiedensohler, A., Moon, D. R., Heard, D. E.,  
1523 Baeza-Romero, M. T., Zheng, M., Wahner, A., Kiendler-Scharr, A., and Zhang, Y.: Influence of aerosol  
1524 copper on HO<sub>2</sub> uptake: a novel parameterized equation, *Atmos. Chem. Phys.*, 20, 15835-15850,  
1525 doi:10.5194/acp-20-15835-2020, 2020.

1526  
1527 Spirig, C., Neftel, A., Ammann, C., Dommen, J., Grabmer, W., Thielmann, A., Schaub, A., Beauchamp,  
1528 J., Wisthaler, A., and Hansel, A.: Eddy covariance flux measurements of biogenic VOCs during ECHO  
1529 2003 using proton transfer reaction mass spectrometry, *Atmos. Chem. Phys.*, 5, 465-481,  
1530 doi:10.5194/acp-5-465-2005, 2005.

1531  
1532 Stone, D., Whalley, L. K., and Heard, D. E.: Tropospheric OH and HO<sub>2</sub> radicals: field measurements and  
1533 model comparisons, *Chem. Soc. Rev.*, 41, 6348-6404, doi:10.1039/C2CS35140D, 2012.

1534  
1535 Stone, D., Sherwen, T., Evans, M. J., Vaughan, S., Ingham, T., Whalley, L. K., Edwards, P. M., Read, K.  
1536 A., Lee, J. D., Moller, S. J., Carpenter, L. J., Lewis, A. C., and Heard, D. E.: Impacts of bromine and  
1537 iodine chemistry on tropospheric OH and HO<sub>2</sub>: comparing observations with box and global model  
1538 perspectives, *Atmos. Chem. Phys.*, 18, 3541-3561, doi:10.5194/acp-18-3541-2018, 2018.

1539  
1540 Taketani, F., Kanaya, Y., and Akimoto, H.: Kinetics of Heterogeneous Reactions of HO<sub>2</sub> Radical at  
1541 Ambient Concentration Levels with (NH<sub>4</sub>)<sub>2</sub>SO<sub>4</sub> and NaCl Aerosol Particles, *J. Phys. Chem. A*, 112,  
1542 2370-2377, doi:10.1021/jp0769936, 2008.

1543  
1544 Taketani, F., Kanaya, Y., and Akimoto, H.: Heterogeneous loss of HO<sub>2</sub> by KCl, synthetic sea salt, and  
1545 natural seawater aerosol particles, *Atmos. Environ.*, 43, 1660-1665, doi:10.1016/j.atmosenv.2008.12.010,  
1546 2009.

1547

1548 Tan, D., Faloon, I., Simpas, J. B., Brune, W., Shepson, P. B., Couch, T. L., Sumner, A. L., Carroll, M.  
1549 A., Thornberry, T., Apel, E., Riemer, D., and Stockwell, W.: HO<sub>x</sub> budgets in a deciduous forest: Results  
1550 from the PROPHET summer 1998 campaign, *J. Geophys. Res.: Atmos.*, 106, 24407-24427,  
1551 doi:10.1029/2001jd900016, 2001.

1552  
1553 Tan, Z., Fuchs, H., Lu, K., Hofzumahaus, A., Bohn, B., Broch, S., Dong, H., Gomm, S., Häsel, R., He,  
1554 L., Holland, F., Li, X., Liu, Y., Lu, S., Rohrer, F., Shao, M., Wang, B., Wang, M., Wu, Y., Zeng, L.,  
1555 Zhang, Y., Wahner, A., and Zhang, Y.: Radical chemistry at a rural site (Wangdu) in the North China  
1556 Plain: observation and model calculations of OH, HO<sub>2</sub> and RO<sub>2</sub> radicals, *Atmos. Chem. Phys.*, 17, 663-  
1557 690, doi:10.5194/acp-17-663-2017, 2017.

1558  
1559 Tan, Z., Rohrer, F., Lu, K., Ma, X., Bohn, B., Broch, S., Dong, H., Fuchs, H., Gkatzelis, G. I.,  
1560 Hofzumahaus, A., Holland, F., Li, X., Liu, Y., Liu, Y., Novelli, A., Shao, M., Wang, H., Wu, Y., Zeng, L.,  
1561 Hu, M., Kiendler-Scharr, A., Wahner, A., and Zhang, Y.: Wintertime photochemistry in Beijing:  
1562 observations of RO<sub>x</sub> radical concentrations in the North China Plain during the BEST-ONE campaign,  
1563 *Atmos. Chem. Phys.*, 18, 12391-12411, doi:10.5194/acp-18-12391-2018, 2018.

1564  
1565 Tan, Z., Lu, K., Hofzumahaus, A., Fuchs, H., Bohn, B., Holland, F., Liu, Y., Rohrer, F., Shao, M., Sun,  
1566 K., Wu, Y., Zeng, L., Zhang, Y., Zou, Q., Kiendler-Scharr, A., Wahner, A., and Zhang, Y.: Experimental  
1567 budgets of OH, HO<sub>2</sub>, and RO<sub>2</sub> radicals and implications for ozone formation in the Pearl River Delta in  
1568 China 2014, *Atmos. Chem. Phys.*, 19, 7129-7150, doi:10.5194/acp-19-7129-2019, 2019.

1569  
1570 Tan, Z., Hofzumahaus, A., Lu, K., Brown, S. S., Holland, F., Huey, L. G., Kiendler-Scharr, A., Li, X.,  
1571 Liu, X., Ma, N., Min, K.-E., Rohrer, F., Shao, M., Wahner, A., Wang, Y., Wiedensohler, A., Wu, Y., Wu,  
1572 Z., Zeng, L., Zhang, Y., and Fuchs, H.: No Evidence for a Significant Impact of Heterogeneous  
1573 Chemistry on Radical Concentrations in the North China Plain in Summer 2014, *Environ. Sci. Technol.*,  
1574 54, 5973-5979, doi:10.1021/acs.est.0c00525, 2020.

1575  
1576 Tan, Z., Fuchs, H., Hofzumahaus, A., Bloss, W. J., Bohn, B., Cho, C., Hohaus, T., Holland, F.,  
1577 Lakshmisha, C., Liu, L., Monks, P. S., Novelli, A., Niether, D., Rohrer, F., Tillmann, R., Valkenburg, T.,  
1578 Vardhan, V., Kiendler-Scharr, A., Wahner, A., and Sommariva, R.: Seasonal variation of nitryl chloride  
1579 and its relation to gas-phase precursors during the JULIAC campaign in Germany, *Atmos. Chem. Phys.*  
1580 *Discuss.*, 2022, 1-30, doi:10.5194/acp-2022-386, 2022.

1581  
1582 Tanaka, P. L., Riemer, D. D., Chang, S., Yarwood, G., McDonald-Buller, E. C., Apel, E. C., Orlando, J. J.,  
1583 Silva, P. J., Jimenez, J. L., Canagaratna, M. R., Neece, J. D., Mullins, C. B., and Allen, D. T.: Direct  
1584 evidence for chlorine-enhanced urban ozone formation in Houston, Texas, *Atmos. Environ.*, 37, 1393-  
1585 1400, doi:10.1016/S1352-2310(02)01007-5, 2003.

1586  
1587 Teng, A. P., Crouse, J. D., and Wennberg, P. O.: Isoprene peroxy radical dynamics, *J. Am. Chem. Soc.*,  
1588 139, 5367-5377, doi:10.1021/jacs.6b12838, 2017.

1589  
1590 Thornton, J. A., Kercher, J. P., Riedel, T. P., Wagner, N. L., Cozic, J., Holloway, J. S., Dubé, W. P.,  
1591 Wolfe, G. M., Quinn, P. K., Middlebrook, A. M., Alexander, B., and Brown, S. S.: A large atomic

1592 chlorine source inferred from mid-continental reactive nitrogen chemistry, *Nature*, 464, 271-274,  
1593 doi:10.1038/nature08905, 2010.

1594

1595 Vaughan, S., Ingham, T., Whalley, L. K., Stone, D., Evans, M. J., Read, K. A., Lee, J. D., Moller, S. J.,  
1596 Carpenter, L. J., Lewis, A. C., Fleming, Z. L., and Heard, D. E.: Seasonal observations of OH and HO<sub>2</sub> in  
1597 the remote tropical marine boundary layer, *Atmos. Chem. Phys.*, 12, 2149-2172, doi:10.5194/acp-12-  
1598 2149-2012, 2012.

1599

1600 Vilà-Guerau de Arellano, J., van den Dries, K., and Pino, D.: On inferring isoprene emission surface flux  
1601 from atmospheric boundary layer concentration measurements, *Atmos. Chem. Phys.*, 9, 3629-3640,  
1602 doi:10.5194/acp-9-3629-2009, 2009.

1603

1604 Wang, F., Hu, R., Chen, H., Xie, P., Wang, Y., Li, Z., Jin, H., Liu, J., and Liu, W.: Development of a field  
1605 system for measurement of tropospheric OH radical using laser-induced fluorescence technique, *Optics*  
1606 *Express*, 27, A419-A435, doi:10.1364/OE.27.00A419, 2019.

1607

1608 Whalley, L. K., Edwards, P. M., Furneaux, K. L., Goddard, A., Ingham, T., Evans, M. J., Stone, D.,  
1609 Hopkins, J. R., Jones, C. E., Karunaharan, A., Lee, J. D., Lewis, A. C., Monks, P. S., Moller, S. J., and  
1610 Heard, D. E.: Quantifying the magnitude of a missing hydroxyl radical source in a tropical rainforest,  
1611 *Atmos. Chem. Phys.*, 11, 7223-7233, doi:10.5194/acp-11-7223-2011, 2011.

1612

1613 Whalley, L. K., Stone, D., Dunmore, R., Hamilton, J., Hopkins, J. R., Lee, J. D., Lewis, A. C., Williams,  
1614 P., Kleffmann, J., Laufs, S., Woodward-Massey, R., and Heard, D. E.: Understanding in situ ozone  
1615 production in the summertime through radical observations and modelling studies during the Clean air for  
1616 London project (ClearfLo), *Atmos. Chem. Phys.*, 18, 2547-2571, doi:10.5194/acp-18-2547-2018, 2018.

1617

1618 Whalley, L. K., Slater, E. J., Woodward-Massey, R., Ye, C., Lee, J. D., Squires, F., Hopkins, J. R.,  
1619 Dunmore, R. E., Shaw, M., Hamilton, J. F., Lewis, A. C., Mehra, A., Worrall, S. D., Bacak, A., Bannan,  
1620 T. J., Coe, H., Percival, C. J., Ouyang, B., Jones, R. L., Crilley, L. R., Kramer, L. J., Bloss, W. J., Vu, T.,  
1621 Kotthaus, S., Grimmond, S., Sun, Y., Xu, W., Yue, S., Ren, L., Acton, W. J. F., Hewitt, C. N., Wang, X.,  
1622 Fu, P., and Heard, D. E.: Evaluating the sensitivity of radical chemistry and ozone formation to ambient  
1623 VOCs and NO<sub>x</sub> in Beijing, *Atmos. Chem. Phys.*, 21, 2125-2147, doi:10.5194/acp-21-2125-2021, 2021.

1624

1625 Winiberg, F. A. F., Dillon, T. J., Orr, S. C., Groß, C. B. M., Bejan, I., Brumby, C. A., Evans, M. J., Smith,  
1626 S. C., Heard, D. E., and Seakins, P. W.: Direct measurements of OH and other product yields from the  
1627 HO<sub>2</sub> + CH<sub>3</sub>C(O)O<sub>2</sub> reaction, *Atmos. Chem. Phys.*, 16, 4023-4042, doi:10.5194/acp-16-4023-2016, 2016.

1628

1629 Wolfe, G. M., Thornton, J. A., Bouvier-Brown, N. C., Goldstein, A. H., Park, J. H., McKay, M., Matross,  
1630 D. M., Mao, J., Brune, W. H., LaFranchi, B. W., Browne, E. C., Min, K. E., Wooldridge, P. J., Cohen, R.  
1631 C., Crouse, J. D., Faloona, I. C., Gilman, J. B., Kuster, W. C., de Gouw, J. A., Huisman, A., and Keutsch,  
1632 F. N.: The Chemistry of Atmosphere-Forest Exchange (CAFE) Model – Part 2: Application to  
1633 BEARPEX-2007 observations, *Atmos. Chem. Phys.*, 11, 1269-1294, doi:10.5194/acp-11-1269-2011,  
1634 2011.

1635

1636 Wolfe, G. M., Cantrell, C., Kim, S., Mauldin Iii, R. L., Karl, T., Harley, P., Turnipseed, A., Zheng, W.,  
1637 Flocke, F., Apel, E. C., Hornbrook, R. S., Hall, S. R., Ullmann, K., Henry, S. B., DiGangi, J. P., Boyle, E.  
1638 S., Kaser, L., Schnitzhofer, R., Hansel, A., Graus, M., Nakashima, Y., Kajii, Y., Guenther, A., and  
1639 Keutsch, F. N.: Missing peroxy radical sources within a summertime ponderosa pine forest, *Atmos. Chem.*  
1640 *Phys.*, 14, 4715-4732, doi:10.5194/acp-14-4715-2014, 2014.

1641

1642